ASSESSMENT OF SPATIAL/TEMPORAL VARIABILITY OF URBAN HEAT ISLAND EFFECT: A CASE STUDY IN THE CENTRAL DISTRICTS OF İZMİR

A Thesis Submitted to
the Graduate School of Engineering and Sciences of
İzmir Institute of Technology
in Partial Fulfillment of the Requirements for the Degree of

MASTER OF SCIENCE

in City Planning

by
Filiz AY

March 2024
İZMİR

We approve the thesis of **Filiz AY**

Examining Committee Members:

Assoc. Prof. Dr. Deniz GERÇEK KURT
Department of City and Regional Planning, İzmir Institute of Technology

Asst. Prof. Dr. Zeynep ELBURZ
Department of City and Regional Planning, İzmir Institute of Technology

Assoc. Prof. Dr. Nur Sinem PARTİGÖÇ
Department of City and Regional Planning, Pamukkale University

08 March 2024

Assoc. Prof. Dr. Deniz GERÇEK KURT
Supervisor, Department of City and
Regional Planning, İzmir Institute
of Technology

Prof. Dr. Koray VELİBEYOĞLU
Head of the Department of City and
Regional Planning

Prof. Dr. Mehtap EANES
Dean of the Graduate School of
Engineering and Sciences

ACKNOWLEDGMENTS

First and foremost, I want to extend my heartfelt gratitude to my advisor, Assoc. Prof. Dr. Deniz GERÇEK KURT, whose significant contributions were instrumental in crafting my master's thesis. Throughout my academic journey, her invaluable insights, suggestions, and unwavering support were pivotal in its preparation.

Afterwards, I extend my appreciation to Asst. Prof. Dr. Zeynep ELBURZ and Assoc. Prof. Dr. Nur Sinem PARTİGÖÇ, for graciously serving on the jury, meticulously evaluating my work, and providing constructive criticism.

I also want to express my deepest thanks to my dear family, who stood by me every step of the way, believing in me wholeheartedly and offering endless support. My beloved mother, Derya AY, who has been my pillar of strength, my cherished father, Selim AY, and my exceptional brother, Mahmut Sezgin AY, your unconditional assistance means the world to me.

To my dear fiancé, Boğaçhan BALÇIKLI, I owe a debt of gratitude for your unwavering support and love, enduring every challenge with me throughout the thesis process.

Lastly, I am immensely grateful to my close friends and beloved cousins for their well-wishes and unwavering encouragement. Special thanks to Aslı BAYRAKDARLAR, Merve DOĞRAMACI, Serhat DURNASUYU, R. Ezgi TEKİN ELMAS, and Birsu ÇINAR for their invaluable assistance in completing this work. Your support has been vital to my success, and I dedicate this achievement to each one of you.

I was able to achieve my goal thanks to your support, which is extremely vital to my success. I want to express my heartfelt thanks to all of you who didn't leave me alone during this challenging process and supported me with endless dedication. I dedicate this work to all of you.

ABSTRACT

ASSESSMENT OF SPATIAL/TEMPORAL VARIABILITY OF URBAN HEAT ISLAND EFFECT: A CASE STUDY IN THE CENTRAL DISTRICTS OF İZMİR

The rapid increase in urban population leads to changes in land use/land cover (LULC) and environmental problems such as Urban Heat Islands. Temperatures in cities being higher than their rural surroundings is a climatic phenomenon known as Urban Heat Island (UHI). Besides direct measurements of air temperature, Land Surface Temperature (LST) that characterizes Surface Urban Heat Island (SUHI) is widely used to determine the impact of UHI.

This study aims to determine the spatial/temporal variability of the SUHI effect in the central districts of İzmir for the years 1990, 2000, 2006, 2012, and 2018. Landsat satellite images were used for LST, Normalized Difference Vegetation Index (NDVI), Normalized Difference Water Index (NDWI), Normalized Difference Building Index (NDBI), Urban Index (UI), and albedo, while the CORINE land cover dataset was used for LULC maps.

In the study, the relationship between LST and LULC, and spectral indices was analyzed using zonal statistics, correlation, and regression analyses. In 2018, the highest LST values were observed for pastures, industry, commercial areas, transportation units, and mines, respectively. There is a high positive correlation between LST and NDBI, UI, Albedo, and a negative correlation with NDVI, respectively, while there is a moderate positive correlation with NDWI. In the regression model, 60.4% of the variability of the dependent variable is explained by NDBI and NDVI. NDBI (71.3%) and NDVI (7.6%) indices were the most effective factors on SUHI formation. The SUHI effect was more comprehensively evaluated across five different regions adding built-up indices into the variable set. It is concluded that the changes in LST values, together with the built environment indices, are largely influenced by changes in LULC.

Keywords: *Urban Heat Island, Surface Urban Heat Island, Land Surface Temperature, Spectral Indices*

ÖZET

KENTSEL ISI ADASI ETKİSİNİN MEKÂNSAL/ZAMANSAL DEĞİŞKENLİĞİNİN DEĞERLENDİRİLMESİ: İZMİR İLİ MERKEZ İLÇELERİ ÖRNEĞİ

Kentsel nüfusun hızla artması arazi kullanımı/arazi örtüsünde (AK/AÖ) değişikliklere ve Kentsel Isı Adaları gibi çevresel sorunlara neden olmaktadır. Şehirlerdeki sıcaklıkların kırsal çevrelerden daha yüksek olması, Kentsel Isı Adası (KIA) olarak bilinen bir iklim olgusudur. Hava sıcaklığının doğrudan ölçümlerinin yanı sıra, Yüzey Isı Adasını (YIA) karakterize eden Yer Yüzey Sıcaklığı (YYS), KIA'nın etkisini belirlemek için yaygın olarak kullanılmaktadır.

Bu çalışma, İzmir'in merkez ilçelerindeki YIA etkisinin mekânsal/zamansal değişkenliğini 1990, 2000, 2006, 2012 ve 2018 yılları üzerinden belirlemeyi amaçlamaktadır. Landsat uydu görüntülerinin termal verileri kullanılarak; YYS, Normalize Edilmiş Fark Bitki Örtüsü İndeksi (NDVI), Normalize Edilmiş Fark Su İndeksi (NDWI), Normalize Edilmiş Yerleşim Alanı İndeksi (NDBI), Kent İndeksi (UI) ve Albedo, CORINE arazi örtüsü veri seti kullanılarak ise AK/AÖ haritaları oluşturuldu.

Çalışmada YYS ile AK/AÖ ve spectral indeksler arasındaki ilişki zonal istatistik, korelasyon ve regresyon analizleri ile incelendi. 2018 yılındaki en yüksek YYS değerleri sırasıyla meralar, sanayi, ticari alanlarda, ulaşım birimlerinde ve maden ocaklarında gözlendi. YYS ile sırasıyla NDBI, UI, Albedo arasında yüksek düzeyde pozitif bir ilişki ve NDVI ile negatif bir ilişki bulunurken, NDWI ile arasında orta düzeyde pozitif bir ilişki vardır. Regresyon modelinde bağımlı değişkendeki değişimin %60,4'ü NDBI ve NDVI tarafından açıklandı. NDBI (%71,3) ve NDVI (%7,6) endeksleri SUHI oluşumunda en etkili faktörlerdir. YIA etkisi, değişken setine yapılaşma indeksleri eklenerek beş farklı bölgede daha kapsamlı bir şekilde değerlendirildi. YYS değerlerindeki değişikliklerin, yapılı çevre indeksleri ile birlikte büyük ölçüde AK/AÖ'deki değişimlerden etkilediği sonucuna varıldı.

Anahtar Kelimeler: *Kentsel Isı Adası, Yüzey Isı Adası, Yer Yüzey Sıcaklığı, Spektral İndeksler*

TABLE OF CONTENTS

LIST OF FIGURES

Figure	**Page**

LIST OF TABLES

Table **Page**

LIST OF ABBREVIATIONS

AUHI: Atmospheric Urban Heat Island

CLC: CORINE Land Cover

CORINE: Coordination of Information on the Environment

DN: Digital Number

ETM +: Enhanced Thematic Mapper Plus

GIS: Geographical Information Systems

LULC: Land Use/Land Cover

LSE: Land Surface Emissivity

LST: Land Surface Temperature

MLR: Multiple Linear Regression

MNDWI: Modified Normalized Difference Water Index

NIR: Near Infrared

NDBI: Normalized Difference Built-up Index

NDWI: Normalized Difference Water Index

NDVI: Normalized Difference Vegetation Index

OLI: Operational Land Imager

PBL: Planetary Boundary Layer

SUHI: Surface Urban Heat Island

SWIR: Shortwave Infrared

TIRS: Thermal Infrared Sensor

TM: Thematic Mapper

TOA: Top of Atmosphere

TSMS: Turkish State Meteorological Service

UBL: Urban Boundary Layer

UCL: Urban Canopy Layer

UHI: Urban Heat Island

UI: Urban Index

USGS: United States Geological Survey

CHAPTER 1

INTRODUCTION

Urbanization, accelerated with the Industrial Revolution, is a socio-economic process that causes the spatial distribution of the population to shift from rural areas to urban areas, and the growth of cities. Urban populations are increasing rapidly due to global population growth, and economic change[1,2]. It is stated that the world population, which is increasing day by day, will reach approximately 8.5 billion in 2030 and 9.7 billion in 2050[3]. It is estimated that 68% of the world's population will live in cities by 2050[4].

Rapid urbanization does not only cause the population to increase in cities. At the same time, it is a process of land use transformation that creates significant differences in the physical environment. With the increase in human activities associated with industrialization, climate changes in cities have accelerated due to the increase in fossil fuel consumption, greenhouse gas emissions, and transformations in urban landscape (covering natural surfaces with artificial surfaces)[5,6]. As a result of this change, it has been observed that the temperatures in cities tend to increase, and the urban climate differs from the rural surroundings[1].

Due to population growth in cities, social, economic, and environmental problems also increase[7]. People living in cities directly face the consequences of global climate changes such as natural disasters (rising sea levels, extreme weather events, etc.), poor quality water, and air, infertile soil, ecosystem, and land loss[8]. Urbanization, and urban land expansion characterized by demographic changes are the most radical, and irreversible form of land use[9]. Therefore, the effects of urbanization, and global climate change are of crucial importance for developing cities' climate change adaptation[8].

Cities create microclimate areas by creating local climate zones[10]. This situation causes different temperatures, surface flow, and wind conditions according to their environment[11,12]. Urbanization causes the rural cover types such as soil, water, and vegetation to be replaced with impervious surfaces such as concrete, metal, and asphalt[13]. Construction materials with high heat capacity, and low permeability properties used on urban surfaces (concrete, asphalt, etc.) absorb more solar heat than the materials used in rural areas[14,15]. Heat absorption on these surfaces then spreads to the environment, causing a significant temperature increase leading to the formation of “UHI” as a microclimatic environmental problem[16,17]. UHI, one of the most discussed issues of climatic events that occur with urbanization, is defined as the temperature in urban areas being higher than the temperature of the surrounding rural areas[18,19]. In other words, it is seen as the urban scale equivalent of global warming[20]. UHI phenomenon was first researched by Luke Howard in 1810, and the term was first used by Timothy Richard Oke[17].

With the rapid change in the built environment, cities are expanding horizontally while growing vertically. High building densities cause the microclimate in urban areas to differ significantly from the climate in rural areas[7]. Therefore, it is inevitable to observe UHI effects in urban areas where green areas decrease because of the densification of construction[12]. UHI causes increased energy consumption and bills, human health problems, air pollution and temperature increase, and environmental impacts. The main negative impacts on human health are heat stroke, heat exhaustion, respiratory problems, cardiovascular disorders, dehydration, and sleep disorders[21]. The UHI effect varies depending on the morphological structure of the city[12]. The UHI effect becomes more pronounced as wind speeds are generally low, and air temperatures are high in urban areas[19]. Features that determine the geometry of the city, such as the width of streets, and avenues, and the height of buildings affect the formation of the UHI effect[22,23]. While this formation, which occurs mostly at night, provides positive effects in the winter months, it causes extreme temperature increases in summer[24].

Nowadays, with the rate of urbanization reaching the highest levels, there is a growing interest in national/regional/urban, and micro-scale studies aimed at reducing the UHI effect, which negatively affects human health. There is a vast amount of studies in the literature examining the relationship between urban, and urbanization dynamics, and UHI. In general, these studies have revealed that the transformation of natural areas into hard, and impervious ground as a result of urbanization causes the UHI effect to accelerate, and increase. Therefore, it is very important to determine the UHI effect in cities. UHI’s are categorized under two main headings: Atmospheric UHI’s (AUHI), and Surface UHI’s (SUHI)[25]. There are two ways to demonstrate the UHI effect. The UHI effect is demonstrated by measuring temperature variations in the atmosphere at different heights in urban areas (AUHI) and by measuring temperature variations on the surface

(SUHI)[26]. In this context, Atmospheric UHI's are observed by direct measurements of weather stations, and mobile transits, while Surface UHI's are observed by indirect measurements such as remote sensing[27].

Remotely sensed imagery, which helps reveal the effect of the UHI, is used to measure the ground surface temperature[28]. Mapping ground surface temperatures is an important tool in scientific studies on issues such as climate change, LULC, and weather forecasting[29,30]. For the first time in the literature by Rao, P. (1972) studies have been carried out to detect Surface UHI's using remote sensing techniques. Observation of temporal surface temperature changes, and comparison of LULC changes are provided by thermal images obtained from satellites[31,32]. SUHI is characterized by LST, and it is detected by remote sensing methods commonly using MODIS, Landsat OLI/TIRS, Landsat TM, Landsat ETM+, Sentinel, ASTER, and SPOT images which enable determination of spatial variation, and changes in LST[32,33]. Studies examining LST values are critical to improving urban living conditions and making sustainable planning in the future[34].

In our country, it is predicted that the current effects of climate change will continue to increase in the future. For this reason, the central districts (11 districts) of İzmir, Türkiye's third-largest city, were chosen as the research area. İzmir is an important city for Türkiye with its economic, cultural, and historical rich history, and geographical location. At the same time, the city faces various challenges related to water resources, and environmental factors. This situation causes UHI effect to be observed intensively in İzmir. In this context, the study aims to determine the spatial, and temporal UHI effect in the central districts of İzmir city, and to propose measures to reduce the effect. The UHI effect is clearly seen in İzmir, especially during the summer months. This creates risks for urban quality of life (air pollution, water pollution, lack of green space, climate change, etc.). In this context, the study aims to evaluate the effect of SUHI on LST values in terms of LULC change, spectral indices, and built-up indices. For compatibility with the CORINE data set compared to LULC for LST 1990, 2000, 2006, 2012, and 2018. For this reason, in order to determine the UHI effect in the central districts of İzmir, July, and August, which are the hottest months in the summer; LST was created in the ArcGIS environment using Landsat 8 OLI/TIRS, Landsat 7 ETM+, and Landsat 5 TM thermal satellite images for the years 1990, 2000, 2006, 2012, and 2018. In the study, urban parameters such as LST (dependent variable) calculated from satellite images, and Normalized Difference Vegetation Index (NDVI), Normalized Difference Water Index

(NDWI), Normalized Difference Built-up Index (NDBI), Urban Index (UI), and Albedo (independent variable) were used. The relationship between them has been determined. Factors affecting UHI formation in the central districts of İzmir have been determined. Air temperature values of meteorological stations containing the same dates as Landsat satellite images were compared with LST values. The relationship between LST, and urban parameters was determined by correlation analysis, and Multiple Linear Regression (MLR) analysis. The effects of land use types on LST were determined by calculating LST statistics for CORINE LULC classes. For a comprehensive assessment of a larger set of variables defining the urban environment, LST and LULC relationships in the study area were evaluated. As a result of the analysis, built-up indices as urban parameters were determined using data on the number of buildings, green areas, and average number of mean household's size. Five different built environment textures were selected with the built-up indices determined as population density, building area density, and mean floor height, together with the LST and LULC maps of 2018. Changes in land use and urban parameters were detected depending on the LST values in these regions. Thus, the effects that may have caused UHI formation in the central districts of İzmir were determined. Finally, suggestions are made to reduce the UHI effect within the scope of the urban planning.

1.1. Problem Definition

The numbers, frequencies, and areas of impact of climatic, and meteorological disasters, which have become a global issue beyond environmental problems due to climate change, are increasing, and are said to continue to affect the world in the long term. Along with climate change, a significant increase in various weather events has been observed in many regions of the world in recent years[35,36]. Natural disasters, which have always existed throughout history, and will continue to exist in the future, threaten life on Earth, and have significant socio-economic impacts[36,37]. The possible risks of natural disasters are increasing due to factors such as the rapid growth of the world population, concentration of population in risky areas, overuse of natural resources, industrialization, unplanned urbanization, and inadequate infrastructure, while also accelerating the UHI effects in cities[37]. Global climate has warmed by 0.5°C over the last hundred years due to greenhouse gas emissions contributing to global warming[38] and climate change from human activities, and it is stated that the world will warm between 1.4°C and 5.8°C within the next century[39].

It has been found that meteorological disasters, which constitute a large part of natural disasters, have increased in the last twenty years. According to EM-DAT, one of the world's leading disaster databases, 7348 disaster events have been recorded worldwide in the last twenty years[40]. According to the "WMO Atlas of Mortality and Economic Losses From Weather, Climate and Water Extremes" report published in 2021, it is stated that 11072 natural disasters related to weather, climate, and water occurred worldwide between 1970 and 2019 (Figure 1)[41]. Half of all recorded disasters during this period, 45% of fatalities, and 74% of economic losses are attributed to meteorological disasters[40].

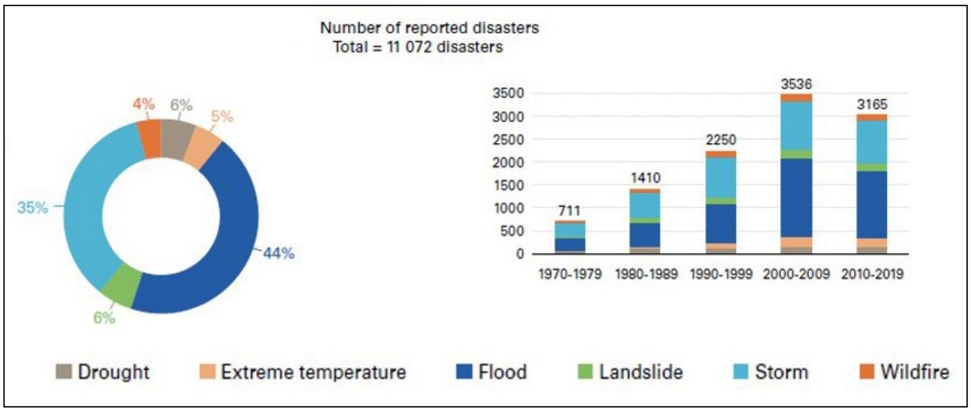

Figure 1. Distribution of the number of natural disasters originating from weather, climate and water occurring worldwide in 10-year periods (1970-2019)

(Source: WMO[41])

In the coming years, it is stated that the general temperature increase in the Mediterranean Basin, including Türkiye, will reach 1°C-2°C, and the annual average temperature in Türkiye will increase by 2.5°C-4°C in the coming years[38]. As a result, drought is expected in large areas, and particularly in the inland regions, the number of heatwaves, and extremely hot days is expected to increase. It is emphasized in IPCC reports, and national, and international scientific model studies that Türkiye will have a warmer, drier, and more uncertain climate structure in the near future[42]. Türkiye, which is among the countries at risk in terms of the potential effects of global climate change (excluding tropical storms, and active volcanoes), is predicted to experience a decrease in water resources, and ecological disturbances due to the expected increase in natural disasters associated with climate change[35,36].

Our country, which has a wide geography and various climate regions, experiences a large number and variety of severe meteorological events, including storms, floods, hail, frost, snow, and drought[35]. Serious increasing trends in the numbers of meteorological disasters have been observed in Türkiye's long-term distribution of meteorological disaster numbers from 1940 to November 30, 2022. The highest number of extreme events in Türkiye occurred in 2022 with 1030 extreme events. The majority of extreme events are constituted by heavy rainfall (Figure 2)[43].

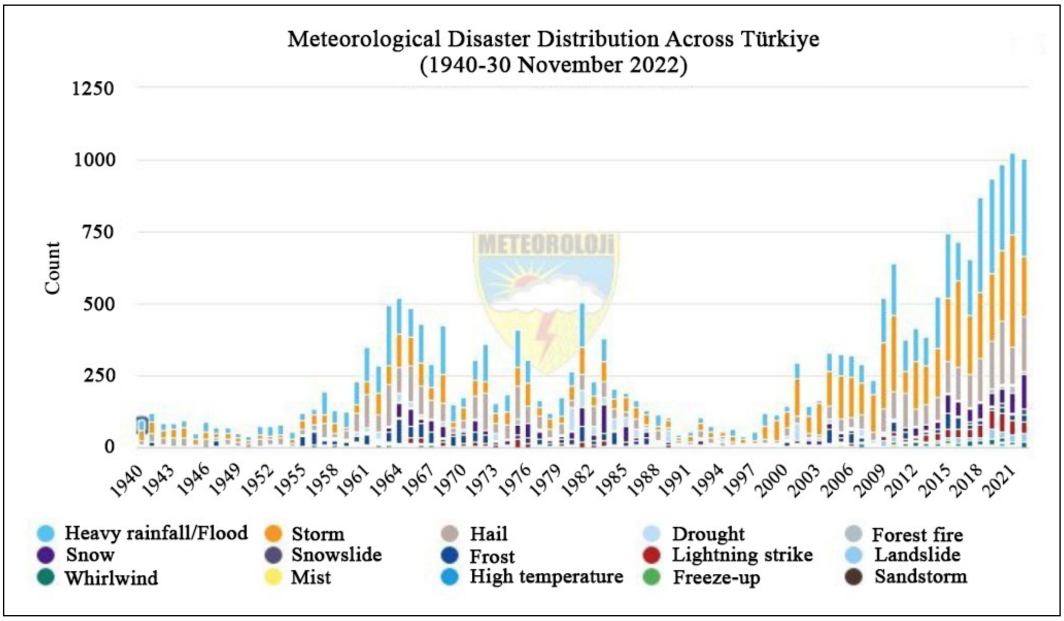

Figure 2. Meteorological disasters between 1940-30 November 2022 number of extreme events for many years

(Adapted from Turkish State Meteorological Service[43])

In the Mediterranean Basin, anthropogenic climate change has been observed on many variables in recent years. In the future, the region is expected to be one of the regions most affected by climate change, especially in terms of precipitation and hydrological cycle[44].

Among the provinces where meteorological disasters have been most prevalent in recent years, İzmir ranks third[37]. Located under the influence of the Mediterranean climate, winters in İzmir are mild, and rainy, while summers are dry and hot. The annual average temperature is 17.9°C, and the highest rainfall occurs in December, January, and February. Due to its geographical location, and climatic characteristics, İzmir province is susceptible to various natural disasters. Among these disasters are frequent occurrences of storms, and whirlwinds with speeds exceeding 100 km/h during the winter, and spring periods, floods, and water deluge resulting from heavy rainfall, widespread lightning strikes resulting from rainfall frequently occurring as thundery showers, short-term episodic droughts, and forest fires. Additionally, İzmir has experienced the largest forest fire in the city's history[45].

The rapid urbanization of İzmir brings about various problems, particularly those associated with the UHI effect. Due to rapid urbanization, decreasing green areas, and increasing use of impermeable materials such as asphalt and concrete, issues such as temperature rise in city centers, discomfort, increased energy consumption, decreased water resources, air pollution, and loss of biodiversity arise. Additionally, with the increasing population, there have been significant changes in LULC. Due to LULC changes such as deforestation and industrialization, the accumulation of greenhouse gases in the atmosphere is rapidly increasing and contributing to the formation of UHI[46]. Therefore, it is considered that meteorological disasters caused by UHI effects will continue to pose a risk for İzmir in the coming years. Therefore, it is important to implement urban planning, environmental policies, and land use management measures to cope with climate change and the UHI effect.

1.2. Aim and Scope of the Study

This study aims to temporally and spatially reveal the changes between LULC and LST created using multispectral imagery and to determine the relationships between UHI, SUHI, and spectral and built-up indices at the micro-scale. In line with this aim, the objectives are defined as follows: (1) detecting the changes LST values over time in the study area; (2) determining the effects of LULC on LST values; (3) elucidating the quantitative relationship between SUHI effect, and urban parameters; (4) providing recommendations for reducing the UHI effect from the perspective of urban planning.

The geographical scope of this study encompasses 11 districts in the İzmir Metropolitan Region. The temporal scale of the study covers the months of July, and August, characterized by intense UHI effects, and higher air temperatures in the Urban Canopy Layer (UCL). Satellite imagery, and CLC data for 1990, 2000, 2006, 2012, and 2018 are used in the study. The dependent variable of the study is the LST that characterized SUHI. Among the spectral parameters as urban parameters identified through the literature review to affect the formation of SUHI, NDVI, NDWI, NDBI, UI, and Albedo are the independent variables of the study. In terms of methodological aspects, this study employs correlation analysis, and MLR analysis to determine the relationships between LST, and urban parameters; it utilizes specific methodologies such as zonal statistics to understand, and evaluate the relationship between LST, and land use. Built-up indices (population density, building area density, mean floor height, and surrounding green areas larger than 2 ha), LST, LULC, and spectral indices were evaluated by dividing them into different regions. In conclusion, this study aims to provide information to shed light on policies, and strategies to reduce or mitigate the heat island effect in urban areas.

1.3. Research Questions

This study investigates the UHI effect in the central districts of İzmir province. Based on the problem and the aim of the study, several research questions are determined. In this regard, this study intends to find answers to the following research questions:

- How do land use/land cover classes affect LST values?
- How are the spectral indices as urban parameters related to LST/SUHI?
- What findings emerge from comparing LST values with built-up indices as urban parameters?

1.4. Structure of the Thesis

This thesis consists of six chapters.

The first two chapters include the literature review, and information about the study, while the subsequent four chapters cover the study area, the data used, the methodology used in the study, the results of the study, and the conclusions.

The first chapter includes general information about the thesis, explanations about why this topic is important, the problem, the research questions, and the aim, and scope of the study.

The second chapter of the discussed thesis study describes the methods employed to assess the Urban Heat Island (UHI) effects stemming from the Urban Climate. It also includes SUHI and LST concepts.

The third chapter, general information about the study area is provided. In addition, the data, and data sources used in the study are detailed in this part.

The fourth chapter, the methodology of the study is explained in detail under four headings: data preparation, assessment of the LST's relationship with LULC change and spectral indices, comparison of LST with different built environment textures, and comparison of Air Temperature and LST values.

The fifth chapter, explains the results of the methods examined and shows the maps of the study area. The effects of the SUHI in the study area are discussed in this part.

The last chapter provides an overview of the results obtained from the study. Additionally, suggestions that will contribute to future studies are explained in this part.

CHAPTER 2

LITERATURE REVIEW

In this part of the thesis, general information about Urban Climate, the UHI effect, SUHI as one of the actors of UHI variability, and LST as a parameter of SUHI is emphasized. Subsequently, relevant studies on the examination of the relationship between LST values and different urban parameters (spectral indices and built-up indices) are discussed, and the expected findings regarding these indices are presented based on the conducted research.

2.1. Urban Climate

Climate is the long-term pattern of weather conditions in a given region, which is constantly changing and is the most fundamental factor shaping life. Climate, which is determined by the climate system of a region, also varies in different parts of the world[47,48]. Climate is an interactive system consisting of five basic components: atmosphere, hydrosphere, land surface, biosphere, and cryosphere (Figure 3). Many physical, chemical and biological interactions occur between these interrelated components of the climate system[49]. Changes in long-term records of elements such as solar radiation, temperature, humidity, precipitation, atmospheric pressure and wind, and natural or anthropogenic changes in the components of the climate system result in climate change[49,50]. Therefore, changes in even one of the climate elements have a direct impact on human health and quality of life, causing changes in thermal comfort level and ecological balance[51].

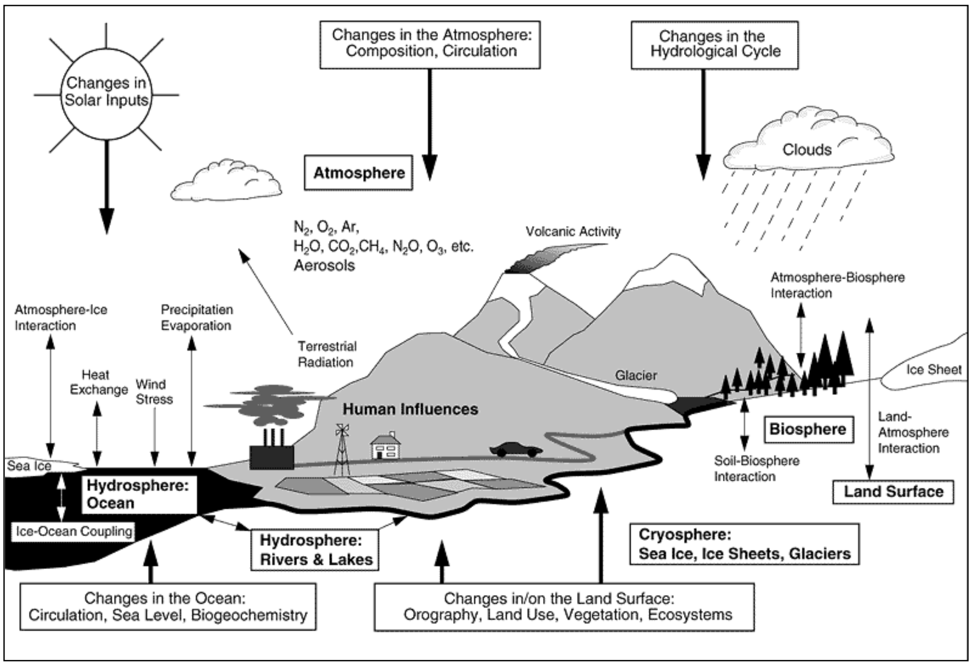

Figure 3. Components of the global climate system and interactions

(Source: IPCC[49])

The world climate has been changing continuously for centuries. Since the industrial revolution (second half of the 18th century), there has been an accelerating process of climate change due to human activities. While most of this process, which is closely related to global warming and the increase in greenhouse gases in the atmosphere, which directly cause climate change and environmental impacts, is caused by natural causes; the release of greenhouse gases (carbon dioxide, nitrogen oxides, methane, etc.) and solid/liquid substances in the atmosphere as a result of human activities also contributes significantly[52,53].

It was first stated in 1957 by Roger Randall Dougan Revelle that global warming could cause a large-scale climate change[54]. It is predicted that the amount of CO_2, one of the greenhouse gases in the atmosphere, will increase from past to present. With this situation causing global warming, it is stated that there will be difficulties in controlling climate changes locally and regionally[55]. As a result of global climate change; temperature increase in the atmosphere, temperature increase on the water surface, sea level rise, change in precipitation cycle, increase in annual precipitation amount, increase in evapotranspiration and more frequent and intense unusual events are among the observed effects[56].

In the literature, the serious effects of land use changes on climate have been expressed by many studies. Urbanization, one of the land cover changes, negatively affects climate, biodiversity and ecological systems at regional scale. In particular, urbanization reduces biodiversity, destroys natural habitats, reduces green areas and disrupts ecosystem balance, causing significant changes in surface temperatures and air temperaturesolmaktadır[53,57]. With this change, it has been observed that there are significant changes in local, regional and even global climate (Figure 4). Physical processes that affect climate and result from land use change include albedo, surface roughness, topography and the cycling of water vapor and greenhouse gases between the atmosphere and the earth[58].

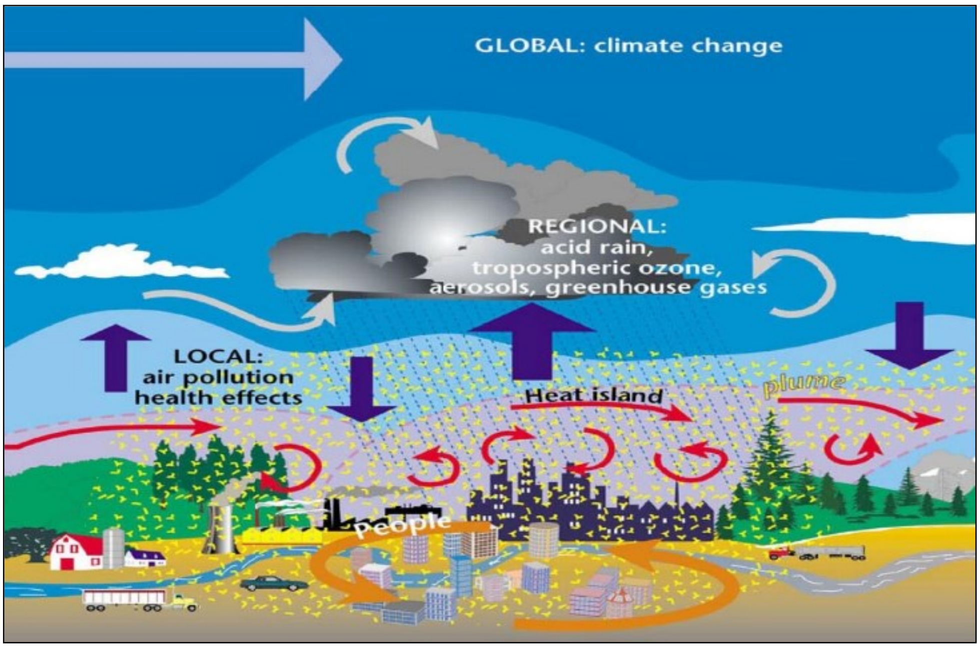

Figure 4. Effects of urbanization on climate

(Source: Carmichael[58])

Cities are places where great transformations occur and can easily adapt to changing conditions[58]. The urban ecosystem, which forms a complex network and includes interactions between various elements, refers to the balance of biotic (human, plant, animal) and abiotic (air quality, temperature, light, atmosphere) factors generally found in urban environments[59].

In terms of urban planning, urban ecosystem is defined as the ecological infrastructure that includes both the infrastructure in the built environment, and the plants, and water surfaces that provide ecosystem services at different spatial scales such as buildings, streets, and neighborhoods[60]. In summary, the urban ecosystem is where green areas are destroyed, impervious surfaces, and structural areas are dense, natural drainage, and water flow are changed; Urban ecosystem can be described as spaces where transformations occur in water, energy, vegetation, topography, and materials[58]. As a result of these changes in urban areas, climatic conditions such as air temperature, humidity, wind, and precipitation that differ compared to the rural environment are expressed as urban climate, which varies at regional, and local scale[61]. Urban climate emerges as a component of urban ecology, and must be examined in terms of planning. For this reason, the features of the physical space shaped by cities should be reviewed along with global or local conditions.

The local climate that differs as a result of the interactions between built-up areas, and the regional climate is called "Urban Climate"[62]. Urban climate science began with the work of Luke Howard in the 1800s[63]. This study, which is the first systematic urban climate study, measured the temperature differences in the city of London and the surrounding rural areas in 1815. All effects that caused the formation of an UHI were identified. It has been suggested by Howard that artificial temperatures arise in cities due to the structure of the city, excess population, and fuel consumption[64]. The climate of cities emerges as a modified version of the surrounding macroclimatic conditions, and is affected by thermal conditions, and air pollutants. Stating that the urban climate is not completely unique, Landsberg (1981)[11] states that the climate undergoes a modification by being affected by the large-scale climatic conditions in the environment. Due to changes, climatic conditions in cities differ from rural areas (Table 1). In cities; It is observed that when wind speed is lower, pollutants are increased in density, wind direction changes, temperature is higher, radiation is blocked, precipitation is higher, and clouds are more abundant[65]. In the urban environments, higher temperatures are observed at night, and in some cases during the day compared to the rural areas. UHI, which emerges due to this temperature difference, is a microclimate phenomenon that occurs as a result of the deterioration of the environmental energy balance in urban areas[66].

Table 1. Comparison of Climate Variables Between Urban and Rural Areas (Source: WHO[65])

Meteorological Parameter		Urban Areas Compared with Rural Areas
Radiation	Solar Radiation	Less
	Ultraviolet Radiation (Winter)	Less
	Ultraviolet Radiation (Summer)	Less
	Sunshine Duration	Less
Air temperature	Annual Mean	Higher
	Radiation Days	Higher
	Minimum Temperature	Higher
	Maximum Temperature	Higher
Humidity	Relative	Less
	Absolute	No Change
Fog		Less
Cloudiness		More
Precipitation	Annual Mean	More
	Snow	Less
Wind	Mean Wind-Speed	Less
	Calms	More
	Gusts	More
Contaminants	Particles	More
	Gases	More

According to Roth (2013)[67], urban climates are characterized by a combination of processes occurring at various scales, depending on the biophysical nature of cities and the layered structure of the urban atmosphere. According to Stewart and Oke (2009)[68], the scale also provides the conceptual framework for modeling each type, identifying the factors and processes that influence and generate each heat island[69]. Cities are classified as horizontal and vertical according to different atmospheric and spatial characteristics[68].

Human-made factors determine the horizontal boundaries of the city, and cities that change over time expand. Due to this change, climatic changes also increase over time. UHIs are analyzed in three scales: meso, local, and micro[70]. Mesoscale refers to the climatic scale that includes the entire city[71]. Local-scale refers to the climatic scale formed by the aggregation of microscale units. Typical local scales range from one to several kilometers horizontally[72]. The microscale is defined by individual buildings, trees, and intervening areas forming an urban canopy. This scale includes the roughness substrate on the vertical. Typical microscales range from one meter to several hundred meters horizontally[59].

Depending on atmospheric properties; The city can be examined in three main vertical layers: Planetary Boundary Layer (PBL), Urban Boundary Layer (UBL), and Urban Canopy Layer (UCL). Heat islands can be characterized according to different layers of the urban atmosphere and various surfaces and can be divided into three categories: Canopy Layer UHI (CLUHI), Boundary Layer UHI (BLUHI) and Surface UHI (SUHI) (Figure 5)[73]. PBL is the most general, and largest layer. This layer is where climate events occur, and atmospheric changes end. UBL is the layer below the urban impact limit, which is the boundary separating the UCL, and the free atmosphere. The boundary called the "UCL" on the vertical, covers the gaps between the roughening elements such as buildings, and trees. The UCL, which is the layer with the highest human impact, is also the layer with the highest concentration of pollutants in the air[71]. CLUHI and BLUHI are Atmospheric Urban Heat Island (AUHI) as they indicate the heating of the urban atmosphere, while SUHI refers to the relative temperature of urban surfaces relative to the surrounding rural areas[73].

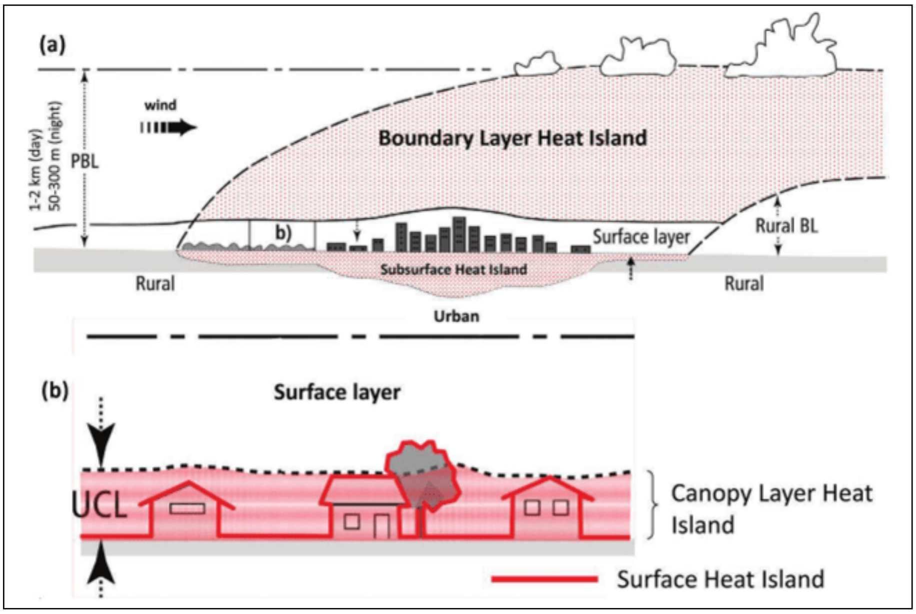

Figure 5. Climatic scales and vertical layers found in urban areas

(Source: The Handbook of Natural Resources[73])

It is necessary to know the characteristics of urban areas that affect the atmosphere to this extent. These characteristics are; urban structure (i.e. distance, height of buildings, width and area of streets), urban cover/surface cover (i.e. built/paved levels, vegetated surfaces, soil surfaces, water surfaces and bare surfaces), urban fabric/texture of building materials and urban metabolism (i.e. heat, water and pollution from human activities)[65].

2.2. Urban Heat Island (UHI)

With the development of cities, buildings, roads, and other infrastructure, replaces open land, and vegetation, causing the destruction of these areas. Consequently, permeable humid surfaces transform into impervious, and dry surfaces[25]. The most prominent atmospheric modification resulting from urbanization is known as the "UHI"[67]. The increasing temperatures in cities are the most significant change in climatic factors and have become a concerning issue for humans[67].

UHI phenomenon implies that the urban areas have higher temperatures than their rural surroundings[17]. The most prominent climatic indicator of urbanization, the UHI, was first defined for the city of London in 1820 by Luke Howard[26]. The profile of heat islands that can occur during the day or night throughout the year is closely related to urban morphology[12,20]. The temperature difference between urban, and rural areas often occurs on calm nights, caused by the faster cooling of rural areas compared to cities, and the accumulation of heat by roads, buildings, and other structural elements in cities. Temperature values can vary according to land use types, and seasons, especially with urban centers having much higher temperature values compared to the surrounding rural areas[20]. The change in temperature values according to land use type is shown in Figure 6.

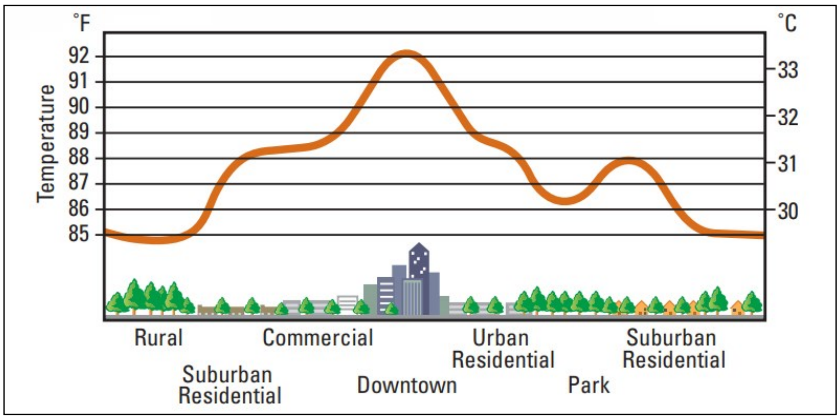

Figure 6. Urban heat island profile

(Source: EPA[20])

UHI and SUHI are two important concepts that express thermal differences in cities. While human influence is not the main factor in the formation of the SUHI, human activities are the main factor in the formation of the UHI. Analyzes performed using land temperatures indicate SUHI, while analyzes performed using air temperatures indicate UHI[74].

UHI is caused by factors such as construction in urban areas and the capacity of surfaces to absorb and emit sunlight. The temperature in city centers is generally higher than rural areas. UHI is directly related to urbanization and urban development[75].

UHI are analyzed under two main headings: AUHI and SUHI[25]. Table 2 shows the main characteristics of UHI types.

Table 2. Characteristics of UHI Types

(Source: EPA[25])

Feature	**Surface UHI**	**Atmospheric UHI**
Temporal Development	• Present at all times of the day and night • Most intense during the day and in the summer	• May be small or non-existent during the day • Most intense at night or predawn and in the winter
Peak Intensity (Most intense UHI conditions)	• More spatial and temporal variation: - Day: 18 to 27°F (10 to 15°C) - Night: 9 to 18°F (5 to 10°C)	• Less variation: - Day: -1.8 to 5.4°F (-1 to 3°C) - Night: 12.6 to 21.6°F (7 to 12°C)
Typical Identification Method	• Indirect measurement: - Remote sensing	• Direct measurement: - Fixed weather stations - Mobile traverses
Typical Depiction	• Thermal image	• Isotherm map • Temperature graph

Characteristic of urban climate, UHI is usually marked by maximum sunlight exposure during daylight hours and low wind speeds during the night[76]. Figure 7 shows that the magnitude of temperature differences in UHI intensity varies temporally, and spatially depending on local weather conditions, location, and urban characteristics[77]. Surface and atmospheric temperatures vary in areas where land use is different. While daytime surface temperatures vary more than air temperatures, nighttime temperature values appear to be quite similar to each other[78].

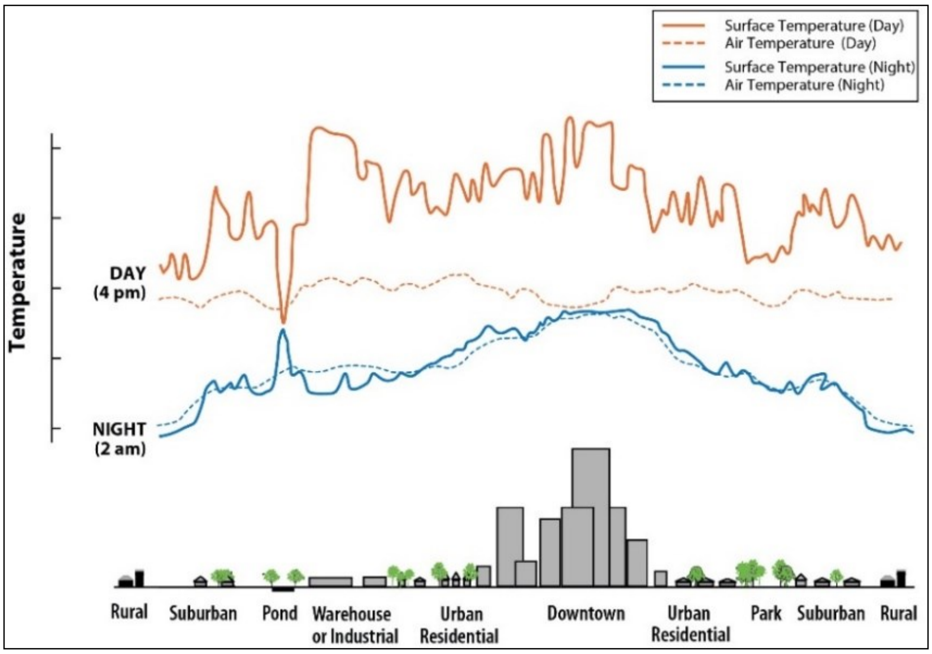

Figure 7. Variation of surface and atmospheric temperature according to land use area (Source: EPA[25])

The layers of the Atmospheric UHI and Surface UHI are shown in Figure 8. Atmospheric UHI: It is divided into two different subcategories: Boundary Layer UHI (BLUHI) and Canopy Layer UHI (CLUHI). The reason for this difference is that the atmosphere has different layers and different surface types[68].

- **Surface UHI** typically reaches its highest values during the daytime and is defined as the spreading temperatures on the three-dimensional urban surface of the city. Roof surfaces, walls, and ground surfaces constitute Surface UHI, and it is important to distinguish the energy exchanges between them[79].

Atmospheric UHI is further categorized into:

- **Boundary Layer UHI (BLUHI)** is defined as a combination of many local-scale effects occurring throughout the boundary layer. It can extend up to several hundred meters above the surface and is most pronounced during nighttime[12].
- **Canopy Layer UHI (CLUHI)** is the air temperature within the UCL that lies below roof level on the streets and is limited by building height. Like BLUHI, it is usually most pronounced during nighttime[68].

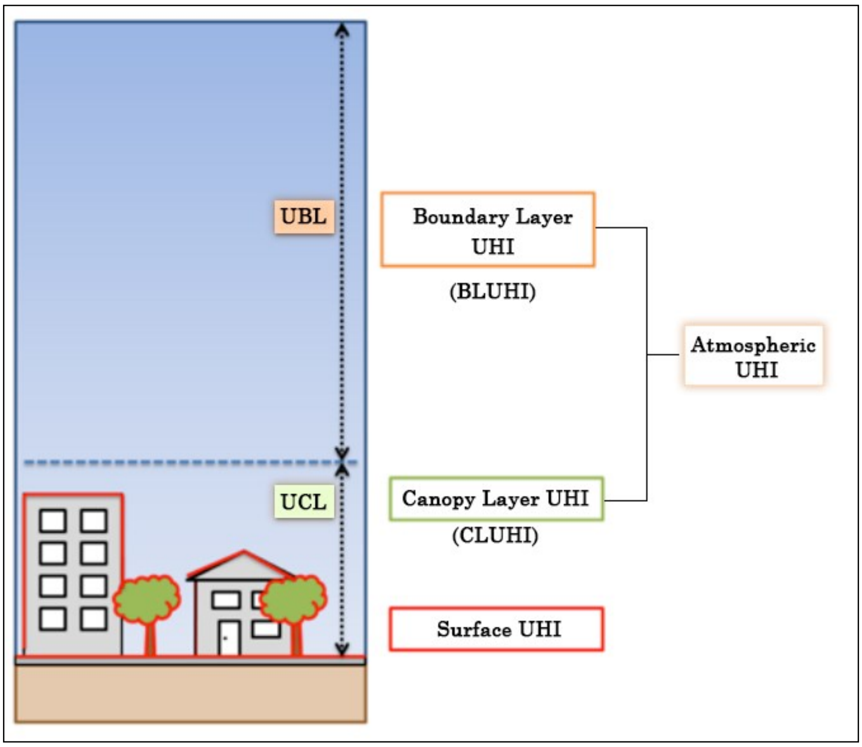

Figure 8. Types of urban heat islands

(Source: Harris and Coutts[80])

The general characteristics of UHI were defined by Oke (1982)[17]. UHI intensity; It decreases with increasing wind speed, decreases with increasing cloudiness, is highest in anticyclonic conditions, is higher in summer or the hot half of the year, and tends to increase with the increase in the size and/or population of the city, is highest at night. The UHI effect may disappear during daylight hours, may be cooler in surrounding areas than in rural areas, and increases costs for heating and cooling[17].

As shown in Table 3, Oke (1982)[17] also states that the reasons for the occurrence of UHI differ according to the UCL.

Table 3. Causes of Urban Heat Island Formation

(Source: Oke[17])

Altered energy balance terms leading to a positive thermal anomaly	Features of urbanization underlying energy balance changes
Canopy Layer	
1. Increased absorption of short-wave radiation	Canyon geometry- increased surface area and multiple reflections
2. Increased long-wave radiation from the sky	Air pollution- greater absorption and re-emission
3. Decreased long-wave radiation loss	Canyon geometry- reduction of sky view factor
4. Anthropogenic heat source	Building and traffic heat losses
5. Increased sensible heat storage	Construction materials-increased thermal admittance
6. Decreased evapotranspiration	Construction materials-increased 'water proofing'
7. Decreased total turbulent heat transport	Canyon geometry - reduction of wind speed

There are many factors contributing to the temperature difference between urban and rural areas, playing a significant role in urban planning, environmental health, and climate change, which determine the extent of the temperature difference. Figure 9 illustrates the factors affecting UHI. Anthropogenic effects and the urban texture of the city increase the UHI.

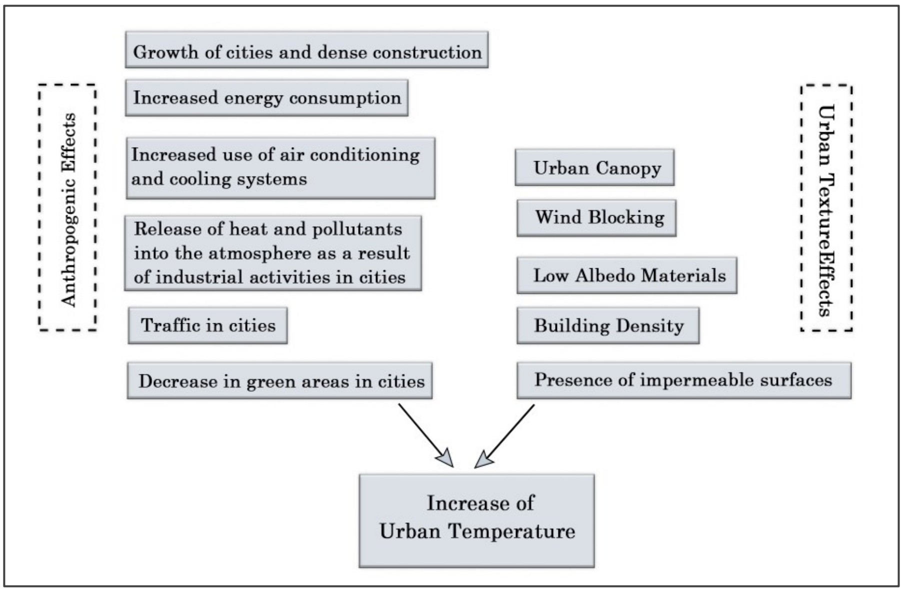

Figure 9. Process of UHIs formation

(Adapted from Nuruzman[81]; Pandya[82])

In this study, Nuruzzaman[81] and Pandya[82] explained the factors affecting UHI mentioned in Figure 9. These factors:

- Surfaces absorb radiation and trap heat due to the use of materials with low albedo. Dark surfaces have higher absorption of solar radiation
- Heat is trapped in the atmosphere, leading to further warming, due to pollutants causing heat trapping in the atmosphere. building materials store solar heat and release it at night.
- Reduced wind speed and decreased atmospheric convection result from tall buildings and uncontrolled construction in wind corridors.
- Narrow passages created by tall buildings increase wind speed and intensify air pollution by creating a canyon effect.
- Urban canopies obstruct direct sunlight from reaching the ground, trapping heat in the atmosphere.
- Decreased green spaces due to changes in land cover. Increased impervious surfaces like roads and parking areas trap heat within the city. paved surfaces heat up faster and prevent the intake of rainwater in the soil.
- Vehicles, air conditioning units, buildings and industrial facilities all radiate heat into the urban environment. These anthropogenic or anthropogenic waste heat sources contribute to the heat island effect.
- Human-generated CO_2 emissions contribute to higher temperatures in urban areas.

The combination of these factors in cities increases temperatures, leading to the formation of the UHI effect[81]. Figure 10 shows how UHI affects human life.

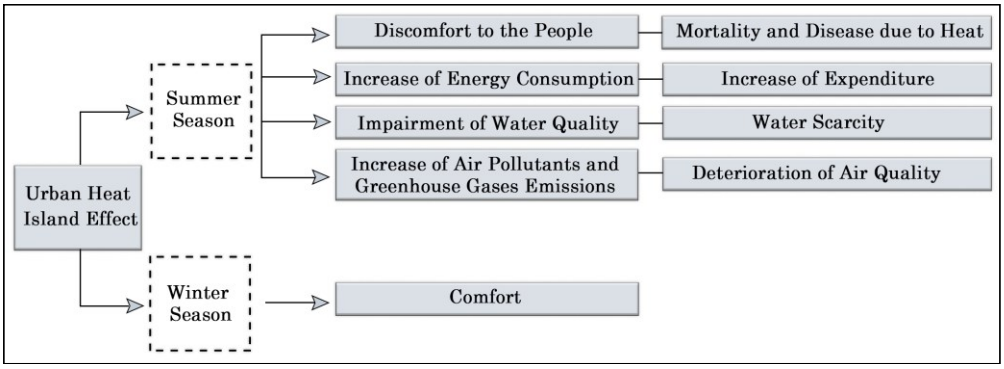

Figure 10. Effects of UHI formation
(Adapted from Nuruzzaman[81]; EPA[83])

The effects of UHIs can create serious problems during the summer months, especially in dry and tropical regions. Increasing temperatures and air pollution can cause respiratory difficulties, heat cramps, general discomfort, heat exhaustion, and even deaths among people living in city centers[81,83]. Vulnerable populations, such as the elderly, young children, low-income individuals, and those who spend working hours outdoors, are at greater risk[83].

Particularly during the summer months, high temperatures increase general electricity and energy demand. The increased demand is due to the desire for building cooling and providing comfort to the public. Increased air conditioning usage results in waste heat generation and overloading of systems, leading to excessive spending by individuals and governments[83,84].

UHI contribute to a decrease in water quality and rapid changes in water temperature through thermal pollution, causing serious problems for aquatic life. Increased pollution due to decreased sewage flow affects rivers, lakes, and ponds, leading to water scarcity[83].

Increased energy and electricity demand result in burning more fossil fuels, leading to high emissions of greenhouse gases and air pollutants. Pollutants also increase the formation rates of ground-level ozone, fine particulate matter, and acid rain, leading to air quality issues and global climate change[83,85].

During the winter season, the temperature increase due to the UHI effect provides comfort to people[86].

2.3. Land Surface Temperature (LST)

SUHI is a type of UHI and is often used when UHI cannot be measured or there is insufficient data. Often referred to as an alternative, SUHI is considered an important tool for assessing UHI impacts by reflecting surface temperature differences in urban areas[87].

The SUHI, present during both day and night, exhibits its effects more prominently during bright daylight hours[75]. While the daytime surface temperature difference between the city center and rural areas ranges from 10°C to 15°C, the nighttime surface temperature difference ranges from 5°C to 10°C[88]. The size of SUHI varies by season due to changes in sunlight intensity, land cover, and weather conditions. The most intense UHI occurs during the summer months when the sky is clear, and winds are calm. Heavy cloud cover in cities reduces daytime heating, while strong winds reduce the temperature difference between urban and rural areas[25]. SUHI are detected by LST obtained by thermal infrared sensors, typically used on airborne or satellite platforms[79].

LST, calculated from satellite-based thermal infrared (TIR) data, dates back to the 1970s[89]. As the direct driving force in the exchange of long-wave radiation and turbulent heat fluxes at the surface–atmosphere interface, LST is one of the most important parameters in the physical processes of surface energy and water balance at local through global scales[90].

At the surface-atmosphere interface, LST is the temperature radiated by the earth's surface. The main source of this heat is the Sun. Light energy reaching the earth from the sun turns into heat energy and heats objects. The materials used in urbanization and construction absorb the energy reaching the earth without reflecting it back. Therefore, it causes LST to increase. LST is shown as an important factor that affects various types of events on Earth. LST data is a frequently preferred data type in vegetation change analysis, LULC change analyses, global warming studies, and meteorological studies[30].

Atmospheric UHI are detected by air temperatures obtained from a network of meteorological stations by direct measurement techniques, while Surface UHI are detected by LST obtained by thermal infrared sensors usually used on airborne or satellite platforms[79].

There are many studies in the literature where LST is determined with remote sensing images. LST values produced with remotely sensed images are effectively used to reveal the effects of land cover changes on climate conditions with Geographic Information Systems (GIS)[91].

Remote sensing is the remote collection of information about objects without direct contact using sensors. Remote sensing involves the analysis and interpretation of measurements of the electromagnetic spectrum that is reflected or emitted and observed or recorded from an observation point that is not in contact with an observer or target[92]. Figure 11 shows the electromagnetic spectrum.

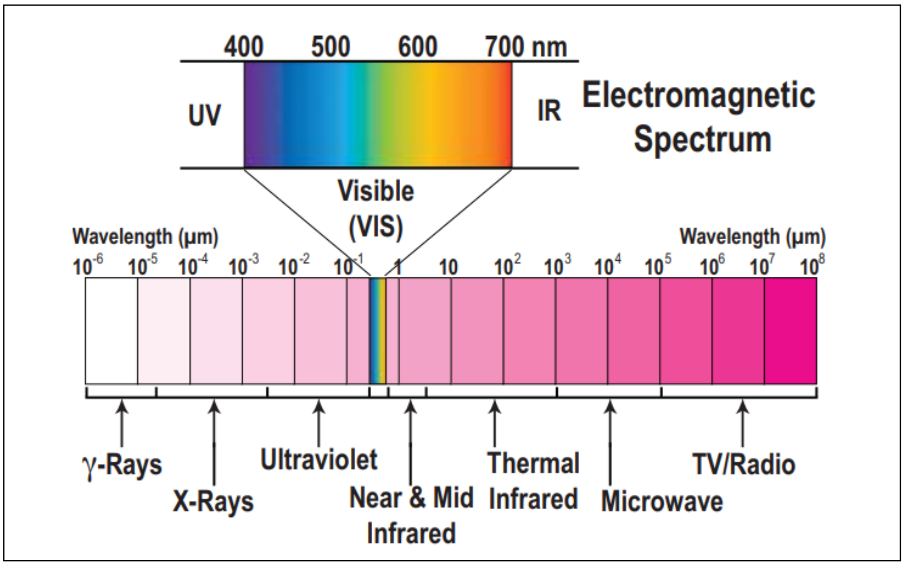

Figure 11. Electromagnetic spectrum

(Source: Camps-Valls et al.[93])

The electromagnetic spectrum is a continuous energy medium and is divided into specific regions. Almost all regions of the electromagnetic spectrum are used in remote sensing. However, visible (VIS), infrared (IR) and visible (VIS) and microwave (MW) regions constitute the main spectral regions[93]. The wavelength of the visible region used in remote sensing satellites to obtain information about the earth's surface varies between 400-700 nm. The wavelength of the infrared region varies between between 760 - 1000000 nanometers. The only region that the human eye can perceive is the visible region. The colors of this region range from red to violet, but the primary colors are red (600-700 nm.), green (500-600 nm.) and blue (400-500 nm.). LST maps are created using sensors capable of detecting the surface radiance temperature values in the thermal infrared wavelength range of the electromagnetic spectrum. It usually includes bands between 8000-14000 nanometers[94].

2.4 Studies Examining the Relationship Between LST with Urban Parameters

UHI and SUHI are closely related to various characteristics that define the urban environment. These characteristics can be related to factors such as the density of development in urban areas, the presence of green areas, the presence of water surfaces. Furthermore, UHI and SUHI can be represented by spectral indices and built-up indices.

There are various studies that examine the relationship between LST with built-up indices, and spectral indices to determine the UHI effect.

Spectral indices such as Albedo, Normalized Difference Vegetation Index (NDVI), Normalized Difference Built-up Index (NDBI), Enhanced Vegetation Index 2 (EVI2), and Soil Adjusted Vegetation Index (SAVI) are commonly used in UHI studies. Additionally, other indices like Urban Index (UI), Index-based Built-up Index (IBI), Enhanced Built-up and Bareness Index (EBBI), New Built-up Index (NBI), Normalized Difference Barren Index (NDBaI), Normalized Multi-Band Drought Index (NMDI), Bare Soil Index (BSI), Dry Built-up Index (DBI), and Normalized Difference Impervious Surface Index (NDISI) are widely employed.

Built-up indices such as Population Density (PD), Sky View Factor (SVF), Mean Building Height, Building Footprint Density, Land Use/Land Cover (LULC), Road Network Density (RND), and Building Footprint Density (BVD) are commonly used in UHI studies.

Studies using remote sensing imagery to determine LST and examining the impact of urban parameters and LULC on SUHI are provided in Table 4, based on the literature review.

A comprehensive assessment of these parameters is important for understanding and managing UHI impacts.

Some of the selected studies in the last ten years using remote sensing imagery to determine LST and examining the influence of urban parameters and LST in Table 4 based on the literature review.

Table 4. Summary of Studies with LST in National and International Literature

Parameters	Author(s)/Year	Study Area	Data	Aim of the Study	Results
Land Surface Temperature **(LST)**, and Land Use/Land Cover **(LULC)**	Stathopoulou and Cartalis /2007[95]	Major cities in Greece (Athens, Thessaloniki, Patra, Volos and Heraklion)	Landsat 7 ETM+, and CORINE Land Cover	Determining the "hottest" surfaces in the urban environment of each city and relating LST values to land uses	Complex urban areas have been identified as 'hot spots' in the city. It has been concluded that the LST value at these points is high due to the increasing ratio of asphalt and concrete-covered surfaces and the solar heating of open areas associated with mines and vacant lands.
	Jiang and Tian / 2010[96]	Beijing, China	Landsat 5 TM, and Landsat 7 ETM+	Examining the impact of land use changes on LST	It was stated that land use change is an important factor for the increase in LST value and there is a strong positive relationship between LULC and LST.
	Şekertekin and Marangoz /2019[97]	Zonguldak metropolitan region, Türkiye	Landsat 8 OLI/TIRS	Investigating the relationship between LULC and LST	While high LST values were obtained in residential areas and open areas, it was observed that there were lower LST values in forested and vegetated areas.
	Ünal Çilek /2022[98]	Adana city center, Türkiye	Landsat 8 OLI/TIRS	The examination of the impact of LULC on the Surface Urban Heat Island (SUHI) using the obtained LST for winter and summer seasons	It has been determined that LST values are highest in the discontinuous medium-density urban fabric, industrial and commercial units, and isolated structures in winter months, while they are higher in commercial units, highways, and associated land, sports and leisure facilities, and continuous urban fabric in summer months.

(cont. on next page)

Table 4. (cont.)

Parameters	Author(s)/Year	Study Area	Data	Aim of the Study	Results
Land Surface Temperature **(LST)**, Land Use/Land Cover **(LULC)**, Normalized Difference Vegetation Index **(NDVI)**, and Normalized Difference Built-up Index **(NDBI)**	Tran et al. / 2017[94]	Inner city area of Hanoi, Vietnam	Landsat 5 TM, Landsat 7 ETM+, and Landsat 8 OLI/TIRS	Determining the relationship between LULC changes and LST values in the context of urbanization and analyzing the correlation between LST, NDVI, and NDBI for all LULC types in the study area	The relationship between LST and NDVI, NDBI within each LULC type was examined. It was determined that there was a negative correlation between LST and NDVI, and a positive correlation between LST and NDBI. As a result, it was determined that there was a non-linear relationship between LULC and LST.
Land Surface Temperature **(LST)**, Normalized Difference Vegetation Index **(NDVI)**, and Normalized Difference Built-up Index **(NDBI)**	Malik et al. /2019[99]	Kandaihimmat Watershed, India	Landsat 8 OLI/TIRS	Development of the relationships between LST values with NDBI and NDVI for all seasons (January, May, and October)	It is seen that LST values are higher on built-up and bare surfaces and lower in areas with healthy vegetation, that there is a strong positive relationship between LST and NDBI, that there is a strong negative relationship between LST and NDVI, that NDBI is not only used to analyze LST but also for any It has been determined that it can also be used to determine the urban heat island effect in an area.
Land Surface Temperature **(LST)**, Land Use/Land Cover **(LULC)**, and Normalized Difference Built-up Index **(NDBI)**	Külahlıoğlu et al. / 2022[100]	Adana, Türkiye	Landsat 7 ETM+, and Landsat 8 OLI/TIRS	Investigation of the relationship between NDBI, LULC, impervious surfaces, and LST in order to reveal the effect of the Urban Heat Island (UHI) in Adana province	While there is a positive correlation between impervious surfaces and LST, there is a negative correlation between urban green areas and forest areas (land use) and LST.

(cont. on next page)

Table 4. (cont.)

Parameters	Author(s)/Year	Study Area	Data	Aim of the Study	Results
Land Surface Temperature **(LST)**, Land Use/Land Cover **(LULC)**, Normalized Difference Vegetation Index **(NDVI)**, Enhanced Vegetation Index 2 **(EVI2),** Soil Adjusted Vegetation Index **(SAVI),** Normalized Difference Built-up Index **(NDBI),** Urban Index **(UI)**, Index-based Builtup Index **(IBI)**, New Built-up Index **(NBI),** Enhanced Built-up and Bareness Index **(EBBI),** and Normalized Difference Impervious Index **(NDII)**	Daramola et al. / 2018[101]	Ibadan, Nigeria	Landsat 5 TM, Landsat 7 ETM+, and Landsat 8 OLI/TIRS	Evaluation of changes in LULC of Ibadan city for the years 1984, 2000, and 2016 and examining the impact of changes in LULC on LST and related indices.	It has been observed that the decrease in vegetated surfaces and the increase in impervious surfaces revealed by the built-up index increase the LST values. It was found that the increase in the built-up area of Ibadan showed a net change of 8% and the Urban Index (UI) was the indicator that best predicted the LST. Negative correlation between LST and vegetative indices (NDVI, SAVI, and EVI2); A positive correlation was observed between impervious surface indices (NDII, NDBI, EBBI, IBI, NBI, and UI) and LST.
Land Surface Temperature **(LST)**, Normalized Difference Built-up Index **(NDBI),** Normalized Difference Barren Index **(NDBaI)**, and Urban Index **(UI)**	Macarof et al. / 2017[102]	Iași, Romaniaisthe	Landsat 8 OLI/TIRS	Investigation of the relationship between LST with urban indices (NDBaI, NDBI, and UI) in the Iasi municipality area	There is a strong linear relationship between LST and urban indices (UI and NDBI), while the correlation between LST and NDBaI is lower; The R2 value was found to fluctuate significantly from above 0.4 for NDBI and UI to approximately zero for NDBaI. Therefore, it has been determined that the correct indicators of SUHI effects are NDBI and UI indexes in this study.

(cont. on next page)

Table 4. (cont.)

Parameters	Author(s)/Year	Study Area	Data	Aim of the Study	Results
Land Surface Temperature **(LST)**, and Normalized Difference Vegetation Index **(NDVI)**	Türkyilmaz et al. / 2020[103]	Çanakkale, Türkiye	Landsat 5 TM, Landsat 8 OLI/TIRS, and General Directorate of Meteorology	It was examined how well LST values represent the air temperature. Calculation of LST values with Artis & Carnahan, Single Channel, Single Window, Radiative Radiation Equations, examination of land cover/land use and the relationship between NDVI and LST.	It has been determined that there is a negative correlation between NDVI and LST values, temperature deviations occur between air temperature values at meteorological stations and LST values, and the Artis & Carnahan equation is the most successful method for Çanakkale province. The lowest LST values were observed in forested areas, park areas, and green areas, and the highest LST values were observed in urban areas and empty areas where reinforced concrete and asphalt structures are dense.
	Tonyaloğlu / 2019[104]	Aydın province, Efeler and İncirliova districts , Türkiye	Landsat 5 TM, and Landsat 8 OLI/TIRS	Examining the relationships between LST, NDVI, and building density, evaluating the effects of urbanization on the urban thermal environment.	It was determined that there was a negative correlation between LST and NDVI values, and a positive correlation between building density and LST.

(cont. on next page)

Table 4. (cont.)

Parameters	Author(s)/Year	Study Area	Data	Aim of the Study	Results
Land Surface Temperature **(LST)**, Normalized Difference Built-up Index **(NDBI)**, Urban Index **(UI),** Soil Adjusted Vegetation Index **(SAVI),** and Modified Normalized Difference Water Index **(MNDWI)**	Halder et al. / 2021[105]	Kolkata metropolitan and surrounding area, India	Landsat 8 OLI/TIRS	Examining the UHI using thermal remote sensing data and analyzing the relationship of the LST distribution with different spectral indicators.	NDVI and SAVI show a negative correlation with LST, while NDBI and UI show a positive correlation. It has been determined that in recent times, Kolkata has encountered high temperatures due to anthropogenic activities such as urbanization, industrialization, population pressure, and vegetation degradation, with the excessive use of public transportation playing a significant role in this.
Land Surface Temperature **(LST),** Normalized Difference Built-up Index **(NDBI),** Soil Adjusted Vegetation Index **(SAVI)**, and Normalized Difference Bareness Index **(NDBal)**	Akyürek / 2020[106]	Kocaeli, Türkiye	Landsat 8 OLI/TIRS	Examining the statistical relationship between LST values and SAVI and NDBI images, and determining what effect there is between wind speed and directions and LST.	LST values have an inverse relationship with SAVI and a linear relationship with NDBI, when wind maps are examined, they do not show a reducing effect on LST, regions with high industrialization and geothermal activity have high LST values, LST values are ranked from high to low; It has been determined that these areas are listed as industrial facilities, urban areas, agricultural and green areas and water zones.

(cont. on next page)

Table 4. (cont.)

Parameters	Author(s)/Year	Study Area	Data	Aim of the Study	Results
Land Surface Temperature **(LST)**, Normalized Difference Vegetation Index **(NDVI),** Normalized Difference Built-up Index **(NDBI)**, Normalized Multi-Band Drought Index **(NMDI)**, and Normalized Difference Water Index **(NDWI)**	Guha et al. / 2020[107]	Raipur, India	Landsat 8 OLI/TIRS	Determination of urban heat island (UHI) and non-urban heat island (non-UHI) regions of Raipur City through LST, examining the relationship of LST with NDVI, NDWI, NDBI and NMDI	It has been observed that the urban heat island develops mainly in the northern and southern surroundings of the city and the range of LST in the common UHI for four different seasons varies from 25.72°C to 35.69°C. It was concluded that LST showed a strong positive correlation with NDBI, a moderate to strong negative correlation with NMDI, and within UHI, NDVI and NDWI showed a stronger correlation with LST (NDVI-negative, NDWI-positive) compared to other indices.
Land Surface Temperature **(LST)**, Land Use/Land Cover **(LULC)**, Normalized Difference Vegetation Index **(NDVI)**, Normalized Difference Built-up Index **(NDBI)**, Normalized Difference Barren Index **(NDBaI),** and Normalized Difference Water Index **(NDWI)**	Nimish et al. / 2020[108]	Kolkata Metropolitan Area, India	Landsat 5 TM, Landsat 7 ETM+, and Landsat 8 OLI/TIRS	Establishing the relationship between surface temperature and land use/land cover, determining the change in surface temperature and examining the relationship between LST with NDVI, NDBI, NDBal, NDWI	It was observed that the residential area in the study area grew threefold in a period of twenty years, and a decrease in vegetation and other classes led to an average increase of 10.6 degrees in surface temperature. While a positive correlation was observed between LST with NDBI and NDBIal, a negative correlation was observed between LST with NDVI and NDWI. During the study period, changes in the landscape became evident in the center and towards the north; It was concluded that there was an increase in LST in these areas as an effect of this.

(cont. on next page)

Table 4. (cont.)

Parameters	Author(s)/Year	Study Area	Data	Aim of the Study	Results
Land Surface Temperature **(LST)**, Land Use/Land Cover **(LULC)**, and Normalized Difference Vegetation Index **(NDVI)**	Kaçmaz and Gürbüz /2022[109]	Aksaray, Türkiye	Landsat 8 OLI/TIRS, Landsat 5 TM, MODIS MOD11A1, and CORINE Land Cover	A temporal study of the influence of land use/land cover change on land surface temperature in Aksaray Province from 1990 to 2018	When analyzing the correlation between LST values and LULC data, it was discovered that wetlands and forest areas had lower temperature values, while artificial areas, bare areas, moors, heathland, natural grassland areas and agricultural areas had higher temperature values. It was concluded that NDVI values are generally concentrated around 0 because the largest area of the province is covered by dry agricultural areas and barren areas.
Land Surface Temperature **(LST)**, Land Use/Land Cover **(LULC)**, Normalized Difference Vegetation Index **(NDVI),** Normalized Difference Built-up Index **(NDBI)**, Urban Index **(UI)**, Normalized Difference Water Index **(NDWI),** Normalized Difference Impervious Index **(NDISI),** Bare Soil Index **(BSI),** and Dry Built-up Index **(DBI)**	Khan et al. / 2021[110]	Beijing, China	Landsat 8 OLI/TIRS	Investigating the effect of LULC indices (built-up, bare soil, and barren land, etc.) on LST and determining the effect of green areas in the study area on LST	While there was a positive relationship between built-up areas (NDBI, DBI, UI, NDISI), bare soil (BSI) indices with LST, it was found that there was a strong negative relationship between LST with NDVI and NDWI. It is concluded that the LULC index can be used to describe LULC-type LSTs and provide useful information to city managers and urban planners in the design of smart green cities.

(cont. on next page)

Table 4. (cont.)

Parameters	Author(s)/Year	Study Area	Data	Aim of the Study	Results
Land Surface Temperature **(LST),** Normalized Difference Vegetation Index **(NDVI)**, and Normalized Difference Impervious Surface **(NDISI)**	Łęczek and Łachowski / 2023[111]	The city of Wloclawek and 12 selected public areas	Landsat 5 TM, and Landsat 8 OLI/TIRS	Examination of the factors (represented by NDVI and NDISI, which are vegetation cover indices) that most affect the high temperature in city centers and its increase compared to its surroundings.	The conclusion is that in the examined public spaces, the impact of NDVI values on LST is higher than that of NDISI; however, it is acknowledged that well-conditioned vegetation is not the sole factor influencing temperature reduction.
Land Surface Temperature **(LST),** Sky View Factor **(SVF),** Population Density **(PD),** Albedo, Normalized Difference Vegetation Index **(NDVI),** Built-up Index, Mean Building Height, Building Footprint Density, Building Volume Density **(BVD),** and Road Network Density **(RND)**	Gerçek, and Güven /2023[112]	Kocaeli province, İzmit district, Türkiye	Landsat 8 OLI/TIRS, and ASTER	Understanding urban climate by investigating the interrelationships between UHI, SUHI and UPs at the micro scale using multivariate statistics and GIS tools.	Daytime LST has a strong negative correlation with NDVI and a strong positive correlation with NDBI and PD. Night LST has a strong negative correlation with NDVI and a strong positive correlation with RND and MBH. The findings indicate that UHI is weakly associated with night LST and daytime LST is not related.

(cont. on next page)

Table 4. (cont.)

Parameters	Author(s)/Year	Study Area	Data	Aim of the Study	Results
Land Surface Temperature **(LST),** and **Albedo**	Andrés-Anaya et al. / 2021[113]	Valladolid, Spain; Industrial zones located in 6 different locations within the province	Landsat 8 OLI/TIRS, Terra (MODIS, and ASTER)	Determination of the correlation between Albedo and LST and examination of Extreme UHI (E-UHI) in selected industrial areas in Valladolid	It has been found that there is a negative correlation between albedo and daytime LST and that building roofs with high albedo values reach lower temperatures. It was concluded that the use of materials with high albedo values in building envelopes would be an effective solution to reduce heat accumulation in cities and improve the temperature drop at night.
	Bonafoni et al. / 2017[114]	Perugia, Central Italy and Aprilia, Central Italy	Landsat 7 ETM+, Landsat 8 OLI/TIRS, and Sky Arrow 650 ERA	Examination of the relationship between albedo and LST in July of two urban areas (the cities of Perugia and Aprilia in Central Italy) using different spaceborne and airborne sensors	As a result of the analysis, they determined that there was an "inverse" relationship expected for the LST and albedo relationship (i.e., LST increased as albedo decreased). It was predicted that surfaces with an albedo value of approximately 0.10 could increase the average surface temperature by more than 60°C in July. It was concluded that this study, conducted at different times, can reveal the average albedo change for the same built-up areas and provide information about the materials that can be used for new settlements.

(cont. on next page)

Table 4. (cont.)

Parameters	Author(s)/Year	Study Area	Data	Aim of the Study	Results
Land Surface Temperature **(LST),** Normalized Difference Vegetation Index **(NDVI),** and **Albedo**	Favretto / 2018[115]	Trieste, North-East of Italy	Landsat 8 OLI/TIRS	Using remote sensing and GIS methods in the Province of Trieste to investigate urban heat island (UHI) impact factors	It has been determined that building density and lack of vegetation cause higher temperatures in the studied region and there is a strong correlation between these variables. It was observed that there was a positive correlation between Albedo and LST, and a negative correlation between LST and NDVI.
	Yücer / 2023[116]	Karabük province, Safranbolu districts, Türkiye	Landsat 8 OLI/TIRS	Revealing the Relationship between LST and NDVI, and albedo	It has been determined that there is a positive relationship between LST and albedo, a negative relationship between LST and NDVI, and a negative relationship between albedo and NDVI, and that the type of material on the surface, the amount of moisture on the surface, vegetation and density are the main factors affecting the relationship between LST, albedo and NDVI. It is concluded that the LULC index can be used to describe LULC-type LSTs and provide useful information to city managers and urban planners in the design of smart green cities.

(cont. on next page)

Table 4. (cont.)

Parameters	Author(s)/Year	Study Area	Data	Aim of the Study	Results
Land Surface Temperature **(LST)**, Land Use/Land Cover **(LULC)**, and **Albedo**	Trlica et al. / 2017[117]	Boston, Massachusetts, USA	Landsat 7 ETM+, and MODIS	Improving urban albedo with high resolution geographical data on the course followed according to previous studies, determining the relationships of albedo measurements with descriptive measures of urban land cover character (canopy cover, impervious fraction and population density) and mid-morning summertime LST values.	Average albedo: It has been determined that it decreases in more densely developed areas with lower tree cover, higher impervious fraction, and higher population density, while areas showing lower albedo show higher mean LST. It was concluded that when evaluating albedo, increasing summer temperature and urbanization should be associated together and used as a part of changing land cover characteristics.
	Odunuga and Badru / 2015[118]	Plateau, North-Central Nigeria (Barakinladi, Jos, and Kafachan environs)	Landsat 5 TM, and Landsat 7 ETM+	Evaluation of the relationship between environmental variables (land cover change, land surface temperature, surface albedo and topography) for the period between 1986 and 2014	As a result of urbanization and agricultural activities; It is concluded that gradual losses in vegetation and increases in mean LST and albedo occur. It has been determined that changing land cover and topography are associated with surface albedo and LST.

CHAPTER 3

STUDY AREA AND MATERIALS

This chapter includes the location, general information, data used in the study, and the sources of the data for the selected area chosen as a case study.

3.1. Description of the Study Area

The province of İzmir, located in the Aegean Region and the third-largest city in Türkiye, is situated between the latitudes of 37°45' and 39°15' North and longitudes of 26°15' and 28°20' East (Governorship of İzmir). İzmir, with an acreage of 12012 km², comprises a total of 30 districts. There are 11 central districts, including Balçova (16 km²), Bayraklı (30 km²), Buca (178 km²), Bornova (220 km²), Çiğli (139 km²), Gaziemir (70 km²), Güzelbahçe (77 km²), Karabağlar (89 km²), Karşıyaka (51 km²), Konak (24 km²), and Narlıdere (50 km²)[119].

The province of İzmir is situated in the Mediterranean climate zone; therefore, summers in İzmir are hot and dry, while winters are mild and rainy. There are factors (differences in physical geography such as elevation, aspect and distance from the coast, precipitation, temperature and insolation) that cause climate differences throughout the province[120]. İzmir ranks third in terms of meteorological disasters caused by climate differences[37]. Along the coastal areas, the annual average temperature fluctuates between 14-18 ºC. In the city, July (27.3 ºC) and August (27.6 ºC) are the hottest months, while January (8.6 ºC) and February (9.6 ºC) are the coldest months[120].

İzmir, besides hosting its historical, cultural, and commercial centers, the center of İzmir stands at the heart of the city's economic and social life. İzmir has an intensified UHI effect due to its dense population, wide range of business activities and climate characteristics. As a result of this effect, electricity consumption increases, water resources diminish, and health problems increase in İzmir with the advent of high temperatures. The urbanization process has led to high building density, decreased green areas, and widespread asphalt roads and concrete structures in İzmir. Additionally, the central districts of İzmir are the most densely populated areas and hubs of commercial and economic activities. Alongside this dense population, large shopping malls, business centers, and factories contribute to increased energy consumption and heating needs, further intensifying the UHI effect. Therefore, the study area selected for examining the phenomenon of UHI and understanding its effects lies within the İzmir Metropolitan Area, comprising 11 central districts. The chosen study area covers an area of 944 km², representing the most densely built-up areas of the city. Figure 12 shows the location of the study area in Türkiye and its location to the surrounding districts and provinces.

Figure 12. Study area

In the province of İzmir between 1938-2022, the mean highest temperature (33.8 ºC) is seen in July, while the mean lowest temperature (6 ºC) is seen in January (Figure 13).

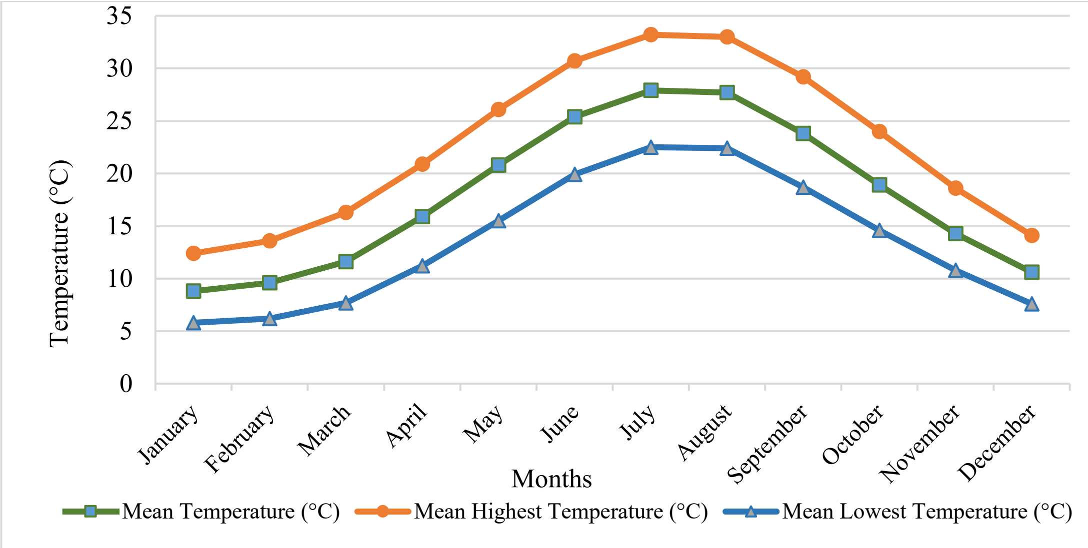

Figure 13. Temperature values of İzmir province between 1938-2022

(Source: TSMS[121])

The hours of sunshine, which is directly related to temperature, is observed at most in July with 12.3 hours in İzmir between 1938 and 2022 (Figure 14).

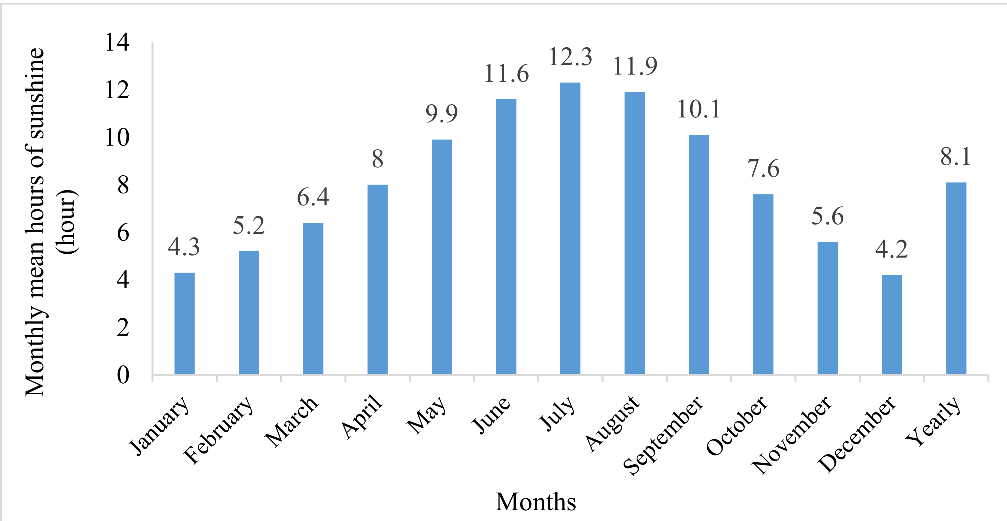

Figure 14. Monthly mean hours of sunshine (hour) for İzmir province between 1938-2022

(Source: TSMS[121])

According to the data from the Turkish Statistical Institute (TÜİK) population census database, the population of the study area was 1780476 in the year 1990, reaching 2966488 in the year 2022. The numerical values of the population shown in Table 5 are shown graphically in Figure 15.

Table 5. The Population of Study Area

(Source: TÜİK[122–124])

Years	Population
1990	1780476
2000	2273388
2007	2649582
2008	2683842
2009	2740306
2010	2786863
2011	2796931
2012	2816632
2013	2842604
2014	2861542
2015	2891492
2016	2916298
2017	2938546
2018	2947000
2019	2972900
2020	2959835
2021	2959355
2022	2966488

The study area shows a rapidly increasing population graph from 1990 to 2022. A population explosion occurred, especially between 1990 and 2007 (Figure 15). The highest population growth over the years has been in the Buca district.

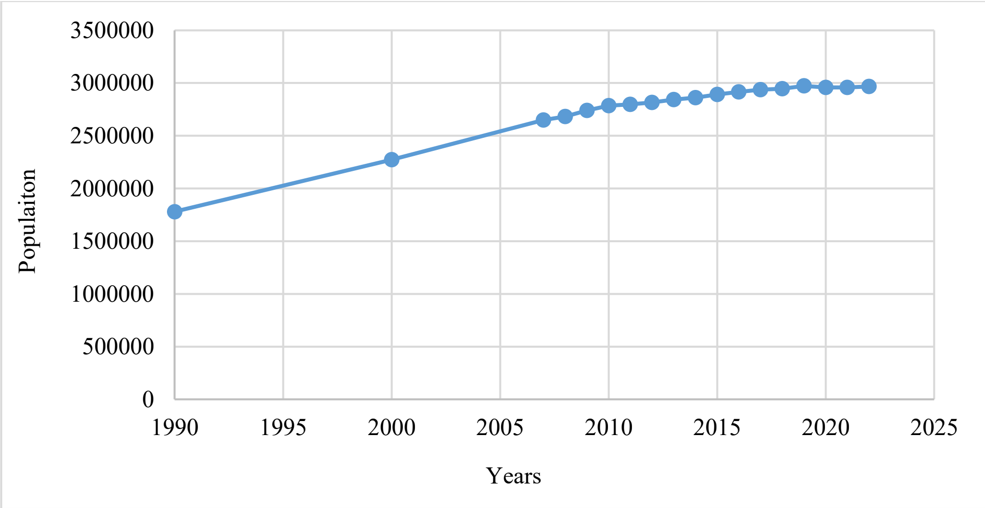

Figure 15. Population distribution diagram of the study area

(Source: TÜİK[122–124])

Rainfall distribution in İzmir shows significant variations according to months and seasons. Generally, more than half of the rainfall occurs from the second half of October until April. Particularly during the winter period, heavy rainfall and storms are observed. The annual average total rainfall amount is 696.7 mm[45,120]. The prevailing wind direction in İzmir is southeast and west. While the wind is unstable and mild during the winter months, it shows stability during the summer months. Generally, the effect of the wind is observed from the sea towards the land[120].

According to the data recorded between 1950 and 2021, a total of 1431 extraordinary events related to meteorological/climate change have occurred in İzmir province (Figure 16). The events occurred as follows: forest fires (1235), landslides (117), heavy rainfall/floods (62), heavy snowfall (10), storms (4), snowslides (2), and strong winds (1). Forest fires are the most common event in the province, accounting for 86.3% of the total events[45].

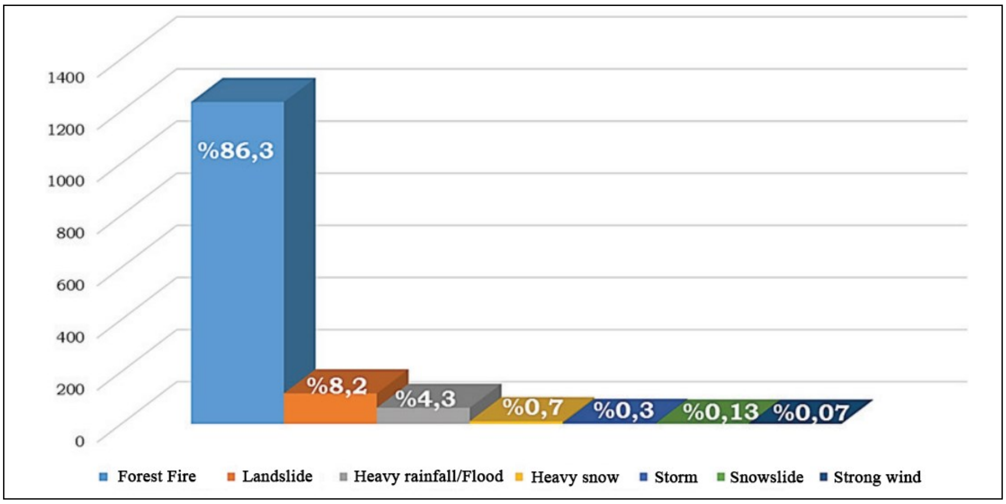

Figure 16. Distribution chart of the number of extraordinary events due to meteorological/climate change in İzmir province

(Source: İRAP[45])

According to the data recorded between 1950 and 2021, a total of 399 extraordinary events related to meteorological/climate change have occurred in the central districts of the study area. Forest fires (367) are the most common events in the central districts. Bornova (92), Buca (73), Balçova (53), and Bayraklı (43) are the most affected districts by this disaster. The second and third most common disasters in the study area are sudden rainfall/heavy rainfall (15) and landslides (7), respectively. River floods occurred only in the Bornova district during these years, while strong winds, storms, and heavy snowfall occurred in the Konak district (Table 6).

Table 6. Number of Extraordinary Events Due to Meteorological/Climate Change in the Central Districts of İzmir Province (Source: İRAP[45])

Central Districts	Sudden Rainfall /Heavy Rainfall	Extreme / Heavy Rainfall	River Flood	Strong Wind	Storm	Heavy Snow	Landslide	Forest Fire
Balçova	-	-	-	-	-	-	-	53
Bayraklı	-	-	-	-	-	-	2	43
Bornova	4	-	1	-	-	-	2	92
Buca	1	-	-	-	-	-	1	73
Çiğli	2	-	-	-	-	-	-	19
Gaziemir	-	-	-	-	-	-	-	19
Güzelbahçe	-	-	-	-	-	-	-	9
Karabağlar	2	1	-	-	-	-	1	11
Karşıyaka	2	-	-	-	-	-	-	35
Konak	4	2	-	1	1	4	-	8
Narlıdere	-	-	-	-	-	-	1	5
Total	**15**	**3**	**1**	**1**	**1**	**4**	**7**	**367**

3.2. Data and Sources

LST, LULC, spectral indices as urban parameters, and built-up indices as urban parameters were used to determine the SUHI effect in the study area.

LST is also analyzed with CORINE land cover data, which is another determinant of the SUHI effect. LST values that change depending on the LULC change allow us to determine how the SUHI effect changes. As a result of the analysis, the mean LST value is calculated for each LULC. Landsat satellite images are the main data used to determine the SUHI effect in the study area. LST, which is among the spectral indices as urban parameters created from satellite images, is the main index of the study. LST allows the SUHI effect to be analyzed through other spectral indices (NDVI, NDWI, NDBI, UI, and albedo). In addition to satellite imagery, it is also possible to examine the SUHI effect based on built-up indices at the building scale. In this study, LST and built-up indices are used and compared with different built environment textures, and evaluations are made based on the findings.

The quantitative data used in the study are categorized under the UHI, divided into two dimensions: Spatial Aspects and Temporal Aspects (Table 7).

CORINE data for 1990, 2000, 2006, 2012, and 2018 were used to detect LULC changes in the study area. In order to make a consistent evaluation, the years 1990, 2000, 2006, 2012, and 2018, when CORINE data were taken as determining factor in creating spectral indices as urban parameters. Landsat 5 TM, Landsat 7 ETM+, and Landsat 8 OLI/TIRS satellite images were used on the dates determined (July-August) in 1990, 2000, 2006, 2012, and 2018. Landsat satellite images and meteorological station data were used to examine the relationship between LST and air temperature. In order to examine the SUHI effect in more detail with built-up indices as urban parameters, representative regions were selected. Data on buildings, number of floors, mean household size, and urban open-green space are used to construct the built-up indices. Detailed information about the data used and their sources is presented in Table 7.

Table 7. Data Used in the Study

Variable Concepts/ Categories	Dimensions	Variable Indicators	Data Sources
Urban Heat Island	Temporal Aspects	Satellite Imagery; -Landsat 8-9 OLI/TIRS (2018) -Landsat 7 ETM+ (2000, 2006, 2012) -Landsat 5 TM (1990)	**Secondary Data** EarthExplorer[125]
		CORINE Land Cover 1990, 2000, 2006, 2012, and 2018 CORINE Land Cover Change 1990-2000 2000-2006 2006-2012 2012-2018	**Secondary Data** Copernicus Land Monitoring Service (CORINE)[126]
		Daily Mean Air Temperature Values of the Stations in the Central District (ºC) (1990, 2000, 2006, 2012, 2018) (July-August)	**Secondary Data** Meteorology 2nd Regional Directorate[127]
	Spatial Aspects	**Built-up Indices**	**Secondary Data**
		-Building -Number of Floors	İzmir Metropolitan Municipality Directorate Branch of Geographical Information Systems[128]
		-Mean Household Size	İzmir ’in Rakamları[129]
		-Urban Open-Green Areas and Forest Areas	OpenStreetMap Overpass Turbo[130]
		Meteorological Station Information -Geographical Coordinates of Meteorology Stations (Latitude, Longitude) -Meteorological Station Name/Number - UTM X, Y Coordinate of Meteorology Stations	**Secondary Data** Meteorology 2nd Regional Directorate[131]

3.2.1. Landsat Satellite Images

The Landsat Program, a series of Earth observation satellite missions jointly managed by NASA and the U.S. Geological Survey; on July 23, 1972, the Earth Resources Technology Satellite (ERTS-1) was launched in cooperation with NASA and was later renamed Landsat 1[132]. The reference system used to define the locations of images collected by Landsat satellites on Earth and adopted by the USGS is the Worldwide Reference System (WRS-1). This grid system is used to catalog Landsat images from Landsat 1 to Landsat 3. Due to the limitations of the WRS-1 system, WRS-2, developed as an extension of this system, is used today. This system, used since Landsat 4, has been developed to cover the Earth with more lines and paths. Additional Landsat satellites have been launched to create a remote sensing data archive.

Landsat 2, Landsat 3, Landsat 4, and Landsat 5 were launched into space in 1975, 1978, 1982, and 1984. Landsat 5 was the longest-operating satellite that observed Earth, working for almost 29 years. The Landsat 6 satellite, which failed to reach orbit in 1993, is not included in successful Landsat counts. Landsat 7, Landsat 8, and Landsat 9 were launched into space in 1999, 2013, and 2021[133]. Landsat 8 and Landsat 9 are the current active satellites in orbit. Landsat satellites are used to document land changes resulting from urbanization, climate change, forestry, agriculture, and human-induced changes and have medium-resolution spectral bands[132].

Apart from Landsat, there are also MODIS, Sentinel, and ASTER satellites used in LST calculations. The Sentinel satellite was first launched in 2014, ASTER and MODIS in 1999, and the SPOT satellite in 1986. In this study, in order to establish the relationship between LULC and LST, satellite images containing the CORINE Land Cover years must be used. ASTER and MODIS satellites cannot be used because they do not contain images from 1990, and Sentinel satellites do not contain images from 1990, 2000, 2006, and 2012.

The Landsat satellite imagery demonstrates continuity, having been regularly sent into orbit since 1972. This long-term continuity is crucial for conducting extended monitoring and change analyses. Additionally, free access is provided and has global coverage. The Landsat satellite series provides imagery in various wavelengths and spectral bands, enabling the identification and analysis of diverse surface features. Therefore, the Landsat satellite, which has become a fundamental component of various scientific research and applications, provides an advantage in time series analysis in this study.

Land Surface Temperature (LST)

Landsat 5 TM, Landsat 7 ETM+, and Landsat 8 OLI/TIRS satellite images are used for this thesis. Satellite images for the years 1990, 2000, 2006, 2012, and 2018 for the calculation of the LST of the study area were obtained free of charge from the Earth Explorer site in the date ranges given in Figure 17. There is no single dated satellite image covering the province of İzmir. Therefore, two suitable dates have been determined for each year covering the province of İzmir. While determining these dates, care was taken to choose the images with the lowest cloudiness rate. Because the increase in cloudiness increases the margin of error in the LST value. Then, these different dated satellite images were converted into a single raster to generate the LST values.

In this study, satellite images from Landsat 8 OLI/TIRS satellite for 2018 (July 3 and August 20), Landsat 7 ETM+ satellite for 2012 (July 10 and July 26), 2006 (July 10 and August 27), and 2000 (July 25 and August 10), and Landsat 5 TM satellite for 1990 (July 6 and August 23) were used to avoid seasonal differences when comparing the results (Figure 17).

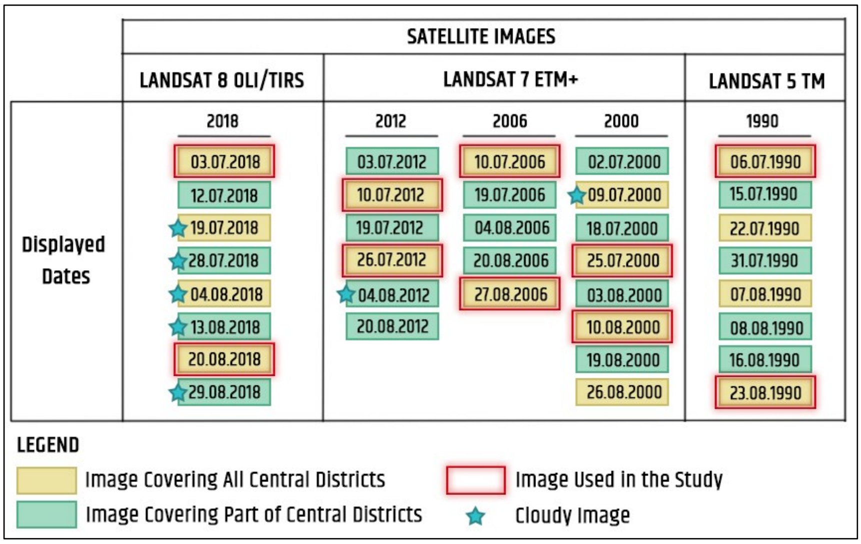

Figure 17. Satellite images used and displayed dates in the study area

After each Landsat satellite operates for a certain period of time, it is replaced by a new generation satellite. Detailed information about all Landsat data used within the scope of this study is given in Table 8, Table 9, and Table 10.

The Landsat 5 TM satellite has a 16-day temporal resolution and 8-bit radiometric resolution. The satellite contains 1 thermal band, and has 7 bands in total (Table 8).

Table 8. Landsat 5 TM Band Combinations

(Source: USGS[134])

Satellite (Sensor)	Spectral Bands	Wavelenght (micrometers/µm)	Resolution (meters)
Landsat 5 (Thematic Mapper-TM)	Band 1-Blue	0.45 - 0.52	30
	Band 2-Green	0.52 - 0.60	30
	Band 3-Red	0.63 - 0.69	30
	Band 4-Near Infrared (NIR)	0.76 - 0.90	30
	Band 5-Shortwave Infrared (SWIR) 1	1.55 - 1.75	30
	Band 6-Thermal	10.40 - 12.50	120 * (30)
	Band 7-Shortwave Infrared (SWIR) 2	2.08 - 2.35	30

Landsat 7 ETM+ satellite has a 16-day temporal resolution and 8-bit radiometric resolution. The satellite contains 1 thermal band and has 8 bands in total (Table 9).

Table 9. Landsat 7 ETM+ Band Combinations

(Source: USGS[135])

Satellite (Sensor)	Spectral Bands	Wavelength (micrometers/µm)	Resolution (meters)
Landsat 7 (Enhanced Thematic Mapper Plus-ETM+)	Band 1-Blue	0.45 - 0.52	30
	Band 2-Green	0.52 - 0.60	30
	Band 3-Red	0.63 - 0.69	30
	Band 4-Near Infrared (NIR)	0.77 - 0.90	30
	Band 5-Shortwave Infrared (SWIR) 1	1.55 - 1.75	30
	Band 6-Thermal	10.40 - 12.50	60 * (30)
	Band 7-Shortwave Infrared (SWIR) 2	2.09 - 2.35	30
	Band 8-Panchromatic (PAN)	0.52 - 0.90	15

Landsat 8 OLI/TIRS satellite has a 16-day temporal resolution and 16-bit radiometric resolution. The satellite contains 2 thermal bands and has 11 bands in total (Table 10).

Table 10. Landsat 8 OLI/TIRS Band Combinations

(Source: USGS[136])

Satellite (Sensor)	Spectral Bands	Wavelenght (micrometers/µm)	Resolution (meters)
Landsat 8 (Operational Land Imager - OLI)	Band 1-Coastal Aerosol	0.43 - 0.45	30
	Band 2-Blue	0.45 - 0.51	30
	Band 3-Green	0.53 - 0.59	30
	Band 4-Red	0.64 - 0.67	30
	Band 5-Near Infrared (NIR)	0.85 - 0.88	30
	Band 6-Shortwave Infrared (SWIR) 1	1.57 - 1.65	30
	Band 7-Shortwave Infrared (SWIR) 2	2.11 - 2.29	30
	Band 8-Panchromatic (PAN)	0.50 - 0.68	15
	Band 9-Cirrus	1.36 - 1.38	30
Landsat 8 (Thermal Infrared Sensor - TIRS)	Band 10-Thermal Infrared (TIRS) 1	10.6 - 11.19	100 * (30)
	Band 11-Thermal Infrared (TIRS) 2	11.50 - 12.51	100

Spectral Indices as Urban Parameters

In the study "How are the spectral indices as urban parameters related to LST/SUHI?" In order to answer the question, NDVI, NDWI, NDBI, UI, and Albedo spectral indices were created from Landsat satellite images. Five maps were created for each index according to the dates determined in Figure 17. In the continuation of the study, each index was correlated with LST, and the relationship between LST and spectral indices was determined. Parameters affecting SUHI formation were determined by examining regression analysis according to the determined correlation.

3.2.2. Land Use/Land Cover (LULC)

Within the scope of the thesis study, CORINE Land Cover (CLC) data produced by Copernicus Land Monitoring Services with an accuracy of 85% and above for the years 1990, 2000, 2006, 2012, and 2018 were used to determine the changes in LULC of the study area.

CORINE (Coordination of Information on the Environment) is a land cover delineation and classification project that aims to produce maps of various land cover classes, biotopes, and air quality on a continental scale as defined by the European Environment Agency. The first CLC dataset of the program initiated in 1985 was produced in 1990. The data, updated every six years, had its latest update in 2018. LULC data are produced for 39 countries, including European Union member states and Türkiye (for 27 countries in 1990). As shown in Table 11, the inventory has 3 hierarchical levels including 44 land cover classes[126,137].

Table 11. CORINE Land Cover Classes

(Source: Copernicus Land Monitoring Service (CORINE)[138]

LEVEL 1	LEVEL 2	LEVEL 3
1. ARTIFICIAL SURFACES	1.1 Urban fabric	1.1.1 Continuous urban fabric
		1.1.2 Discontinuous urban fabric
	1.2 Industrial, commercial and transport units	1.2.1 Industrial or commercial units
		1.2.2 Road and rail networks and associated land
		1.2.3 Port areas
		1.2.4 Airports
	1.3 Mine, dump and construction sites	1.3.1 Mineral extraction sites
		1.3.2 Dump sites
		1.3.3 Construction sites
	1.4 Artificial, non-agricultural vegetated areas	1.4.1 Green urban areas
		1.4.2 Sport and leisure facilities
2. AGRICULTURAL AREAS	2.1 Arable land	2.1.1 Non-irrigated arable land
		2.1.2 Permanently irrigated land
		2.1.3 Rice fields

(cont. on next page)

Table 11. (cont.)

2. AGRICULTURAL AREAS	2.2 Permanent crops	2.2.1 Vineyards
		2.2.2 Fruit trees and berry plantations
		2.2.3 Olive groves
	2.3 Pastures	2.3.1 Pastures
	2.4 Heterogeneous agricultural areas	2.4.1 Annual crops associated with permanent crops
		2.4.2 Complex cultivation patterns
		2.4.3 Land principally occupied by agriculture, with significant areas of natural vegetation
		2.4.4 Agro-forestry areas
3. FOREST AND SEMINATURAL AREAS	3.1 Forests	3.1.1 Broad-leaved forest
		3.1.2 Coniferous forest
		3.1.3 Mixed forest
	3.2 Scrub and/or herbaceous vegetation associations	3.2.1 Natural grasslands
		3.2.2 Moors and heathland
		3.2.3 Sclerophyllous vegetation
		3.2.4 Transitional woodland/shrub
	3.3 Open spaces with little or no vegetation	3.3.1 Beaches, dunes, sands
		3.3.2 Bare rocks
		3.3.3 Sparsely vegetated areas
		3.3.4 Burnt areas
		3.3.5 Glaciers and perpetual snow
4. WETLANDS	4.1 Inland wetlands	4.1.1 Inland marshes
		4.1.2 Peatbogs
	4.2 Maritime wetlands	4.2.1 Salt marshes
		4.2.2 Salines
		4.2.3 Intertidal flats
5. WATER BODIES	5.1 Inland waters	5.1.1 Water courses
		5.1.2 Water bodies
	5.2 Marine waters	5.2.1 Coastal lagoons
		5.2.2 Estuaries
		5.2.3 Sea and ocean

In this study, CLC data were created at Level 2. The dataset for calculating the average LST values of LULC classes with zonal statistics is shown in Figure 18.

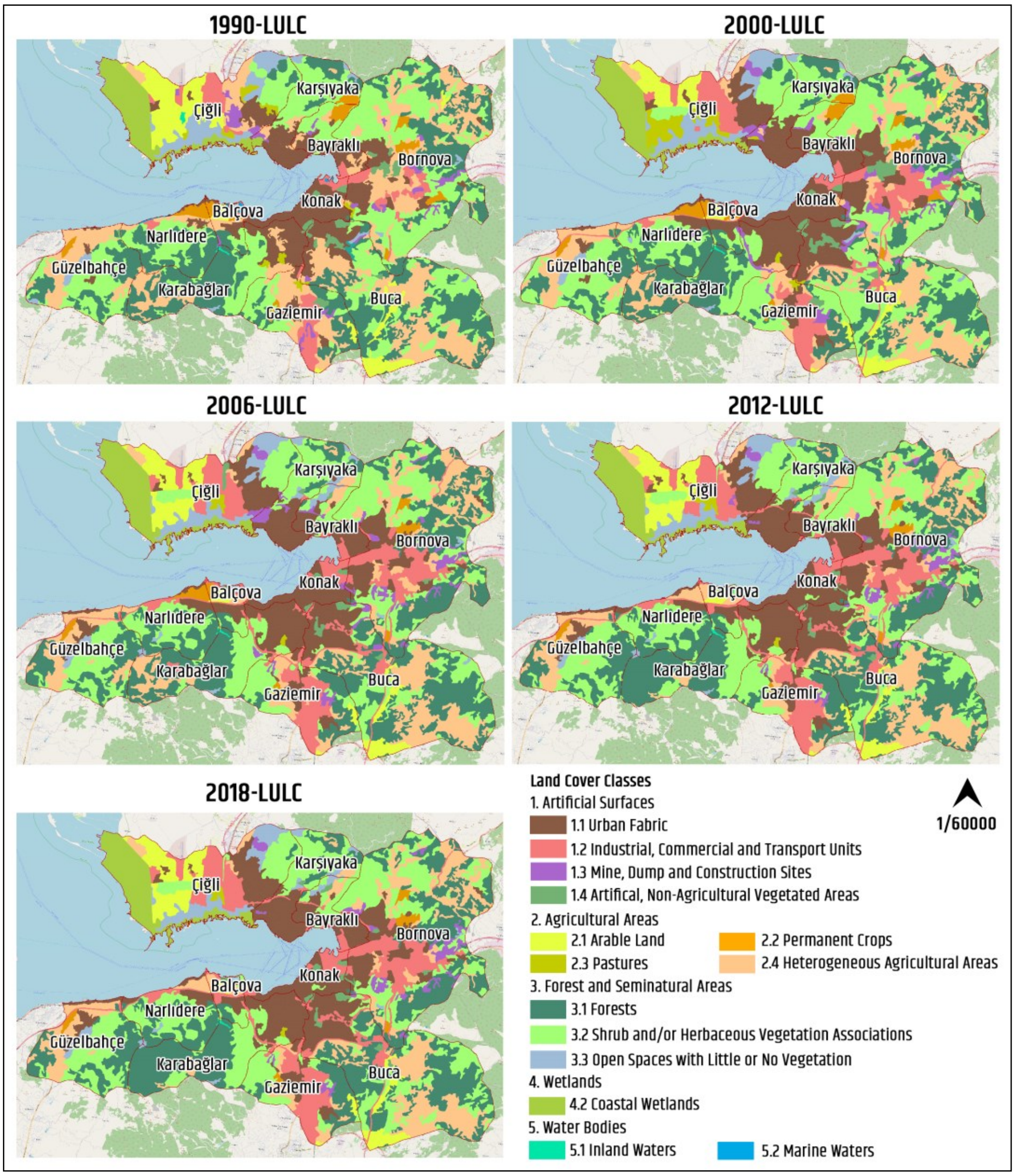

Figure 18. Land cover/use change of study area by years

(Adapted from Copernicus Land Monitoring Service (CORINE)[126])

3.2.3. Data Used in the Representative Regions

Representative regions were selected to evaluate the SUHI effect through different built environment textures. In addition to the change in LST and LULC, buildings, number of floors, mean household size, and urban open-green areas data were used to obtain data on population density, building area density, mean floor height, and green areas larger than 2 ha.

Green areas contribute to the reduction of the SUHI effect due to impervious surfaces. Therefore, it is important to examine green areas in different built environment textures to be selected. The distributions of Urban Open-Green Areas and Forest Areas downloaded from OpenStreetMap Overpass Turbo within the study area are shown in Figure 19. Urban Open-Green Areas include parks, recreation, and cemetery areas with trees. There are a total of 939 ha of Urban Open-Green Area, and 18656 ha of Forest Area within the area. Most urban open-green areas are located in the Bayraklı district, while most forest areas are located in the Buca district (Table 12).

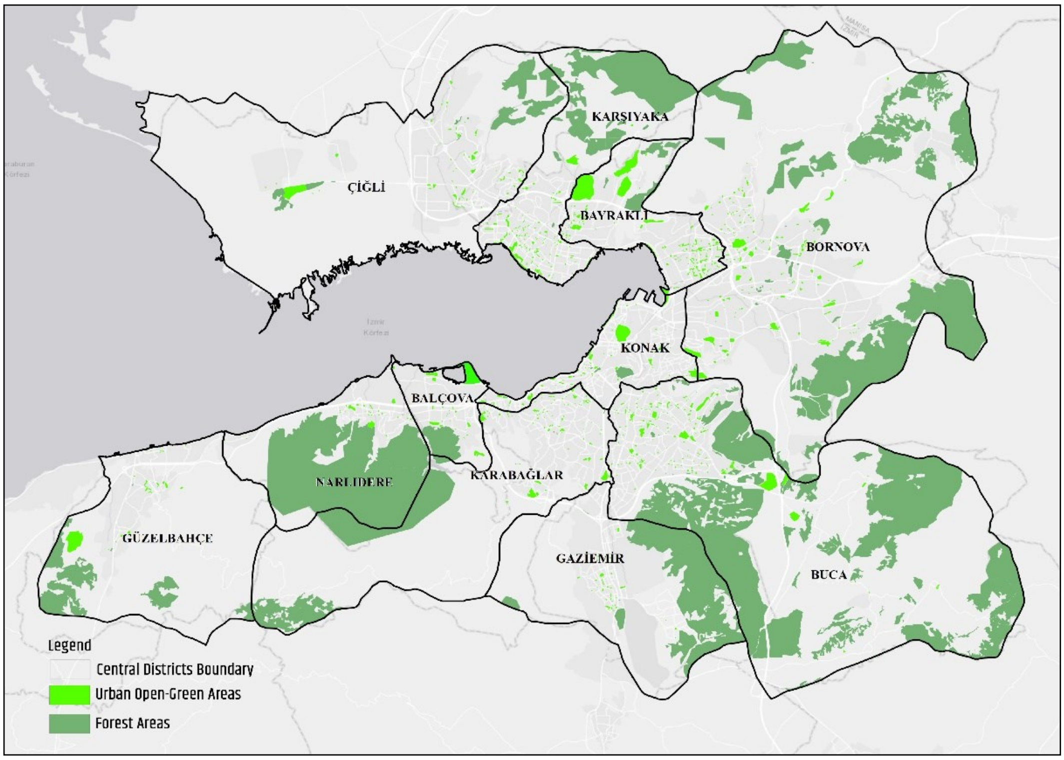

Figure 19. Urban open-green areas and forest areas

(Adapted from OpenStreetMap Overpass Turbo[130])

Table 12. Urban Open-Green Areas Size and Forest Areas Size

(Adapted from OpenStreetMap Overpass Turbo[130])

Central Districts	Urban Open-Green Areas Size (Unit: ha)	Forest Areas Size (Unit: ha)
Balçova	77.2	211.3
Bayraklı	221	151.7
Bornova	128.8	4245.2
Buca	110.6	5819.7
Çiğli	80.3	473.5
Gaziemir	13.9	1539.3
Güzelbahçe	68.4	662
Karabağlar	48.1	1115.2
Karşıyaka	79.2	1335.2
Konak	100.4	40.3
Narlıdere	10.5	3063.5
Total	**938.4**	**18656.9**

Current data on buildings and number of floors in the study area were obtained from İzmir Metropolitan Municipality Directorate Branch of Geographical Information Systems. There are a total of 372029 buildings in the study area. The highest building density is observed in Konak (31.3 building/ha), Bornova (2.7 building/ha), Karabağlar (6.4 building/ha), and Buca (2.9 building/ha) districts, respectively. The district with the lowest building area density is Narlıdere (1.5 building/ha) (Figure 20).

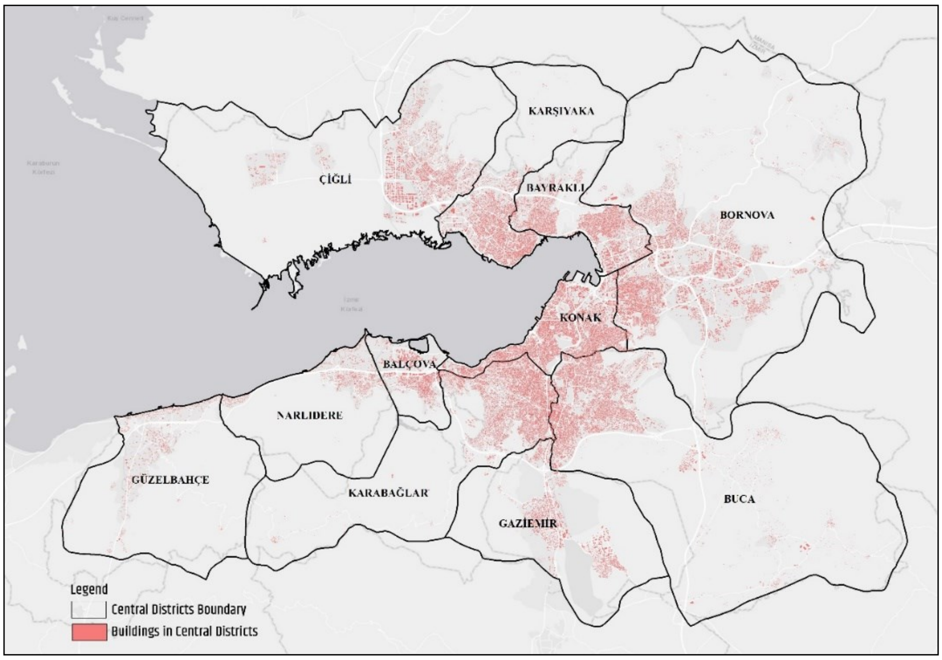

Figure 20. Buildings in study area

(Adapted from İzmir Metropolitan Municipality[128])

There are 43 different number of floors in the study area. While buildings with 1 number of floors are the most, there are only one building each with 40, 41, 42, 48, 49, and 53 number of floors. The number of floors of the buildings is given in Table 13.

Table 13. Number of Floors in Study Area

(Adapted from İzmir Metropolitan Municipality[128])

Number of Floors	Number of Buildings
1-2	197590
3-4	117895
5-6	40991
7-8	9429
9-10	4772
11-12	835
13-14	180
15-16	129
17-18	69
19-20	29
21-22	46
23-24	10
25-26	11
27+	42

Mean household size data was used to calculate the population for selected specific region in the study area. Figure 21 shows the mean household size data for the 11 districts[129].

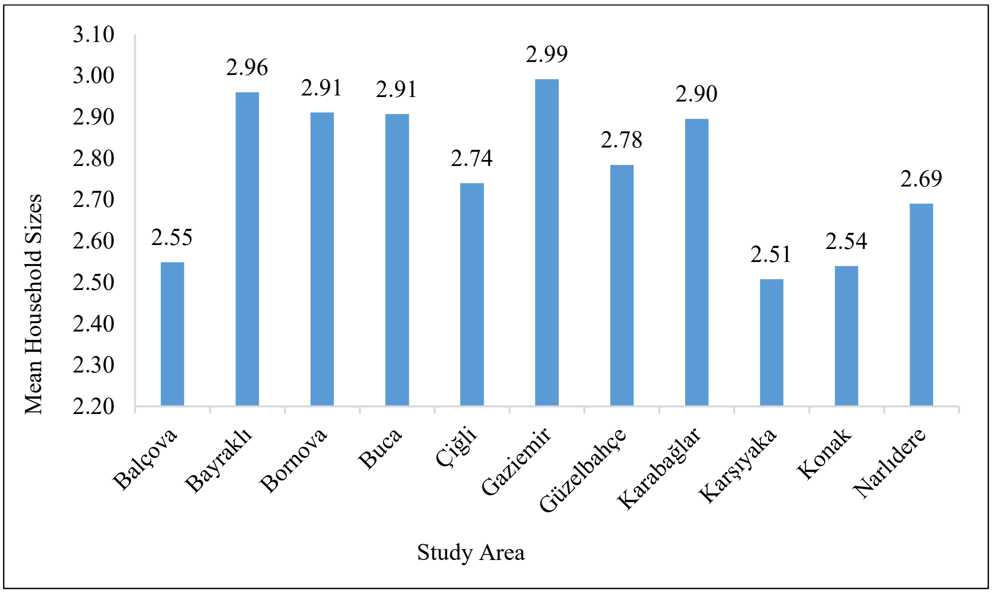

Figure 21. Mean household sizes in study area

(Source: İzmir'in Rakamları[129])

3.2.4. Meteorological Stations in Study Area

Within the scope of the study, the data of fifteen meteorological stations located in the central districts of İzmir province were obtained from Meteorology 2nd Regional Directorate (İzmir Meteoroloji 2. Bölge Müdürlüğü). The locations and names of the stations are shown in Figure 22.

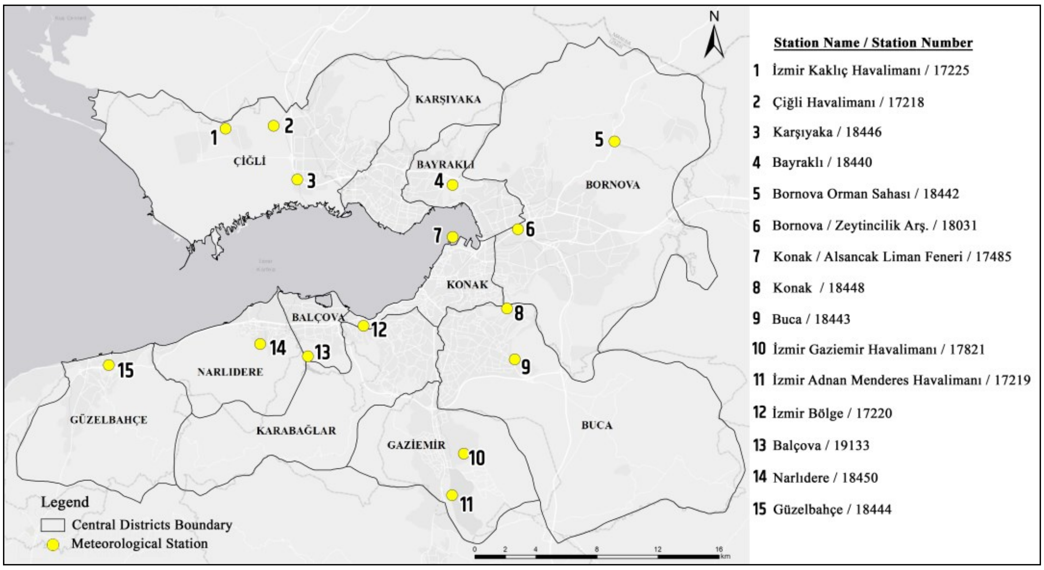

Figure 22. Meteorological stations in study area

(Source: Meteorology 2nd Regional Directorate[131])

In order to compare the air temperature values of the meteorological stations with the LST values, air temperature data were obtained from the 2nd Regional Directorate of Meteorology. It is important to choose the appropriate time interval to determine the relationship between LST and air temperature. Therefore, the air temperature data are the same as the dates on which Landsat satellite images were used. Data on 3 July and 20 August for 2018, 10 July and 26 July for 2012, 10 July and 27 August for 2006, 25 July and 10 August for 2000, and 6 July and 23 August for 1990 were used. Air temperatures for these dates are shown in detail in Table 14.

There are two stations for 1990 and 2000, four stations for 2006, six stations for 2012, and fifteen stations for 2018. While İzmir Bölge/17220 and İzmir Adnan Menderes Havalimanı/17219 stations have been used since 1990, nine stations have started to be used as of 2018.

Table 14. Mean Air Temperature Value on Specific Days at Meteorological Station

(Source: 2nd Regional Directorate of Meteorology[127])

	Air Temperature Value (°C)									
	1990		**2000**		**2006**		**2012**		**2018**	
Station Name / Station Number	**6 July**	**23 August**	**25 July**	**10 August**	**10 July**	**27 August**	**10 July**	**26 July**	**3 July**	**20 August**
Çiğli Havalimanı / 17218	0	0	0	0	26.9	27.8	30.6	27.8	29.3	29.9
İzmir Adnan Menderes Havalimanı / 17219	26.4	25.9	26.0	20.1	26.9	26.8	30.8	28.9	30.1	30.3
İzmir Bölge / 17220	28.5	28.0	30.9	30.2	27.5	29.1	30.9	28.8	29.2	30.4
İzmir Kaklıç Havalimanı / 17225	0	0	0	0	27.2	0	31.3	29.3	32.1	0
İzmir Gaziemir Havalimanı / 17821	0	0	0	0	0	0	32.7	31.8	32.4	0
Bornova/Zeytincilik Arş. (TAGEM) / 18031	0	0	0	0	0	0	31.8	26.8	31.0	30.5
Bayraklı / 18440	0	0	0	0	0	0	0	0	29.5	30.8
Bornova Orman Sahası / 18442	0	0	0	0	0	0	0	0	28.3	27.5
Buca / 18443	0	0	0	0	0	0	0	0	29.5	29.9
Güzelbahçe / 18444	0	0	0	0	0	0	0	0	26.9	28.3
Karşıyaka / 18446	0	0	0	0	0	0	0	0	29.3	31.1
Konak / 18448	0	0	0	0	0	0	0	0	28.8	28.4
Narlıdere / 18450	0	0	0	0	0	0	0	0	28.6	28.5
Konak/Alsancak Liman Feneri / 17485	0	0	0	0	0	0	0	0	29.9	29.6
Balçova / 19133	0	0	0	0	0	0	0	0	27.8	29.0

CHAPTER 4

METHOD

This chapter describes the methodologies used to assess the SUHI effect with LULC variation, spectral indices and built-up indices as urban parameters. The method followed for the analysis and examination of the SUHI effect occurring in the study area is depicted in the flowchart (Figure 23). Method flowchart includes inputs, and analyses and evaluation criteria for products and their relationships.

The flowchart of the method is created within the scope of the three research questions sought to be answered in the study. The inputs in the study are CLC, Landsat, and different built environment textures. The year ranges examined in the study are 1990, 2000, 2006, 2012, and 2018. The reason in determining these years is that these years are radyly available in the CLC dataset.

Within the scope of the research question "How do LULC classes affect LST values?", LULC maps of the CLC dataset for the years 1990, 2000, 2006, 2012, and 2018 were obtained. Average LST values of LULC changes were calculated with the zonal statistics tool in the ArcGIS program. In addition, how the LULC changes over the years were analyzed.

Within the scope of the research question "How are the spectral indices as urban parameters related to LST/SUHI?", NDVI, NDWI, NDBI, UI, and Albedo parameters, especially LST, were created using Landsat satellite images. Appropriate images were obtained for each year in July and August when the SUHI effect is most common. The Landsat types used vary according to the year of launch. The relationships between LST, characterizes the SUHI effect, and other spectral indices were determined by correlation and regression analysis. Although LST images were produced according for different dates, correlation and regression analysis were conducted for the most recent year 2018. The study's independent variables are NDVI, NDWI, NDBI, UI, and Albedo parameters, while LST is the dependent variable.

"What findings emerge from comparing LST values with built-up indices as urban parameters?" To answer the research question, five regions with different built-up environmental textures of 100 hectares were identified, with different LST values in 2018 and where LULC changes were observed. LST was associated with Built-up indices such as mean floor height, building area density, population density, and green areas larger than 2 ha. In line with the divergence in parameters in the regions, the factors causing the SUHI effect were identified.

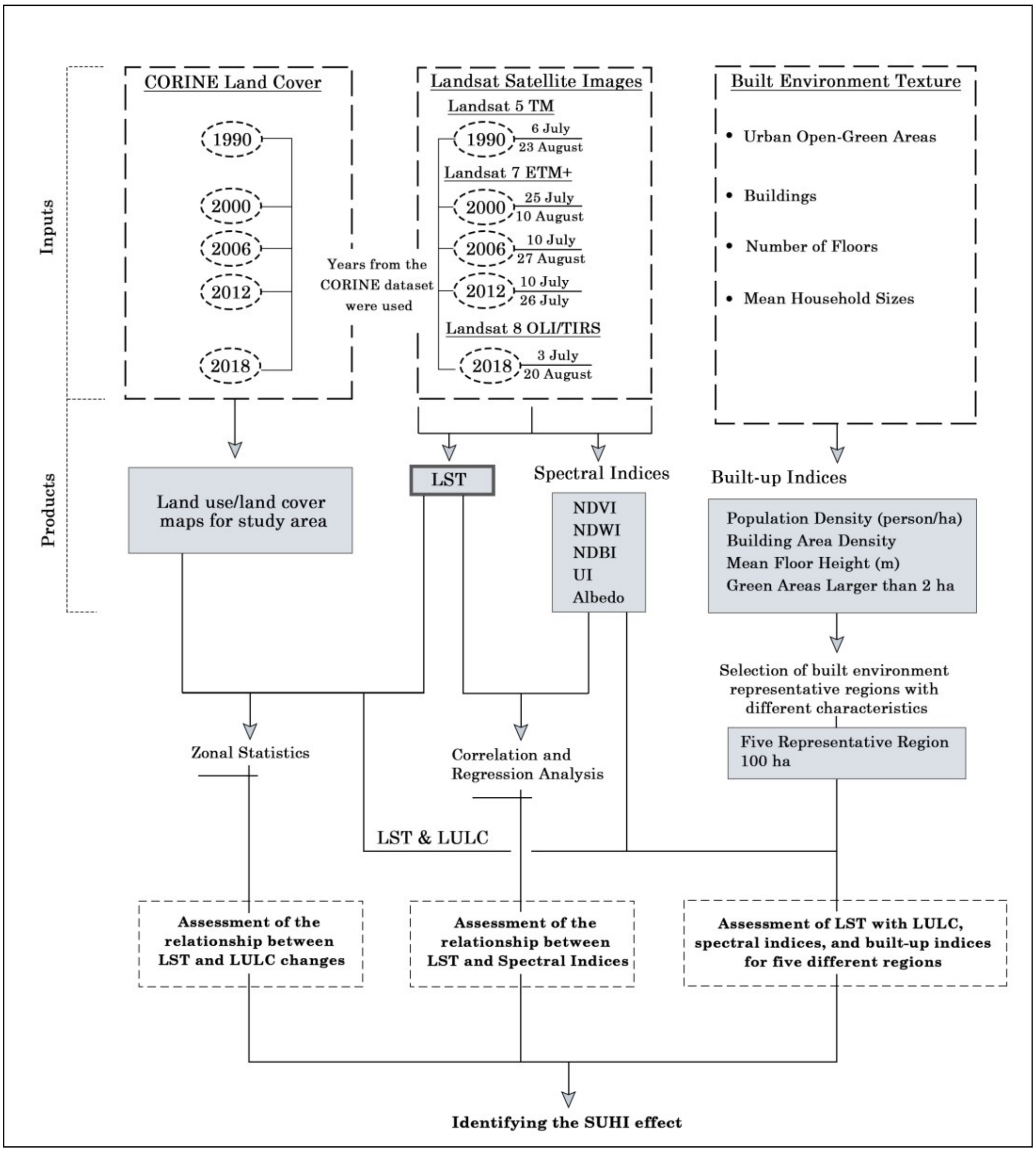

Figure 23. Flowchart for method

4.1. Data Preparation

In order to determine the SUHI effect, a total of six different spectral indices, including LST, NDVI, NDWI, NDBI, UI, and Albedo, have been calculated according to the equations below (Table 15). For each index, maps were created based on Landsat satellite images on the specified dates from 2018.

Table 15. Equations of Spectral Indices as Urban Parameters Used in Study

References	Indices Used	Equation
Stathopoulou and Cartalis, 2007	LST	$T_s = \frac{\mathrm{BT}}{\{1 + [(\lambda * \mathrm{BT}/\rho)\ln\varepsilon_\lambda]\}}$
Jensen, 2000	NDVI	$\mathrm{NDVI} = \frac{\mathrm{NIR} - \mathrm{Red}}{\mathrm{NIR} + \mathrm{Red}}$
McFeeters, 1996	NDWI	$\mathrm{NDWI} = \frac{\mathrm{Green} - \mathrm{NIR}}{\mathrm{Green} + \mathrm{NIR}}$
Zha et al. 2003	NDBI	$\mathrm{NDBI} = \frac{\mathrm{SWIR1} - \mathrm{NIR}}{\mathrm{SWIR1} + \mathrm{NIR}}$
Kawamura et al., 1996	UI	$\mathrm{UI} = \frac{\mathrm{SWIR2} - \mathrm{NIR}}{\mathrm{SWIR2} + \mathrm{NIR}}$
Liang, 2001	Albedo	$\frac{0.356\rho_1 + 0.130\rho_2 + 0.373\rho_3 + 0.085\rho_4 + 0.072\rho_5 - 0.0018}{0.356+0.130+0.373+0.085+0.072}$

4.1.1. Calculation of Land Surface Temperatures (LST)

LST map was created using a raster calculator in ArcGIS (version 10.8.2). The steps shown in Figure 24 are applied to determine the LST and map the SUHI effect. LST maps were created in 6 steps. In the first step, there is Equation (1), in the second step, there is Equation (2), in the third step, there is Equation (3), in the fourth step, there is Equation (4), in the fifth step, there are Equation (5), (6), and (7), and in the last step, there are Equation (8) and (9). In Table 16, the metadata of the satellite images used in the equation are given.

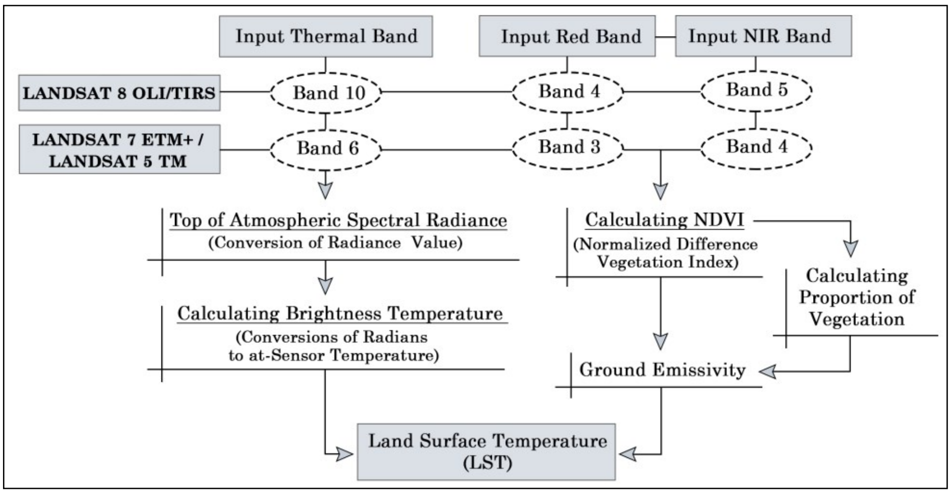

Figure 24. Flowchart for LST

The thermal bands (TIR) of Landsat satellite images are used when determining the SUHI effect. In the study, 6th band was used for Landsat 7 ETM+ and Landsat 5 TM, and only 10th band was used for Landsat 8 OLI/TIRS. The radiance values of the digital numbers (DNs) of the thermal bands were obtained and the brightness temperatures were calculated from these values. NDVI calculations were made using the red (Red) and near infrared (NIR) bands of Landsat satellites. For Landsat 7 ETM+ and Landsat 5 TM, the near infrared (NIR) and red bands (Red) correspond to bands 4 and 3, respectively, and for Landsat 8 OLI/TIRS, bands 5 and 4, respectively. Then, LST values were calculated by creating an image of vegetation proportion and surface emissivity. All the formulas required for the creation of the LST map are shown in steps.

Top of Atmospheric Spectral Radiance

The first step is to convert the digital numbers (DNs) of the Landsat thermal bands (Band 10 and Band 6) to the top of atmospheric (TOA) spectral radiance ($L\lambda$) with the Equation (1) taken from the USGS web page[139].

$$L\lambda = M_L * Q_{\text{cal}} + A_L \tag{1}$$

In this equation in step one, M_L represents the band-specific multiplicative rescaling factor, while Q_{cal} represents the thermal infrared (TIR) band of the images. For this equation, 10th (Landsat 8 OLI/TIRS) and 6th (Landsat 5 TM and Landsat 7 ETM+) bands are used according to the type of satellite images. A_L is the band-specific additive rescaling factor.

Conversion of Radiance to At-Sensor Temperature

In the second step, digital numbers (DNs) are converted to reflection. In the second step, the satellite thermal constants and thermal band data in the metadata file (MTL file) of the downloaded satellite images are used. Thus, TOA spectral radiance ($L\lambda$) is converted to brightness temperature (BT). We convert reflection to BT with the following Equation (2)[139,140].

$$\mathrm{BT} = \frac{K_2}{\ln[(K_1/L\lambda) + 1]} - 273.15 \tag{2}$$

where BT represents the TOA brightness temperature (°C). The band-specific thermal conversion constants from the metadata are K_1 and K_2.

“For obtaining the results in Celsius, the radiant temperature must be revised by adding the absolute zero (approx. −273.15°C)”.

Table 16. Metadata of the Satellite Images

LANDSAT 8	
Thermal constant, Band 10	
K_1	774.8853
K_2	1321.0789
Rescaling factor, Band 10	
M_L	0.0003342
A_L	0.1

(cont. on next page)

Table 16. (cont.)

LANDSAT 7	
Thermal constant, Band 6	
K_1	666.09
K_2	1282.71
Rescaling factor, Band 6	
M_L	0.067087
A_L	-0.06709
LANDSAT 5	
Thermal constant, Band 6	
K_1	607.76
K_2	1260.56
Rescaling factor, Band 6	
M_L	0.055375
A_L	1.18243

NDVI Method for Emissivity Correction

It is evaluated under 3 headings.

-Calculating Normalized Difference Vegetation Index (***NDVI):*** In the third step, Equation (3), the proportion of vegetation estimated by the NDVI is used as an input parameter to measure the land surface emissivity. Vegetation is used to reduce the impact of UHI in urban areas. The LST value is affected by the radiant temperature difference between the vegetation and the urban area[141]. NDVI is obtained by mathematical processing of the near infrared (NIR) and red band (Red). It is important to estimate the NDVI. Because the amount of vegetation available is an important factor, the NDVI can be used to understand general vegetation conditions[142]

$$\mathrm{NDVI} = \frac{\mathrm{NIR} - \mathrm{Red}}{\mathrm{NIR} + \mathrm{Red}}, \tag{3}$$

where NIR represents the near infrared and red represents the red band. Band 4 and band 3 for Landsat 5 TM and Landsat 7 ETM+, respectively; Band 5 and band 4 are used for Landsat 8 OLI/TIRS. NDVI takes a value between -1 and 1 in the Equation (3). Values close to +1 (0.8 - 0.9) are the areas with the highest vegetation density[143]. The calculation of the NDVI is very important for the calculation and correlation of Equation (4) and (5).

-Calculating the Proportion of Vegetation (Pv)

In the fourth step, Equation (4), the plant highly associated with NDVI proportion of vegetation (P_v) is obtained by the following equation. The ratio of the vertical projection area of vegetation (including leaves, stems and branches) on the ground to the total area is expressed as Pv[144]. Pv was developed by Carlson and Ripley (1997) and is an important step for the calculation of Land Surface Emissivity (LSE)[145].

NDVI_v (v: maximum value) and NDVI_s (s: minimum value) values differ for every area and can also be obtained from the histogram. However, in global conditions, the NDVI maximum and minimum values for vegetation and soil are considered 0.5 and 0.2 respectively. For vegetated surfaces, a value of 0.5 may be too low, but overall values from NDVI can also be calculated from the reflection on the surface. However, in the case of an NDVI calculated from TOA reflectivity, a fixed value cannot be said as the maximum and minimum values will depend on atmospheric conditions[145,146].

$$P_v = \left(\frac{\mathrm{NDVI} - \mathrm{NDVI}_s}{\mathrm{NDVI}_v - \mathrm{NDVI}_s}\right)^2 . \tag{4}$$

In the study, the fourth step was calculated by using the maximum and minimum values in the NDVI map created according to the third step.

-Calculating Land Surface Emissivity (LSE)

The contact of the rays from the sun with the objects can occur in three different ways. These three situations are; reflecting, transmitting or absorbing radiation falling on objects. Objects absorb these energies, allowing them to heat up and reach equilibrium temperature. When the objects reach the equilibrium temperature, they emit radiation depending on the object feature and the temperature it has. Emissivity (ε_λ) is also called the radiant ability of the object[146].

To estimate the LSE, the proportion of vegetation step must be completed. Each object has its own unique emissivity value, and the value range varies between 0 and 1. LSE, which largely depends on the characteristics of the land cover (vegetation, soil type, etc.) of the study area, is an important parameter for calculating the LST value[146,147].

In the fifth step, the emissivity (ε) associated with P_v is obtained by the following Equation (5).

$$\varepsilon_\lambda = \varepsilon_{v\lambda} P_v + \varepsilon_{s\lambda} (1 - P_v) + C_\lambda , \tag{5}$$

In this equation, $\varepsilon_{v\lambda}$ is the emissivity value of vegetation surfaces and $\varepsilon_{s\lambda}$ is the emissivity value of soil surfaces. C represents the surface roughness and its constant value is taken as 0.005 (the C value is 0 for homogeneous and flat surfaces)[148]. The Emissivity value of Landsat satellite images varies between 0.96 and 0.99 depending on the structure of the surface and the values are calculated according to Equation (6)[149].

$$\varepsilon_\lambda = \begin{cases} \varepsilon_{s\lambda} , & \text{NDVI} < \text{NDVI}_s , \\ \varepsilon_{v\lambda} P_v + \varepsilon_{s\lambda} (1 - P_v) + C_\lambda , & \text{NDVI}_s \leq \text{NDVI} \leq \text{NDVI}_v , \\ \varepsilon_{s\lambda} + C, & \text{NDVI} > \text{NDVI}_v . \end{cases} \tag{6}$$

If the NDVI value is less than 0, the land is considered to be covered with water (emissivity value = 0.991). Between 0 and 0.2 the land is covered with soil (emissivity value = 0.996), between 0.2 and 0.5 the land is covered with a mixture of soil and vegetation, and if it is greater than 0.5, the land is considered covered with vegetation (emissivity value = 0.973)[146,149].

According to the study of Sobrino et al. (2004)[146], a typical emissivity value of 0.99 is selected for vegetation. The selection of a typical value for soil is more difficult. There is a higher variation of emissivity values for soils compared to vegetation. In the same study, by considering a total of 49 soil spectra, the average soil value was obtained as 0.973 (standard deviation 0.004). In this context, the LSE equation calculated using vegetation cover rate and constants is as follows in Equation (7).

$$\varepsilon_\lambda = 0.004 * P_v + 0.986 \,. \tag{7}$$

Land Surface Temperature (LST)

In the final step, LST or the emissivity-corrected LST (T_s) is calculated using TOA brightness temperature and vegetation emissivity proportion as shown in the Equation (8)[95].

$$T_s = \frac{\mathrm{BT}}{\{1 + [(\lambda * \mathrm{BT}/\rho)\ln\varepsilon_\lambda]\}} \,, \tag{8}$$

In the equation, T_s represents the LST value in Celsius, while λ is the wavelength of the emitted radiance (center wavelength of Band 10 for Landsat 8 (λ = 10.8 μm) and center wavelength of Band 6 for Landsat 7, Landsat 5 (λ = 11.45 μm) is used). BT is the brightness temperature of Band 10 and Band 6. ε_λ is the emissivity calculated using the Equation (9)[95].

$$\rho = \mathrm{h}\,\frac{\mathrm{c}}{\sigma} = 1.438 \times 10^{-2}\ \mathrm{m\,K}\,, \tag{9}$$

The ρ value needs to be calculated to complete step 6 and generate the LST maps. In the equation, σ is Boltzmann's constant (1.38×10^{-23} J/K), h is Planck's constant (6.626×10^{-34} Js), and c is the velocity of light (2.998×10^{8} m/s).

All these steps will be calculated separately for the years 2018, 2012, 2006, 2000, and 1990 and as a result, five LST maps will be obtained.

4.1.2. Spectral Indices as Urban Parameters

Calculation of Normalized Difference Built-up Index (NDBI)

This index was developed by Zha et al. (2003)[150], is designed for automatic mapping of residential areas with Landsat bands. The NDBI index is based on the ability of artificial earth objects to reflect more in the shortwave infrared (SWIR) spectrum than in the near-infrared (NIR) spectrum. Often used to evaluate the SUHI effect, this index uses spectral differences between different surface types. Additionally, the relationship between NDBI and SUHI helps us understand the contribution of urban development to the UHI effect. This allows the detection of built-up areas such as buildings and structures. NDBI is calculated using Equation (10) below[150].

$$\mathrm{NDBI} = \frac{\mathrm{SWIR1} - \mathrm{NIR}}{\mathrm{SWIR1} + \mathrm{NIR}}, \tag{10}$$

SWIR1 and NIR refer to the spectral reflectance values in the shortwave infrared and near-infrared regions, respectively. Band 5 and band 4 for Landsat 5 TM and Landsat 7 ETM+, respectively; band 6 and band 5 were used for Landsat 8 OLI/TIRS. The value of the index ranges from -1 to +1. Values closer to +1 represent more built-up or urban areas. Values close to -1 generally indicate natural areas such as water and vegetation. More pronounced SUHI effects are observed as a result of regions with high NDBI values absorbing more thermal energy[150,151].

Calculation of Urban Index (UI)

The UI parameter allows us to express how the intensity of urbanization affects temperature increase. This index, obtained from satellite images, determines the difference between urban and natural areas. The urban index developed by Kawamura et al. (1996) [153]. takes advantage of the inverse relationship between the near-infrared (NIR) and shortwave infrared (SWIR) reflectance of urban areas in the region[152]. The following is calculated using Equation (11)[153].

$$\mathrm{UI} = \frac{\mathrm{SWIR2} - \mathrm{NIR}}{\mathrm{SWIR2} + \mathrm{NIR}}, \tag{11}$$

Where SWIR2 and NIR refer to the spectral reflectance values in the shortwave infrared and near-infrared regions, respectively. Band 7 and band 4 for Landsat 5 TM and Landsat 7 ETM+, respectively; Band 7 and band 5 were used for Landsat 8 OLI/TIRS. The value of the index ranges from -1 to +1. UI values increase as urban density increases. Higher pixel values indicate denser and more urbanized areas, while lower values represent less developed areas dominated by natural features. Therefore, in urban areas with high UI, greater SUHI effects are observed due to the excessive absorption of sunlight by impervious surfaces[102].

Calculation of Normalized Difference Water Index (NDWI)

The NDWI spectral index is used to detect the presence of water in remote sensing images. An effective indicator of the liquid water content of vegetation, NDWI is less susceptible to atmospheric scattering effects[154]. Developed by McFeeters (1996), NDWI maximizes the reflectance of water by using the green wavelength, while minimizing the reflectance of vegetation and soil cover by using the near-infrared (NIR) wavelength. Therefore, the presence of water is determined by the difference between these two bands. NDWI is calculated using Equation (12)[155].

$$\mathrm{NDWI} = \frac{\mathrm{Green} - \mathrm{NIR}}{\mathrm{Green} + \mathrm{NIR}}, \tag{12}$$

Band 2 and band 4 for Landsat 5 TM and Landsat 7 ETM+, respectively; band 3 and band 5 were used for Landsat 8 OLI/TIRS. The value of the index ranges from -1 to

+1. While water features have positive values, soil and vegetation features have zero or negative values[156]. In order to establish the relationship between NDWI and SUHI, it is important to analyze water availability and temperature changes, especially in urban areas.

Calculation of Albedo

Developed by Liang (2001)[158], Albedo is defined as the reflection of solar radiation in all reflective wavelengths by the surface. Albedo satellite images are calculated with Equation (13) and using blue (ρ_1), red (ρ_2), NIR (ρ_3), SWIR1 (ρ_4), and SWIR2 (ρ_5) bands.

$$\text{Albedo} = \frac{0.356\rho_1 + 0.130\rho_2 + 0.373\rho_3 + 0.085\rho_4 + 0.072\rho_5 - 0.0018}{0.356+0.130+0.373+0.085+0.072}, \qquad (13)$$

The relationship between LST and albedo is negative. Albedo refers to how much a surface reflects sunlight. Colors affect the albedo of a surface. Light-colored surfaces (e.g., white sand, snow) have high albedo, reflecting a large proportion of sunlight, and therefore usually result in low LST values. On the other hand, dark-colored surfaces (e.g. black asphalt) absorb most of the sunlight and therefore have low albedo. Such surfaces can result in higher LST values because the energy from sunlight is largely absorbed and the surface temperature increases[157]. As a result, the color of surfaces is a critical factor in determining albedo values and hence LST.

Blue, red, NIR, SWIR1, and SWIR2 bands are used for the Equation (13). For Landsat 5 TM and Landsat 7 ETM+, these bands are 1, 3, 4, 5, and 7, respectively. For Landsat 8 OLI/TIRS, these are bands 2, 4, 5, 6, and 7. Albedo value varies between 0 and 1. While high albedo values result in low LST values, low albedo values result in high LST values due to absorption[158]. In nature, albedo values cannot approach the 0 and 1 limits. A value of 0.90 is typical for snowy surfaces and values around 0.10 are typical for dark asphalt pavements. The range 0.06-0.10 represents oceans with low albedo and the range 0.80-0.90 represents glaciers with high albedo. The 0.15-0.30 albedo range refers to vegetation, forests and green areas, while the 0.12-0.35 albedo range is usually urban areas. Surfaces with high albedo reflect more sunlight, absorb less heat and have lower temperatures. Therefore, the relationship between Albedo and SUHI is important in this respect[159].

4.2. Assessment of the LST's Relationship with LULC Change and Spectral Indices

The relationships between LST data and LULC, and spectral indices in SUHI effect were determined. Zonal Statistic, Correlation, and Regression analysis methods were used when determining relationships. Spectral indices and LULC values obtained as a result of the analysis were examined.

4.2.1. Assessment of the Relationship between LST and LULC Changes

Zonal statistics involve summarizing the properties of raster cells that intersect or fall within specified regions or polygons. These statistics are commonly used in GIS for analyzing spatial data within defined geographic areas[160]. They are widely employed in various fields such as environmental sciences, geographic analysis, agriculture, ecology, urban planning, and natural resource management. In remote sensing studies, zonal statistics are frequently used to perform statistical analysis of data properties within specified regions or polygons. This statistical method typically operates with raster databases, such as satellite images. Zonal statistics involve mapping each pixel of a raster image to a geographic attribute or value[161]. As a result, statistical summaries such as mean, minimum, maximum, etc., of the data values collected within a specific area (zone) are calculated[160].

In this context, "Zonal Statistic Tool" in the ArcGIS environment was used to evaluate the relationship between LST and LULC changes in the study area. The raster layer containing LST data and LULC polygon layer was used as input. For each LULC class, mean LST values in 1990, 2000, 2006, 2012, and 2018 and their changes according to these years were calculated.

4.2.2. Assessment of the Relationship between LST and Spectral Indices

In studies investigating the formation of UHI, correlation and regression analysis are frequently used to determine the relationship between variables and the effect of a variable on other variables.

To evaluate the relationships between LST and spectral indices, regression and correlation analyses were conducted based on the most recent year (2018) in the study. For the analysis, random points were assigned to the study area with the simple random sampling method. The randomly selected points cover urban areas with varying land use types representing different parts of the city, including regions with higher population density, various land use types across the city, and areas transitioning from the city center towards the outskirts. Therefore, the available number of cases within the study area is 1078. In ArcGIS environment, the "Extract Values to Point" tool extracts the cell values of 1078 random points on the raster images created with spectral indices. IBM-SPSS Statistic program was used for the analysis of the values recorded in the attribute table and the relationship between spectral indices was analyzed.

To measure the strength and direction of the linear relationship between LST and spectral indices variables, Pearson Correlation Analysis was used to calculate the correlation (r) between the variables. MLR analysis- stepwise multiple regression was used to estimate the effects of spectral indices on SUHI. While the spectral indices used in the study are our independent variables, LST was included in the analysis as the dependent variable.

Correlation is the relationship between two or more variables. Correlation analysis is a statistical technique used to test the relationship between two variables and to measure the direction and strength of this relationship, if any. The main purpose of correlation analysis is to explain how the dependent variable will change when the independent variable changes[162]. However, correlation does not establish a cause-and-effect relationship between two variables and does not indicate that the cause of one variable is the other variable[163].

There are two different correlation coefficients used in correlation analysis, Pearson's Product Moment Correlation Coefficient (for linearly distributed variables) and Spearman's Rank Correlation Coefficient (for non-linearly distributed variables[163]. As a result of correlation analysis, the presence of linear relationships and the degree of these relationships are calculated by the correlation coefficient. The correlation coefficient is denoted by "r" and takes values ranging from -1 to +1 as shown in Table 17[162,164].

Table 17. The scale of Correlation Coefficient

(From Selvanathan et al[165])

Pearson's Correlation Coefficient	**Interpretation**
$0 < r \leq 0.19$	Very Low Correlation
$0.2 \leq r \leq 0.39$	Very Correlation
$0.4 \leq r \leq 0.59$	Moderate Correlation
$0.6 \leq r \leq 0.79$	High Correlation
$0.8 \leq r \leq 1.0$	Very High Correlation

A correlation coefficient of "0" means no linear relationship, while a correlation coefficient of "1" is considered a perfect correlation. If the values of both variables tend to increase or decrease together, this indicates a positive correlation and they have positive "r" values. If the value of one of the variables increases while the other decreases, that is, if there is an inverse relationship between the variables, this indicates a negative correlation and they have negative "r" values. The correlation's direction, type and strength can also be evaluated through the scatterplot of the correlation coefficient (r). The graph also allows us to determine whether there is anything that may distort the correlation, such as outliers[164].

Regression analysis is used to measure the cause-and-effect relationship between two or more variables[163]. In other words, it is an attempt to express the effect of one or more independent variables on a dependent variable. First of all, regression analysis is divided into linear regression analysis and non-linear regression analysis according to the linearity of the relationship between variables. In addition, according to the number of variables, it is divided into two as simple regression analysis (one dependent, one independent variable) and multiple regression analysis (more than one independent, one dependent variable)[162]. There are three types of multiple regression. These are; Standard Multiple Regression, Hierarchical MLR, and Stepwise Multiple Regression[163].

In this study, MLR was used because the relationship between variables is linear and has more than one independent variable. MLR, a statistical technique, uses two or more independent variables to predict the outcome of a dependent variable. The stepwise method, which determines the selection of independent variables in the model in regression analysis, evaluates the effects of potential independent variables in the model. Thanks to this method, model selection is made by testing the significance of the model after each variable is added[166]. MLR analysis, which is based on various assumptions, is used to ensure that the regression model works correctly and to assess the reliability of the results obtained. According to Brien and Scott[163], and Taylor[167], the assumptions of regression analysis are explained step by step below.

Assumption 1) A linear relationship between the dependent and independent variables: MLR looks at linear relationships. There should be a linear relationship between the dependent variable and each of the independent variables. The visuals of the scatterplots of each variable should be examined for linearity.

Assumption 2) The independent variables are not highly correlated with each other (Multicollinearity): The fact that the Pearson correlation coefficient of the independent variables is greater than 0.90 indicates that there is a multicollinearity problem. The independent variables influence each other so much that the impact on the dependent variable cannot be clearly read. Assumptions are tested with the Variance Inflation Factor (VIF) method.

Assumption 3) The variance of the residuals is constant (Homoscedasticity): For each value of the dependent variable, the variance of the independent variables should be equal. We can check the relationship between the dependent variable and each variable with scatterplots.

Assumption 4) Independence of observation: The model emphasizes that outliers have a strong influence on the regression equation. This assumption is tested in the early stage of the analysis using scatterplots or the Durbin Watson statistic.

Assumption 5) Multivariate normality: Variables should be normally distributed. This assumption is tested through Normal P-P plot and histogram graphs.

4.3. Assessment of LST with Different Built Environment Texture

In order to address the SUHI effect in the study area more comprehensively, a comparison was made according to the characteristics of the built-up indices, spectral indices, and LULC.

There are many built-up indices as urban parameters that contribute to the SUHI effect. These parameters are population density, building height, land use, infrastructure, and economic activities. This study tries to answer the question "What findings emerge from comparing LST values with built-up indices as urban parameters?". In this context, built-up indices, especially LST, LULC, and spectral indices play an important role in determining the temperature profile of the built environment and determining the urban parameters that contribute to the formation of SUHI.

Cao et al.'s (2011)[168] study suggests that green spaces larger than 2 hectares have a significant cooling effect. Therefore, one of the indices in the study was determined as green areas larger than 2 ha (Figure 19). Built-up indices examined; population density, building area density, mean floor height, and surrounding green areas larger than 2 ha. Examined spectral indices; LST, NDVI, NDWI, NDBI, UI, and albedo.

In this context, five representative regions of 100 hectares were selected from the study area for 2018 (Figure 25). While determining the representative regions, attention was paid to select areas with high population density and different LST values and LULC classes.

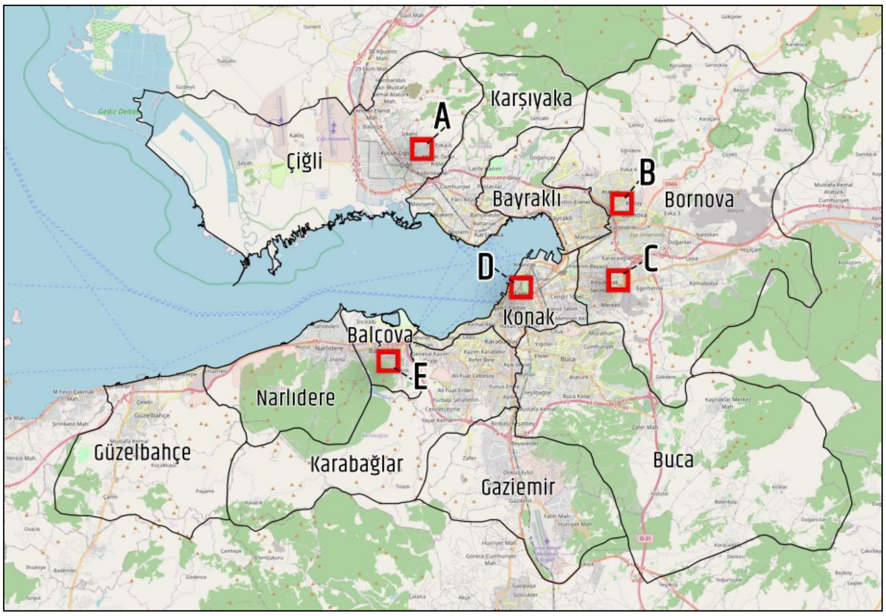

Figure 25. Selection of representative regions

In determining the population in the selected regions, it was assumed that there were an average of 3 apartments on each floor, and the number of household size living in each apartment building (number of floors x 3) was found. The mean number of household size in the district where the population of the region is located (Figure 21) was multiplied by the number of household size in each apartment. As a result, the approximate value of the number of inhabitants in the region was obtained. The population of a building is found by multiplying the total number of households in each building by the average household size in the district where it is located. Approximately the population in the region was obtained by the sum of the populations found for each building. According to the standard published in the İzmir Metropolitan Municipality Building Bylaws[169], each floor must be at least 3.60 meters. Therefore, the building height is obtained by multiplying the number of floors by 3.60 meters.

4.4. Assessment of Air Temperature and LST Values

Assessing the relationship between air temperatures based on meteorological data and surface temperatures measured by LST can help determine how UHI impacts change over time and how they affect air temperatures. The points of meteorological stations only correspond to one or a few pixels on LST images. Since this is insufficient for the assessment, a comparison between LST values and air temperatures for the location of weather stations within a given buffer area should be made. In the studies, various buffer sizes were used depending on the scale difference. Krüger and Givoni[170] used a fixed buffer size of 125 meters in their study and Yokobori and Ohta[171] used a fixed buffer size of 300 meters in their study. In some studies, ranges were determined to determine the buffer width. Yan et al.[172] determined buffers between 20 and 300 meters in their study, and Johnson et al.[173] determined buffers between 50 and 1000 meters in their study. Considering the studies conducted to determine the buffer size, correlation analysis was performed on buffers of five different sizes starting from 100 meters. As a result of the analysis, LST and air temperatures were compared, taking into account the buffer size with the highest correlation coefficient.

The measured air temperature data for all years used in the study can be evaluated for only two stations (İzmir Bölge and İzmir Adnan Menderes Havalimanı) out of fifteen stations taken from Meteorological stations. In order to compare LST and air temperature values, the region of two meteorological stations was determined. As a result of the correlation analysis for the determined region, LST values were created according to the buffer that provided high correlation. The average air temperatures of two stations on certain days in 1990, 2000, 2006, 2012, and 2018 were compared with the average LST values covering the buffer zone at the specified distance. In 2018, with the availability of air temperature data at fifteen different stations, LST values for 2018 for each station were created according to the determined buffer zone distance. The trend between LST values generated per station and air temperatures was analyzed.

CHAPTER 5

RESULTS

5.1. Land Surface Temperature (LST) Maps

Within the scope of the study, LST maps of the study area for the years 1990, 2000, 2006, 2012, and 2018 were created using Landsat 5 TM, Landsat 7 ETM+, and Landsat 8 OLI/TIRS satellite images. It is seen that the minimum and maximum LST values calculated from Landsat satellite images vary between 15.7 ºC and 48.2 ºC. Maps of LST values converted from K to °C unit are shown in Figure 27.

Considering the maximum and minimum values of the LST maps in five years, classification was made with 4°C intervals. In addition, the graph of the minimum, maximum, and mean values calculated from all images is given in Figure 26. When the values are examined, the maximum temperature of 48.2 ºC was calculated from the images of 2012 and the minimum temperature of 15.7 ºC was calculated from the images of 2006. It was determined that the average temperature value of all years was minimum 30.9 ºC and maximum 32.8ºC (Figure 26).

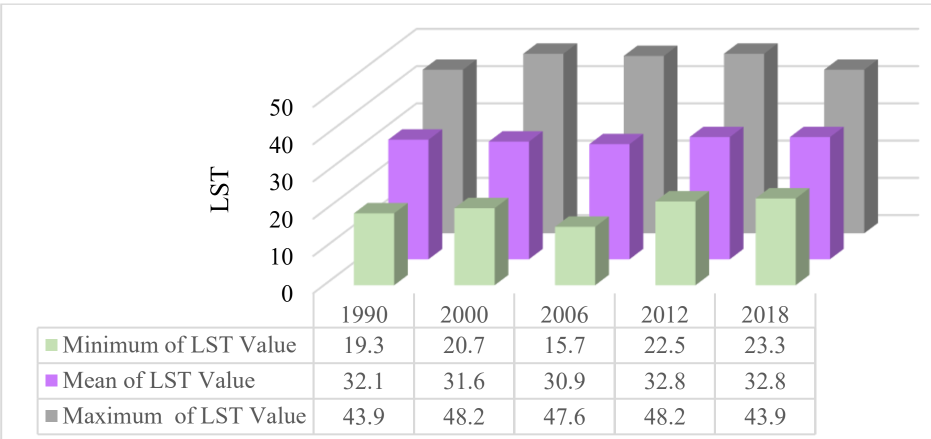

Figure 26. Minimum, maximum, and mean values of LST

LST maps in Figure 27 reveal that the decrease in the LST value in 2006 is greater than the LST values in 1990, 2000, 2012, and 2018. In addition, when the map in 2018 is compared with the maps of other years and the increase in the LST value is greater than the changes in other years. Especially in 2006, the lowest LST value (15.7ºC) was observed in Narlıdere district compared to other years. In 2018, it is determined that the LST values of Çiğli district are higher than other districts. This may be due to the fact that there are "Industrial, Commercial and Transport Units" in the region where the LST value is high.

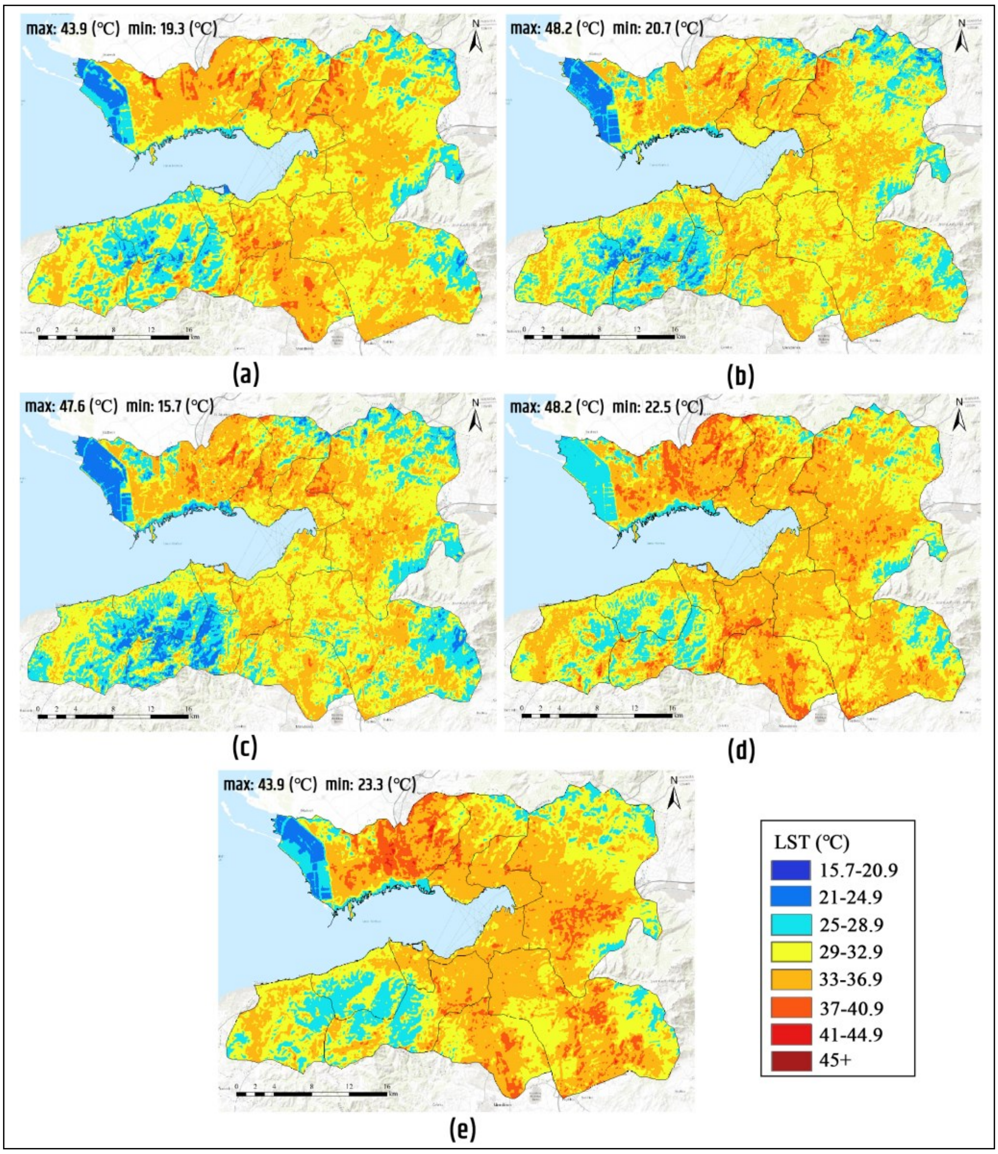

Figure 27. LST maps produced from Landsat images for the years (a) 1990, (b) 2000, (c) 2006, (d) 2012, (e) 2018

5.2. Land Use/Land Cover (LULC)

When the LULC analysis of the years 1990, 2000, 2006, 2012, and 2018 were evaluated, changes are observed in all classes of CORINE Land Cover. Particularly, the most changes are observed in the "Urban Fabric", "Industrial, Commercial, and Transport Units", and "Heterogeneous Agricultural Areas" areas (Table 18).

When Table 18 is examined, the LULC hectares in central districts with the highest total spatial percentage and hectare value are respectively; "Shrub and/or Herbaceous Vegetation Associations", "Forests", "Urban Fabric", "Heterogeneous Agricultural Areas", and "Industrial, Commercial, and Transport Units" areas. "Inland Waters", "Marine Waters", and "Pastures" areas have the lowest total spatial percentage and hectare value within the study area.

From 1990 to 2018, the "Urban Fabric" and "Industrial, Commercial, and Transport Units" areas increased by 4.85% and 6.5%, respectively, reaching 15122 and 9686 hectares in 2018. However, the "Forest Area" increased by only 0.82%. In 2018, the majority of the study area consisted of "Shrub and/or Herbaceous Vegetation Associations Area" (23.75%), "Forests Area" (23.73%), "Urban Fabric" (16.01%), "Heterogeneous Agricultural Areas" (12.54%), and "Industrial, Commercial, and Transport Units" (10.26%).

Table 18. Area Sizes of Study Area According to CORINE Land Cover Classification (Adapted from Copernicus Land Monitoring Service (CORINE)[126])

CORINE Land Cover	Unit	Years				
		1990	2000	2006	2012	2018
1.1 Urban Fabric	Hectare	10535	14164	14529	14988	15122
	%	11.16	15	15.38	15.87	16.01
1.2 Industrial, Commercial and Transport Units	Hectare	3551	6672	8941	9514	9686
	%	3.76	7.06	9.47	10.07	10.26
1.3 Mine, Dump and Construction Sites	Hectare	1400	2059	1985	1404	1514
	%	1.48	2.18	2.10	1.49	1.60
1.4 Artificial, Non-Agricultural Vegetated Areas	Hectare	1029	1225	632	612	631
	%	1.09	1.30	0.67	0.65	0.67
2.1 Arable Land	Hectare	4583	2935	3698	3652	3652
	%	4.85	3.11	3.92	3.87	3.87

(cont. on next page)

Table 18. (cont.)

2.2 Permanent Crops	Hectare	1859	1806	1104	663	663
	%	1.97	1.91	1.17	0.70	0.70
2.3 Pastures	Hectare	657	1402	369	344	344
	%	0.70	1.48	0.39	0.36	0.36
2.4 Heterogeneous Agricultural Areas	Hectare	18013	13380	12923	11991	11841
	%	19.07	14.17	13.68	12.70	12.54
3.1 Forests	Hectare	21635	19581	22475	22987	22408
	%	22.91	20.73	23.80	24.34	23.73
3.2 Shrub and/or Herbaceous Vegetation Associations	Hectare	24552	25027	21412	22023	22429
	%	26.00	26.50	22.67	23.32	23.75
3.3 Open Spaces with Little or No Vegetation	Hectare	2755	2683	2826	2695	2583
	%	2.92	2.84	2.99	2.85	2.74
4.2 Coastal Wetlands	Hectare	3608	3398	3443	3448	3448
	%	3.82	3.60	3.64	3.65	3.65
5.1 Inland Waters	Hectare	79	33	32	32	32
	%	0.08	0.04	0.03	0.03	0.03
5.2 Marine Waters	Hectare	184	75	71	87	87
	%	0.19	0.08	0.07	0.09	0.09
Total Area	Hectare	94440	94440	94440	94440	94440
	%	100	100	100	100	100

The increase and decrease in land cover change between 1990-2000, 2000-2006, 2006-2012, and 2012-2018 are given in Table 19. Overall, between the years, the areas of “Urban Fabric” and “Industrial, Commercial, and Transport Units” increased, while “Arable Land”, “Pastures”, “Permanent Crops”, “Heterogeneous Agricultural Areas”, and “Inland Waters” areas decreased. The highest increase in the “Urban Fabric” and “Industrial, Commercial, and Transport Units” areas is observed during 1990-2000. The highest decrease in the “Arable Land” and “Heterogeneous Agricultural Areas” areas occurred during 1990-2000. Between 2000 and 2006, the highest decrease is observed in the “Pastures” and “Permanent Crops” areas. The forest area decreased by 2.18% between 1990 and 2000. However, no change is observed in six out of fourteen classes in 2012-2018." Numerical values belonging to Table 19 are spatially represented in Figure 28.

Table 19. Changes in the Area Sizes of Central Districts of İzmir, According to the CORINE Land Cover Classification in the Determined Years

(Adapted from Copernicus Land Monitoring Service (CORINE)[126])

CORINE Land Cover Classification	**Unit**	**Central Districts of İzmir**			
		Change Between Years			
		1990-2000	**2000-2006**	**2006-2012**	**2012-2018**
1.1 Urban Fabric	Hectare	3629	365	459	134
	%	3.84	0.38	0.49	0.14
1.2 Industrial, Commercial and Transport Units	Hectare	3121	2269	573	172
	%	3.30	2.41	0.60	0.19
1.3 Mine, Dump and Construction Sites	Hectare	659	-74	-584	110
	%	0.70	-0.08	-0.61	0.11
1.4 Artificial, Non-Agricultural Vegetated Areas	Hectare	196	-593	-20	19
	%	0.21	-0.63	-0.02	0.02
2.1 Arable Land	Hectare	-1648	763	-46	0
	%	-1.74	0.81	-0.05	0
2.2 Permanent Crops	Hectare	-53	-702	-441	0
	%	-0.06	-0.74	-0.47	0
2.3 Pastures	Hectare	745	-1033	-25	0
	%	0.78	-1.09	-0.03	0
2.4 Heterogeneous Agricultural Areas	Hectare	-4633	-457	-932	-150
	%	-4.90	-0.49	-0.98	-0.16
3.1 Forests	Hectare	-2054	2894	512	-579
	%	-2.18	3.07	0.54	-0.61
3.2 Shrub and/or Herbaceous Vegetation Associations	Hectare	475	-3615	611	406
	%	0.50	-3.83	0.65	0.43
3.3 Open Spaces with Little or No Vegetation	Hectare	-72	143	-131	-112
	%	-0.08	0.15	-0.14	-0.11
4.2 Coastal Wetlands	Hectare	-210	45	5	0
	%	-0.22	0.04	0.01	0
5.1 Inland Waters	Hectare	-46	-1	0	0
	%	-0.04	-0.01	0	0
5.2 Marine Waters	Hectare	-109	-4	16	0
	%	-0.11	-0.01	0.02	0

When the LULC change is examined within twenty-nine years, the most change is observed between 1990-2000, and the least change is observed between 2012-2018. However, changes in specific classes are observed between 2000 and 2012 (Figure 28). Fiure 29 shows to which classes the changes of Figure 28 belong.

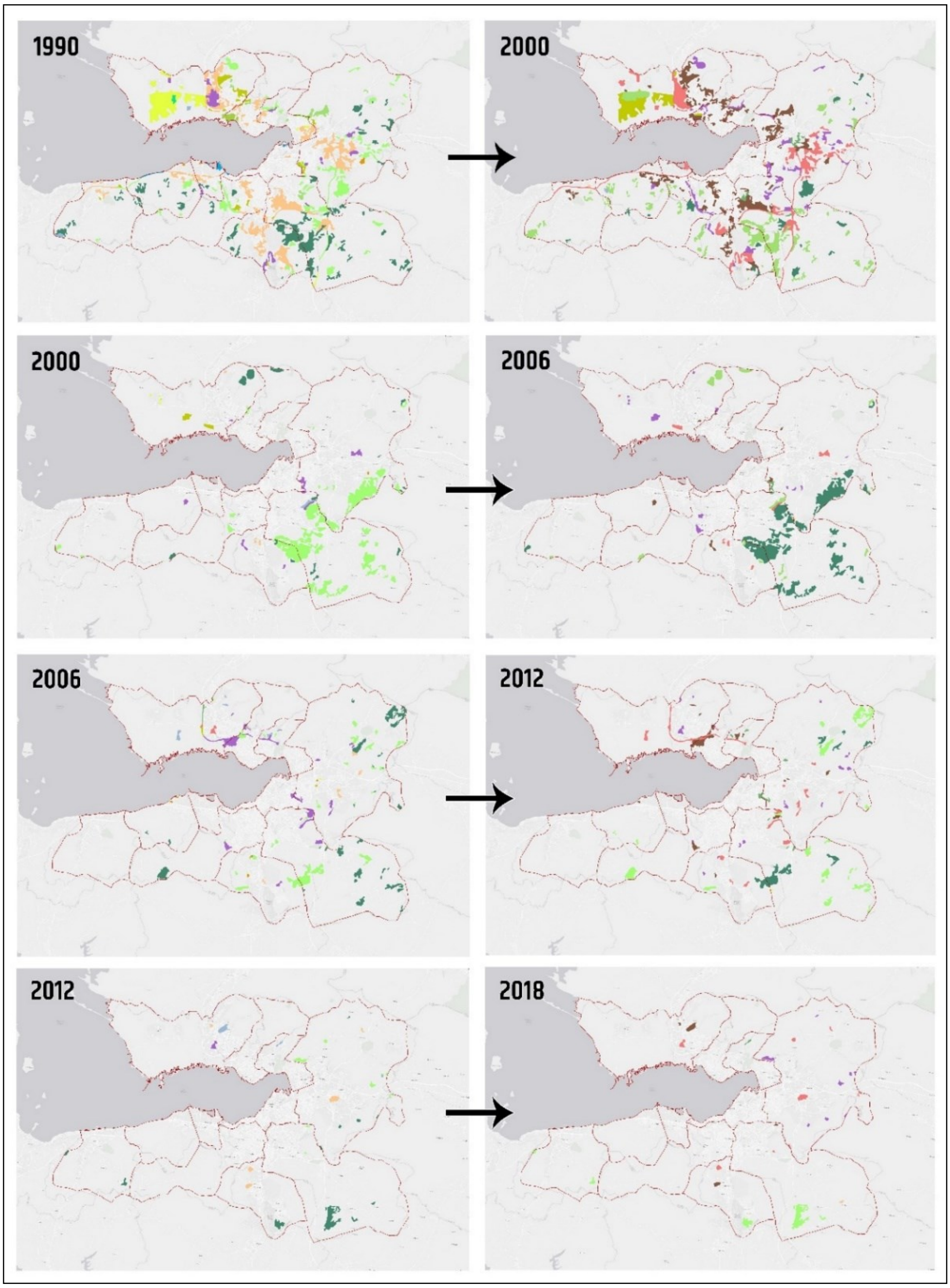

Figure 28. Changes of study area, according to the CORINE land cover classification in the determined years

(Adapted from Copernicus Land Monitoring Service (CORINE)[126])

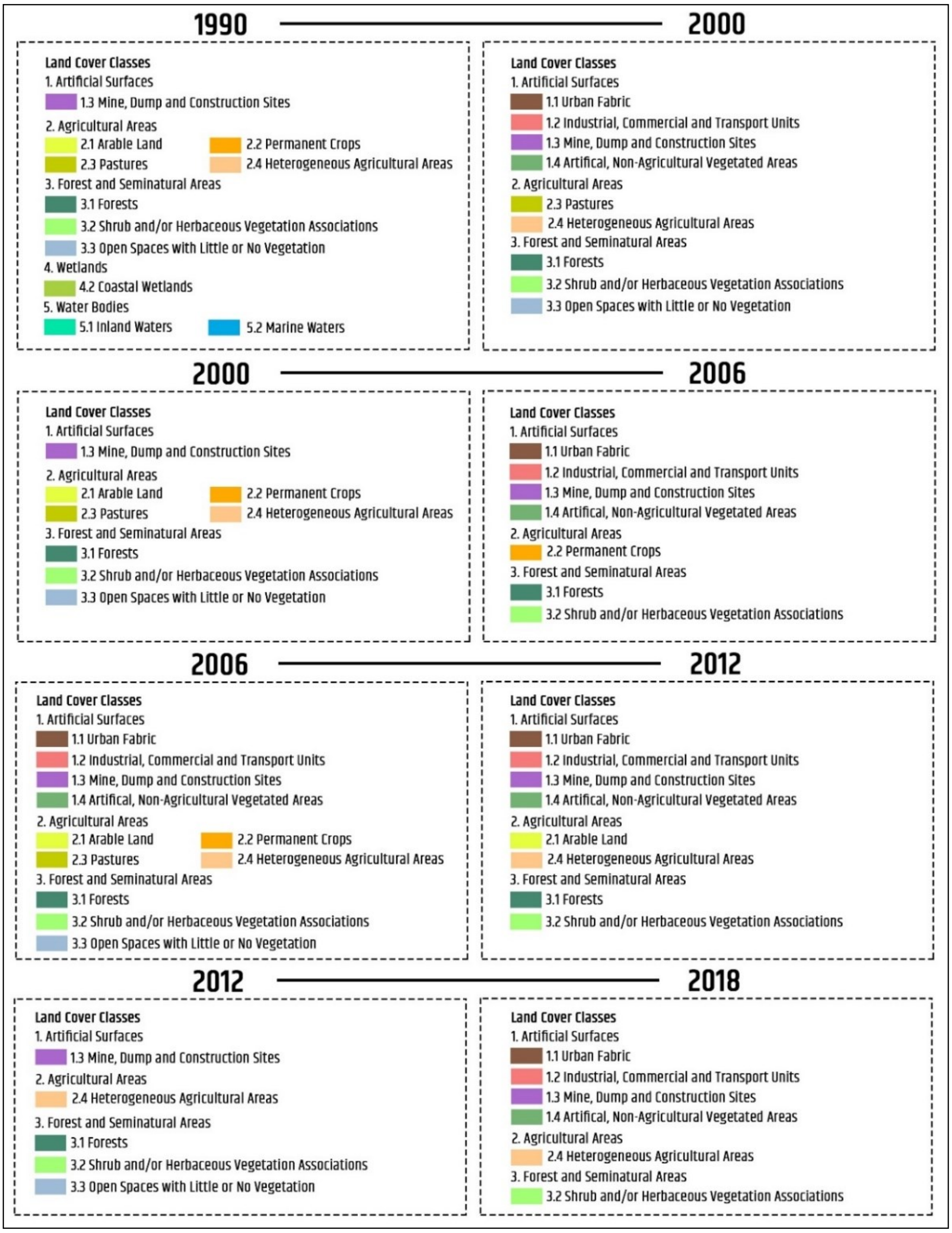

Figure 29. Legends of changes according to the CORINE land cover classification in the determined years

(Adapted from Copernicus Land Monitoring Service (CORINE)[126])

Between 1990-2000:

- The “Arable Land” area has transformed into “Pastures”, “Shrub and/or Herbaceous Vegetation Associations”, “Urban Fabric”, and “Industrial, Commercial, and Transport Units” areas.

- The “Forests” area has transformed into “Shrub and/or Herbaceous Vegetation Associations”, and vice versa.

- “Pastures”, “Permanent Crops”, “Shrub and/or Herbaceous Vegetation Associations”, and “Heterogeneous Agricultural Areas” areas have transformed into the “Urban Fabric” area.

- “Marine Waters”, “Mine, Dump, and Construction Sites”, and “Heterogeneous Agricultural Areas” areas have transformed into the “Industrial, Commercial, and Transport Units” area.

- “Forests” and “Shrub and/or Herbaceous Vegetation Associations” areas have transformed into “Mine, Dump, and Construction Sites” areas.

- The highest rate of change occurred at 20.6% from “Forests (3.1)” to “Shrub and/or Herbaceous Vegetation Associations (3.2)”, and 17.7% from “Heterogeneous Agricultural Areas (2.4)” to “Urban Fabric (1.1)”, respectively.

The districts with the most change are Çiğli, Buca, Bornova, and Gaziemir.

Between 2000-2006:

- The “Forests” area has transformed into “Shrub and/or Herbaceous Vegetation Associations”, and vice versa.

- “Arable Land” and “Pastures” areas have transformed into “Mine, Dump, and Construction Sites”.

- “Open Spaces with Little or No Vegetation” area has transformed into “Shrub and/or Herbaceous Vegetation Associations”.

- “Mine, Dump, and Construction Sites” area has transformed into the “Urban Fabric” area.

- “Pastures” and “Mine, Dump, and Construction Sites” areas have transformed into the “Industrial, Commercial, and Transport Units” area.

- The highest rate of change occurred at 73.9% from “Shrub and/or Herbaceous Vegetation Associations (3.2)” to “Forests (3.1)”.

The most change is observed in the use of “Shrub and/or Herbaceous Vegetation Associations”. There were no changes in the Konak, Balçova, and Bayraklı districts.

Between 2006-2012:

- The “Forests” area has transformed into “Shrub and/or Herbaceous Vegetation Associations”, and vice versa.

- “Mine, Dump, and Construction Sites” area has transformed into the “Urban Fabric” and “Industrial, Commercial, and Transport Units” areas.

- “Permanent Crop’" area has transformed into the “Urban Fabric” area.

- The highest rate of change occurred at 31.4% from “Forests (3.1)” to “Shrub and/or Herbaceous Vegetation Associations (3.2)”.

No LULC change is observed in Güzelbahçe and Balçova districts. There was minimal LULC change in the Konak, Karabağlar, and Narlıdere districts.

Between 2012-2018:

- In the Çiğli district, “Heterogeneous Agricultural Areas” and “Open Spaces with Little or No Vegetation” areas have transformed into the “Urban Fabric” area.

- The “Mine, Dump, and Construction Sites” area has transformed into the “Industrial, Commercial, and Transport Units” area in Gaziemir and Bornova districts.

- In Buca, Gaziemir, and Güzelbahçe districts, the “Forests” area has transformed into the “Shrub and/or Herbaceous Vegetation Associations” area.

- In Gaziemir and Bornova districts, the “Heterogeneous Agricultural Areas” area has transformed into the “Urban Fabric” and “Industrial, Commercial, and Transport Units” areas.

- In the Bornova district, the “Shrub and/or Herbaceous Vegetation Associations” area has transformed into the “Industrial, Commercial, and Transport Units” and “Mine, Dump, and Construction Sites” areas.

- In the Bayraklı district, the “Open Spaces with Little or No Vegetation” area has transformed into the “Artificial, Non-Agricultural Vegetated Areas” area.

- The highest rate of change occurred at 43.9% from “Forests (3.1)” to “Shrub and/or Herbaceous Vegetation Associations (3.2)”.

There was no LULC change in the Karşıyaka, Konak, Karabağlar, Narlıdere, and Balçova districts.

5.3. Assessment of the Relationship between LST and LULC Changes

In this part of the study, the obtained LST values and the relationship of these values with LULC were examined. According to the evaluation results, the average LST values of LULC classes in the period from 1990 to 2018 increased in almost all land classes. When the relationship between LST values and LULC classes is examined, the lowest LST values are in “Marine Water” and “Forests” respectively; the highest LST values are observed in the “Pastures Areas”, “Arable Land”, “Industrial, Commercial and Transport Units Area”, “Mine, Dump and Construction Sites Area”, and “Urban Fabric” area respectively (Table 20).

Table 20. LST Change of LULC Areas of Study Area for the Years 1990, 2000, 2006, 2012 and 2018

CORINE Land Cover Classes	Land Surface Temperature (LST)									
	Mean (°C)					Standard Deviation				
	1990	2000	2006	2012	2018	1990	2000	2006	2012	2018
1.1 Urban fabric	32.8	32.8	32.5	34.0	34.6	1.68	1.41	1.72	1.41	1.40
1.2 Industrial, commercial and transport units	33.1	33.5	33.5	35.2	35.5	1.97	1.71	2.17	1.84	2.06
1.3 Mine, dump and construction sites	33.0	33.0	33.6	35.5	35.4	2.09	1.76	2.23	1.64	1.82
1.4 Artificial, non-agricultural vegetated areas	33.4	32.7	32.8	33.6	34.3	1.88	1.82	1.92	1.63	1.72
2.1 Arable land	34.0	31.7	32.4	34.5	34.6	1.92	2.43	2.81	2.70	2.54
2.2 Permanent crops	30.1	30.6	31.1	32.7	32.9	1.37	1.44	1.64	1.45	1.48
2.3 Pastures	35.2	33.5	36.1	37.0	38.6	2.04	1.71	1.45	1.23	1.60
2.4 Heterogeneous agricultural areas	33.5	32.8	32.1	33.9	33.8	2.12	2.14	2.27	1.99	2.15
3.1 Forests	29.5	29.0	28.1	30.1	29.9	2.39	2.19	2.29	2.06	2.12
3.2 Scrub and/or herbaceous vegetation associations	33.5	32.9	32.3	34.1	33.3	2.50	2.44	2.58	2.35	2.31
3.3 Open spaces with little or no vegetation	33.0	32.7	33.3	34.6	34.5	1.65	1.62	3.06	2.77	3.13
4.2 Coastal Wetlands	27.4	27.1	25.6	27.4	26.6	2.19	1.97	2.46	1.89	1.96
5.1 Inland waters	32.6	28.2	23.7	26.9	26.4	2.91	1.81	0.92	1.12	0.80
5.2 Marine waters	26.3	27.8	26.10	28.34	28.11	2.6	1.30	1.94	1.68	1.87
Mean LST for study area	32.07	31.56	30.94	32.82	32.76	2.79	2.67	3.04	2.67	2.87

It is observed that LST values in LULC areas increase due to the growth of "Urban Fabric, "Industrial, Commercial and Transport Units Area", and "Open Spaces with Little or No Vegetation Areas" over time. It has been determined that LST values have decreased over time due to the decrease in "Inland Waters" areas. However, it is concluded that although the size of the pasture areas decreased, the LST values increased. "Pastures" areas attract more sunlight because they generally have a flat and open surface. Accordingly, it is thought that pasture areas increase the LST value. When the change in the SUHI effect between 1990, 2000, 2006, 2012, and 2018 is examined, it is concluded that the SUHI effect increased by approximately 0.2 °C in the study area.

When the standard deviation results are evaluated, it is seen that the LST values in the LULC classes, especially for the years 2006 and 2018, are higher, that is LST values in 2006 and 2018 showed higher variability than other years. There may be several reasons for this. LULC in a given region may have changed over time. Climate changes can have significant impacts on surface temperature. Between 2006 and 2018, there may have been a particularly pronounced climate change, which could be one reason for the increase in LST values. Different meteorological conditions (e.g. temperature, precipitation, wind) in different years can affect surface temperature. In 2006 and 2018, there may be significant changes in these factors. In order to evaluate this change, it needs to be analyzed together with environmental factors.

5.4. Assessment of Change in Spectral Indices as Urban Parameters

Spectral indices maps produced from Landsat images for 2018 are shown in Figure 30.

NDVI value of the study area in 2018 are between 0.59 and -0.35. These values on the NDVI image show the vegetation level in the study area. White tones represent high NDVI values, and black tones represent low NDVI values. It is seen that NDVI values are predominantly low in the study area. It has been observed that there are large areas with high NDVI values in the southwest of the study area. Narlıdere, Güzelbahçe, and the northern parts of Bornova have vegetation-rich areas. Çiğli Sasalı Zoo and

Balçova İnciraltı Urban Forest are also areas with very high NDVI values. The decrease in the NDVI value co-occurs with the increasing number of buildings in the city center.

NDWI values of the study area in 2018 are between 0.32 and -0.53. These values on the NDWI image show the water surfaces in the study area. White tones represent high NDWI values and black tones represent low NDWI values. Due to the Gediz Delta located in Çiğli, the highest NDWI value in the study area is seen in this region. Values are higher in Konak, Bornova, and Buca districts. The reason for this may be due to the ponds in Buca and Konak. Additionally, the presence of water in park areas also increases the NDWI value.

NDBI values of the study area in 2018 are between 0.34 and -0.46. These values on the NDBI image show the residential areas in the study area. White tones represent high NDBI values, and black tones represent low NDBI values. It has been observed that there are large areas with NDBI values in the study area. Since the NDBI value represents the regions with dense construction, the regions with forest areas are seen in black. Narlıdere and Güzelbahçe districts are calm areas. The increase in white color actually shows that the presence of green areas in those districts is decreasing. Especially green areas, should be increased in these areas.

UI values of the study area are between 0.37 and -0.58. These values on the UI image show urban areas in the study area. White tones represent high UI values, and black tones represent low UI values. It has been observed that there are large areas with UI values in the study area. UI is also similar to NDBI. It showed a similar distribution. Therefore, exclusion of parameters evaluating the same criteria in future studies may lead to more effective evaluations.

Albedo values of the study area are between 0.84 and 0.05. These values on the albedo image define the ability of surfaces in the study area to reflect light. White tones represent high albedo values, and black tones represent low albedo values. It has been observed that there are large areas with low albedo values in the study area. Looking at the albedo colors, it is actually expected that the centers of the districts would not be white. Especially these regions in the study area are the areas with high impervious surfaces. The presence of an industrial area in the Çiğli district causes high LST values and albedo values are very high in this district. On the contrary, low albedo values are expected due to the excess of impervious surfaces in industrial areas. This situation causes us to make wrong theoretical evaluations.

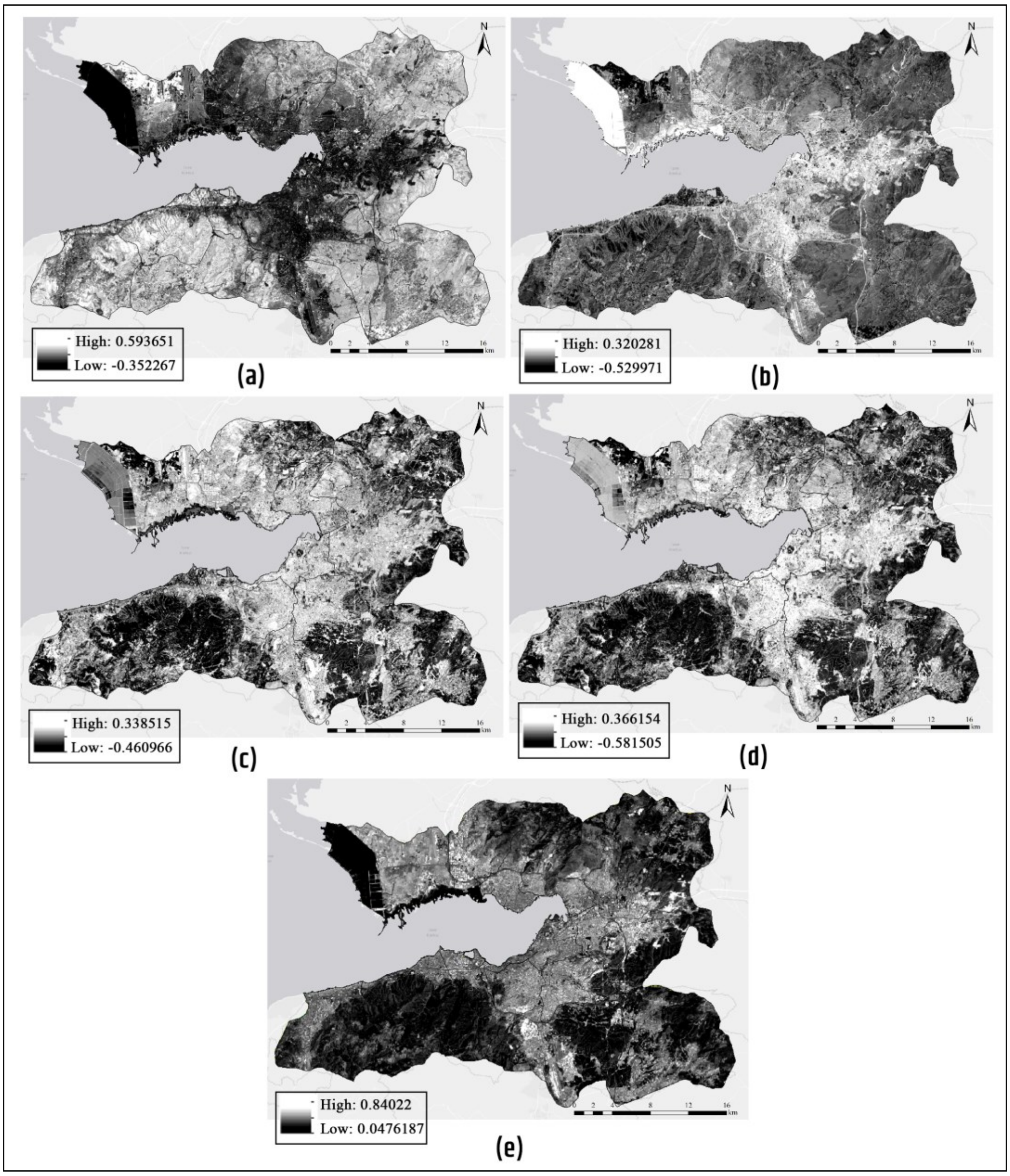

Figure 30. Spectral indices maps produced from Landsat images for the 2018 (a) NDVI, (b) NDWI, (c) NDBI, (d) UI, (e) Albedo

5.5. Assessment of the Relationship between LST and Spectral Indices

Another aspect investigated in this study is the relationship between LST and spectral indices as urban parameters. To assess these relationships, correlation and MLR were conducted. Correlation and Regression Analyses were computed using statistical data analysis methods in the IBM SPSS Statistics environment. To statistically demonstrate the strength of the linear relationship between variables, values of all LST and NDVI, NDWI, NDBI, UI, and albedo maps generated from Landsat images for the year 2018, the most recent year used in the study, were compared to 1078 randomly selected points within the study area. Correlation analysis, a fundamental statistical technique, was employed to examine the relationship between LST (dependent variable) and the selected spectral indices (independent variables). The Pearson correlation coefficient used in the study indicates the degree of linear relationship between variables.

The findings obtained from Pearson Correlation analysis are depicted in Table 21. According to the Pearson Correlation, the magnitude of numerical values represents the strength of the relationship between pairs of variables. Red hues signify a positive correlation, while blue hues indicate a negative correlation. As correlation values approach 1.0, the positive correlation between pairs strengthens, whereas a stronger negative correlation is observed as it approaches -1.0. Correlation values nearing 0 suggest a weak or no correlation between variable pairs. The presence of "**" indicates a statistically significant association at the 0.01 level (Table 21).

Table 21. Pearson Correlation (r) between LST with spectral indices for 2018

Correlations							
		LST	NDVI	NDWI	NDBI	UI	Albedo
Pearson Correlation	LST	**1.000**	**-0.664****	**0.512****	**0.776****	**0.749****	**0.665****
	NDVI	**-0.664****	**1.000**	**-0.936****	**-0.824****	**-0.912****	**-0.633****
	NDWI	**0.512****	**-0.936****	**1.000**	**0.678****	**0.800****	0.472**
	NDBI	**0.776****	**-0.824****	**0.678****	**1.000**	**0.968****	**0.698****
	UI	**0.749****	**-0.912****	**0.800****	**0.968****	**1.000**	**0.721****
	Albedo	**0.665****	**-0.633****	0.472**	**0.698****	**0.721****	**1.000**
Sig. (1-tailed)	LST	.	<.001	<.001	<.001	<.001	<.001
	NDVI	.000	.	.000	.000	.000	.000
	NDWI	.000		.	.000	.000	.000
	NDBI	.000		.000	.	.000	.000
	UI	.000		.000	.000	.	.000
	Albedo	.000		.000	.000	.000	.
N	LST	1078		1078	1078	1078	1078
	NDVI	1078		1078	1078	1078	1078
	NDWI	1078		1078	1078	1078	1078
	NDBI	1078		1078	1078	1078	1078
	UI	1078		1078	1078	1078	1078
	Albedo	1078		1078	1078	1078	1078
Pearson's r > 0.5 (bold), (**) Correlation is significant at 0.01 level. 99% confidence interval							

There exists a high-level and negative correlation between LST and NDVI ($r=-0.664$; $p<0.01$). This indicates that LST values tends to be high in areas with low NDVI, and low in areas with high NDVI values.

There is a moderate-level and positive correlation between LST and NDWI ($r=0.512$; $p<0.01$). This indicates that LST values tends to be high in areas with high NDWI, and low in areas with low NDWI values.

There is a high level of positive correlation between LST and NDBI ($r=0.776$; $p<0.01$). This indicates that LST values tends to be high in areas with high NDBI, and low in areas with low NDBI values.

There is a high level of positive correlation between LST and UI ($r=0.749$; $p<0.01$). This indicates that LST values tends to be high in areas with high UI, and low in areas with low UI values.

There is a high level of positive correlation between LST and Albedo ($r=0.665$; $p<0.01$). This indicates that LST values tends to be high in areas with high Albedo, and low in areas with low Albedo values. However, a negative relationship between LST and albedo is expected to be observed in theory. Because as the surface albedo increases, the ability of the surface to reflect sunlight increases. In this case, as the surface reflects more sunlight back, it receives less heat and this causes the surface temperature to decrease.

The relationship between the variables is also illustrated in the scatterplot in Figure 31.

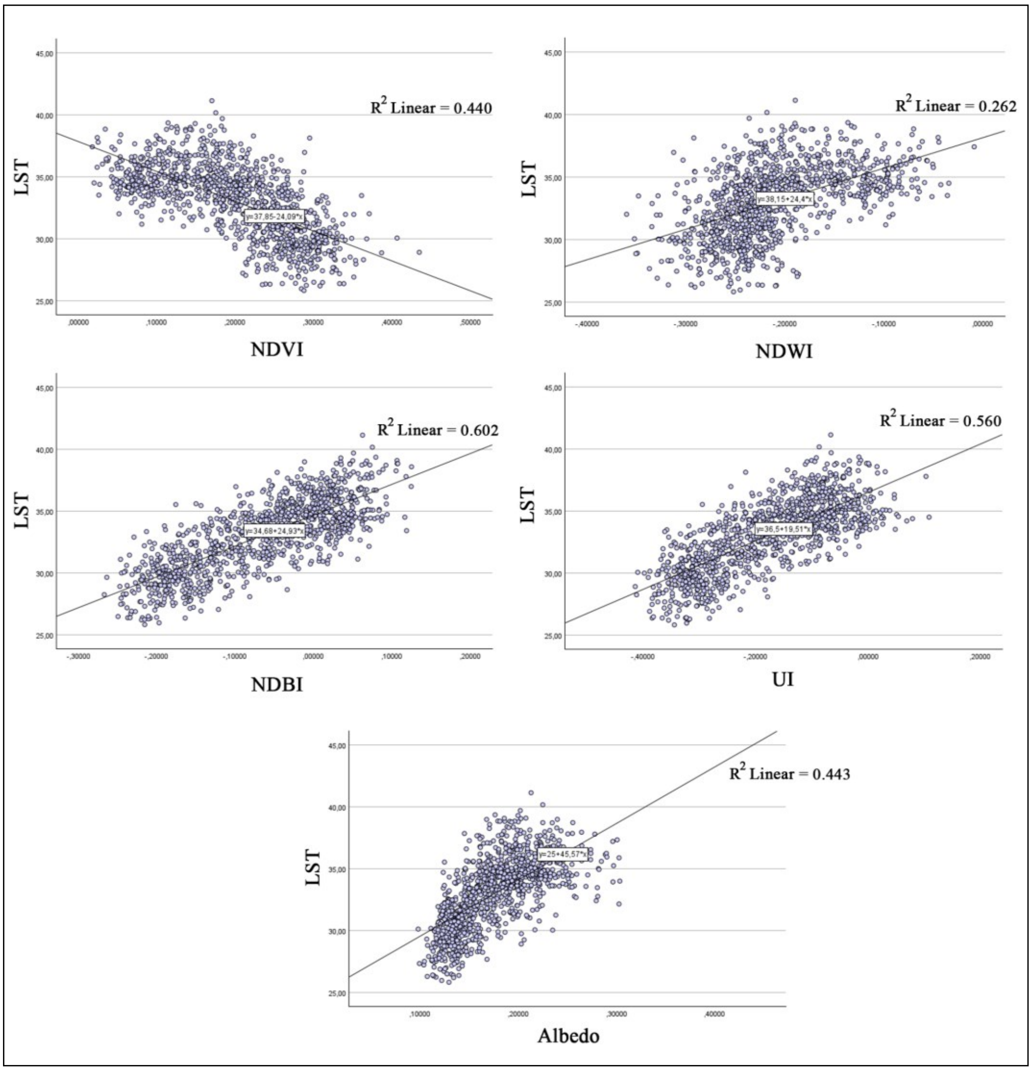

Figure 31. Scatterplots between LST with spectral indices as urban parameters for 2018

Most studies in the literature, assess the relationship between LST and spectral indices usually through correlation analysis. Studies by Tran et al. (2017), Daramola et al. (2018), and Tonyaloğlu (2019) indicate a negative relationship between LST and NDVI. Conversely, studies by Daramola et al. (2018), Khan et al. (2021), and Halder et al. (2021) suggest a positive relationship between NDBI, UI, and LST. Guha et al. (2020) and Yücer (2023) found a positive relationship between Albedo and LST. In the study by Nimish et al. (2020), a positive relationship is observed between NDBI and LST, while a negative relationship is noted between NDVI and NDWI. However, there is no single consensus regarding NDWI. Guha et al. (2020) reported a positive relationship between LST and NDWI, whereas Nimish et al. (2020) concluded a negative relationship between

LST and NDWI. These findings align with the results obtained within the scope of the thesis.

Understanding the correlations between the remote sensing indices used in the study and LST/SUHI is crucial. Indices contributing to SUHI formation should be identified, and strategies to mitigate SUHI effects should be developed.

MLR analysis examines the multivariate relationships between LST and independent variables. With this approach, it will be indicated through which parameters the SUHI effect can be interpreted when there is no LST available. Understanding how the SUHI effect in the absence of LST can vary under the influence of other independent variables is an outcome of regression analysis. Before starting regression analysis, assumptions should be evaluated. Thus, we ensure the accuracy and reliability of the regression analysis.

The first assumption is checked before regression analysis. The linear relationship between the dependent variable and independent variables is examined through scatter plots. Linearity is checked by creating a separate graph for the dependent variable and each independent variable. This process is conducted after correlation analysis (Table 21). Upon examining the graphs, a linear relationship between the dependent variable and independent variables is observed.

According to the stepwise regression method in MLR analysis, a step-by-step approach is used to determine the effects of potential independent variables in the model. At each step, the model's performance is evaluated, and statistically insignificant variables are eliminated, or new variables are added. Table 22 presents the coefficients table resulting from the stepwise regression method. Albedo was not included in the analysis owing to a positive correlation obtained contrary to theoretically reported negative relationship with LST, four models were formed additively for the independent variables NDVI, NDWI, NDBI, and UI, respectively. When examining the 'Standardized Coefficients Beta' column of the models, a negative relationship between LST and UI, and NDWI is inferred. However, they showed a positive correlation in the correlation analysis. Therefore, there is an inconsistency between correlation and regression analysis in data processing. To be on the safe side, it is considered reasonable to eliminate these variables.

Table 22.Table of Coefficients

Coefficients[a]											
Model		Unstandardized Coefficients		Standardized Coefficients	t	Sig.	Correlations			Collinearity Statistics	
		B	Std. Error	Beta			Zero-order	Partial	Part	Tolerance	VIF
1	(Constant)	34.679	0.068		508.592	<.001					
	NDBI	24.935	0.618	0.776	40.338	<.001	0.776	0.776	0.776	1.000	1.000
2	(Constant)	35.096	0.198		176.895	<.001					
	NDBI	22.926	1.089	0.713	21.052	<.001	0.776	0.540	0.404	0.321	3.115
	NDVI	-2.754	1.230	-0.076	-2.239	.025	-0.664	-0.068	-0.043	0.321	3.115
3	(Constant)	34.192	0.230		148.447	<.001					
	NDBI	18.872	1.201	0.587	15.713	<.001	0.776	0.432	0.295	0.252	3.972
	NDVI	-21.347	2.826	-0.588	-7.552	<.001	-0.664	-0.225	-0.142	0.058	17.244
	NDWI	-20.782	2.860	-0.436	-7.267	<.001	0.512	-0.216	-0.136	0.098	10.251
4	(Constant)	34.046	0.236		144.195	<.001					
	NDBI	26.677	3.174	0.830	8.404	<.001	0.776	0.249	0.157	0.036	27.900
	NDVI	-24.290	3.029	-0.669	-8.020	<.001	-0.664	-0.238	-0.150	0.050	19.911
	NDWI	-19.134	2.919	-0.402	-6.556	<.001	0.512	-0.196	-0.123	0.093	10.737
	UI	-8.963	3.376	-0.344	-2.655	.008	0.749	-0.081	-0.050	0.021	48.004
a. Dependent Variable: LST											

Another assumption is that there should be no multicollinearity among the independent variables. For this, the VIF value in Table 22 should be less than 10[174]. When looking at Model 3 and Model 4, it is observed that the VIF values are high. Therefore, due to the multicollinearity problem among the variables in Model 3 and Model 4, Model 2 (NDBI, NDVI) is a more suitable model for regression analysis.

In regression analysis, identifying outliers is important. Std. Residual and Cook's Distance in the Residuals Statistics table are examined (Table 23). The value in the Std. The residual row should fall within the range of -3.29 to +3.29. The maximum value in the Cook's Distance row should not exceed +1[175]. There are no outliers in the analysis.

Table 23. Residuals Statistics

Residuals Statistics[a]					
	Minimum	Maximum	Mean	Std. Deviation	N
Predicted Value	27.2936	38.8234	33.0601	2.26649	1078
Std. Predicted Value	-2.544	2.543	0.000	1.000	1078
Standard Error of Predicted Value	0.056	0.507	0.114	0.037	1078
Adjusted Predicted Value	27.2688	38.8653	33.0601	2.26715	1078
Residual	-5.17454	5.34529	0.00000	1.75625	1078
Std. Residual	-2.941	3.038	0.000	0.998	1078
Stud. Residual	-2.951	3.048	0.000	1.001	1078
Deleted Residual	-5.21123	5.37920	0.00002	1.76484	1078
Stud. Deleted Residual	-2.962	3.059	0.000	1.001	1078
Mahal. Distance	0.075	88.462	3.996	4.782	1078
Cook's Distance	0.000	0.037	0.001	0.002	1078
Centered Leverage Value	0.000	0.082	0.004	0.004	1078

a. Dependent Variable: LST

We interpret whether errors in predictions are normally distributed by examining the Histogram and Normal P-P Plot graphs. Upon reviewing Figure 32 and Figure 33, we observe that errors in predictions are normally distributed.

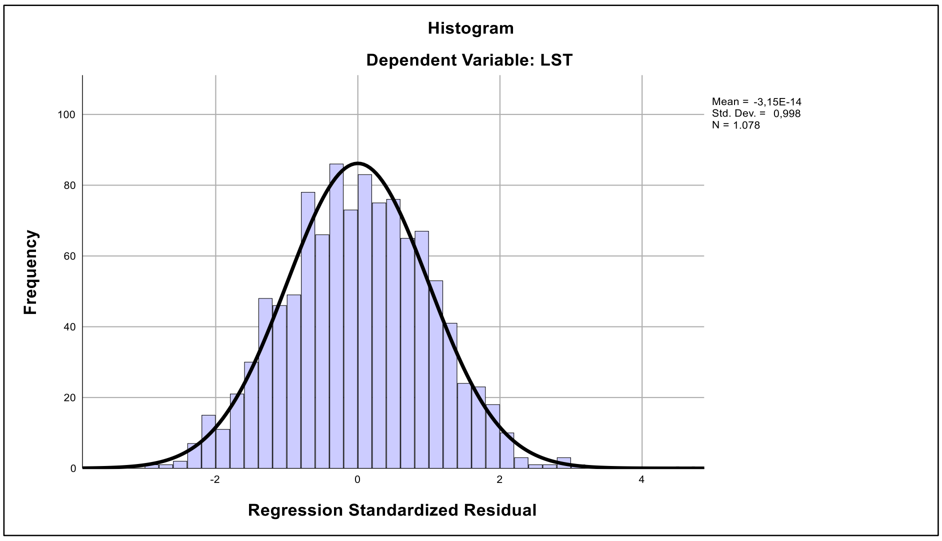

Figure 32. Histogram graph

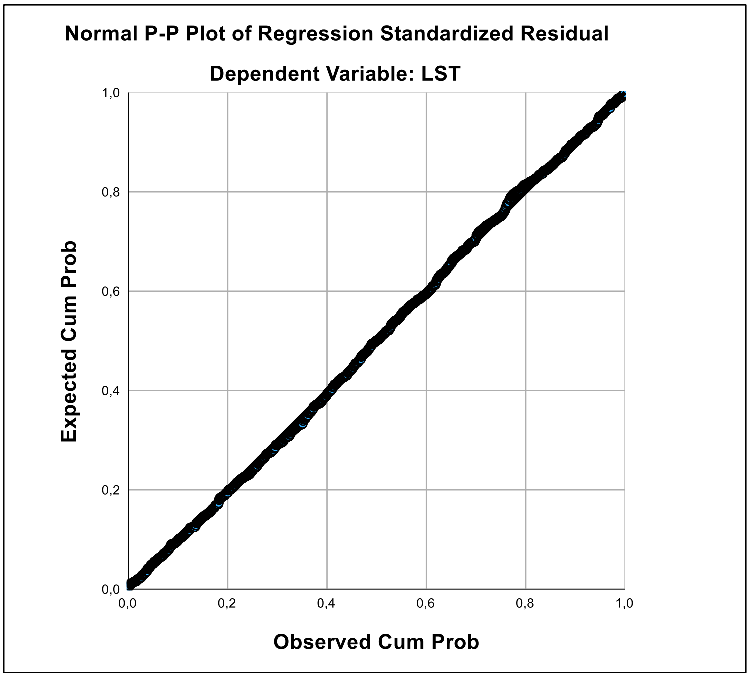

Figure 33. Normal P-P plot of regression standardized residual

In order to satisfy another assumption of regression analysis, Homoscedasticity condition, the points in Figure 34 should be spread as evenly as possible. The points in the figure are widely spread, indicating that the condition is met.

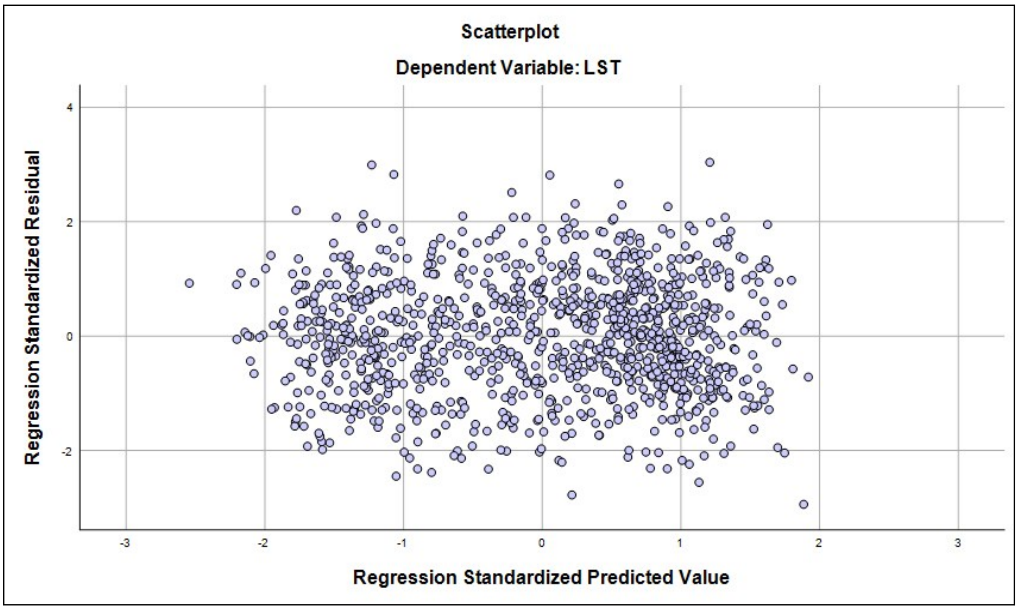

Figure 34. Scatterplot of regression analysis

The final assumption of regression analysis is that the errors should be independent from each other. Accordingly, the Durbin-Watson coefficient in the Model Summary table should be between 1 and 3. Upon examining Table 24, we conclude that the errors are independent from each other. Thus, all assumptions of regression analysis have been met.

Table 24. Model Summary of Regression Analysis

Model Summary[e]						
Model	R	R Square	Adjusted R Square	Std. Error of the Estimate	PRESS	Durbin-Watson
1	0.776[a]	0.602	0.602	1.80986		
2	0.777[b]	0.604	0.603	1.80649		
3	0.789[c]	0.622	0.621	1.76447		
4	0.790[d]	0.625	0.623	1.75952	3354.492	1.963
a. Predictors: (Constant), NDBI						
b. Predictors: (Constant), NDBI, NDVI						
c. Predictors: (Constant), NDBI, NDVI, NDWI						
d. Predictors: (Constant), NDBI, NDVI, NDWI, UI						
e. Dependent Variable: LST						

Table 24 is also a summary table of the model. Shows the results of MLR using the Stepwise method. The appropriate model determined for the regression analysis in this study is Model 2. NDBI and NDVI were used to measure the effects of the independent variables on LST/SUHI. In the model, 60.4% of the variability in the dependent variable is explained by independent variables: NDVI, and NDBI. When looking at the Coefficient table, the NDBI independent variable shows a positive relationship with LST, while NDVI shows a negative relationship. The relative impact of the independent variables on LST/SUHI are in the order NDBI (71.3%) and NDVI (7.6%). In this study, understanding the relationship between dependent and independent variables will help determine the effects that cause the increase in LST values and will be a preliminary study to develop strategies to reduce the SUHI effect.

5.6. Assessment of LST with Different Built Environment Texture

In this study, the SUHI effect was interpreted through LST maps, and temperature differences in the study area were determined. By comparing LST values with spectral indices of five regions, built-up indices, and LULC, the factors that increase/decrease the SUHI effect were determined. While population density, building area density, mean floor height, and green areas larger than 2 ha were evaluated as built-up indices; LST, NDVI, NDWI, NDBI, UI, and albedo images were evaluated as spectral indices. Characteristic features of the built environment in representative regions and results of analysis in these regions are shown in Table 25.

Region A is located in Çiğli district. In region A, the approximate population density is calculated as 360 person/ha. There are 2283 buildings in the area with a building area density of 200. The mean of floor height of the buildings is 7, with floors ranging from 1 to 11. Urban Fabric (1.1) makes up the majority of region A, while Scrub and/or Herbaceous Vegetation Associations (3.2) cover a very small area. There are also none green areas larger than 2 ha in this region. Within these characteristics, the mean LST value in the region is 36.6ºC. The mean values of NDVI (max:0.35, min:0.04), NDWI (max:-0.01, min:-0.37), NDBI (max:0.15, min:-0.23), UI (max:0.13, min:-0.38), and albedo (max:0.37, min:0.09) values are 0.13, -0.16, 0.01, -0.07, and 0.21, respectively. When the spectral indices maps are analyzed, it is seen that NDVI and NDWI values are low in the region. Due to the predominance of urban areas, NDBI and UI values are high.

Region B is located in the Bornova district. In region B, the population density is calculated as approximately 500 person/ha. In the area with 3107 buildings, the building area density is 240. Buildings with floor numbers ranging from 1 to 9, mean floor height is 6.7. While "Urban Fabric (1.1)" constitutes the majority of region B, there are also "Mine, Dump and Construction Sites (1.3)", and "Artificial, Non-Agricultural Vegetated Areas (1.4)". In this region, there is more than 2 ha of green space within area 1.4. (covering 9.7% of the area). Within these characteristics, the mean LST value in the region is 34.6ºC. The mean values of NDVI (max:0.47, min:0.01), NDWI (max:-0.04, min:-0.41), NDBI (max:0.10, min:-0.26), UI (max:0.08, min:-0.45), and albedo (max:0.46, min:0. 15) values are 0.15, -0.17, -0.02, -0.11, and 0.22, respectively. When the spectral indices maps are analyzed, the NDWI value is lower than the NDVI value in the region. Due to the predominance of urban areas, NDBI and UI values are high.

Region C is located in Bornova district. In region C, the approximate population density is calculated as 480 person/ha. There are 2221 buildings in the area with a building area density of 300. The number of floors is between 1 and 29, mean floor height is 9. There are also buildings with 37 (1), 38 (1), and 41 (1) floors. While the majority of region C is composed of "Urban Fabric (1.1)", there are also "Industrial, Commercial and Transport Units (1.2)", and "Heterogeneous Agricultural Areas (2.4)". There are also none green areas larger than 2 ha in this region. Within these characteristics, the mean LST value in the region is 35.3ºC. The average values of NDVI (max:0.30, min: -0.05), NDWI (max:0.08, min:-0.29), NDBI (max:0.11, min:-0.18), UI (max:0.12, min:-0.29), and albedo (max:0.32, min:0.08) values are 0.08, -0.11, -0.002, -0.07, and 0.21, respectively. When the spectral indices maps are examined, the NDVI value in the region is lower than the NDWI value. Due to the predominance of urban areas, NDBI and UI values are high.

Region D is located in Konak district. The approximate population density is calculated in the region as 430 people/ha. There are 1463 buildings in the area and the building area density is 320. Buildings with floor numbers ranging from 1 to 13, mean floor height is 13.9. There are also 25 (1) and 35 (1) floor buildings in the region. In region D, there are "Urban Fabric (1.1)", "Industrial, Commercial and Transport Units (1.2)", and "Artificial, Non-Agricultural Vegetated Areas (1.4)". In this area, there is a green area of more than 2 ha known as Kültürpark within the 1.4 area (covering 36.6% of the area). Within the scope of these characteristics, the mean LST value in the region is 32.3ºC. The mean values of NDVI (max:0.41, min:0.01), NDWI (max:0.03, min:-0.39), NDBI (max:0.19, min:-0.31), UI (max:0.21, min:-0.44), and albedo (max:0.48, min:0.09) in the region are; 0.14, -0.16, -0.06, -0.14, and 0.19. When the spectral indices maps are analyzed, the NDVI value in the region increased in direct proportion to the size of the green area. Wetlands within the green area also increased the NDWI value. NDBI and UI values decreased as the urban area decreased.

Region E is located in Balçova district. The approximate population density is calculated in the region 580 people/ha. There are 2085 buildings in the area with a building area density of 280. Buildings with floor numbers ranging from 1 to 11, mean floor height is 13.2. While the majority of the E region consists of "Urban Fabric (1.1)" area, there are also "Forests (3.1)", and "Scrub and/or Herbaceous Vegetation Associations (3.2)" areas in the region. There are also none green areas larger than 2 ha in this region. Within the scope of these characteristics, the maximum, minimum and mean LST values in the region are 35.2ºC, 27.9ºC, and 33ºC respectively. The average values of NDVI (max:0.37, min:0.03), NDWI (max:-0.07, min:-0.36), NDBI (max:0.19, min:-0.29), UI (max:0.19, min:-0.44), and albedo (max:0.44, min:-0. 11) values are 0.16, -0.18, -0.05, -0.13, and 0.18, respectively. When the spectral indices maps are analyzed, NDVI value increases in forest areas. NDWI value also increased. Due to the predominance of urban areas, NDBI and UI values are high except for forest areas.

It is considered inadequate to evaluate the LST value with the built-up indices of population density, mean floor height, and building area density alone. When the built-up indices, which have an increasing effect on the LST value, are evaluated with other features in the region, it is determined that there are also decreases in the LST value.

NDVI and NDWI values vary depending on the presence of green areas and wetlands. Especially green areas larger than 2 ha, wetlands and forest areas within green areas increase the NDVI value. Even if the building area density and mean floor density of the buildings around the green areas are high, the LST value is low. Even though the population density of region B is (500 people/ha), the LST value is low due to the green area around it. Although the mean floor height and population density are higher in E region, the mean LST value is 33ºC. Although the building area density and mean floor height are high in region D, the LST value is low thanks to the Kültürpark located in the area.

It has been determined that LST has the highest temperature values in areas where "Urban Fabric (1.1)", "Industrial, Commercial, and Transport Units (1.2)", "Mine, Dump and Construction Sites (1.3)", and "Heterogeneous Agricultural Areas (2.4)"have a higher share. NDBI and UI values are higher in areas with dense residential areas where there are fewer natural features capable of mitigating high temperatures.

Therefore, the most effective built-up indices on LST are green areas larger than 2 ha. It cannot be said that other indices alone affect LST. When evaluated together with the LULC change, meaningful results emerge.

Table 25.Characteristic Features of the Built Environment in Representative Regions and Results of Analysis in These Regions

	Representative Region				
	Region A	**Region B**	**Region C**	**Region D**	**Region E**
Location of Map					
Building Area Density					
LST	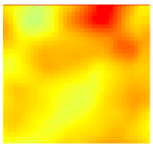	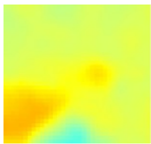	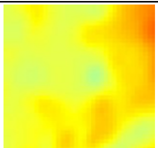	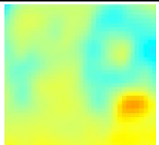	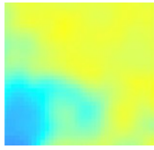
LULC		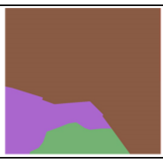		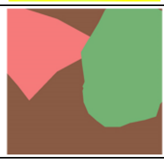	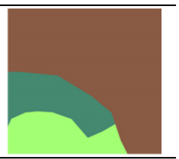
NDVI	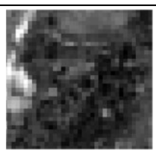	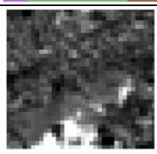	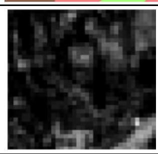	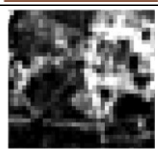	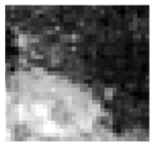
NDWI	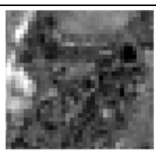	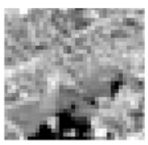	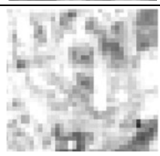	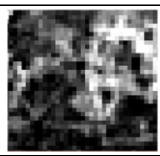	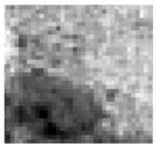
NDBI	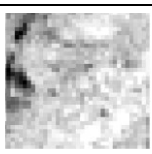	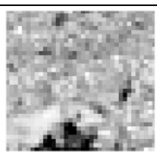	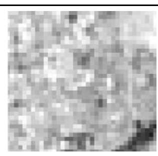	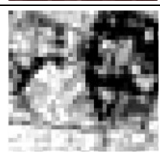	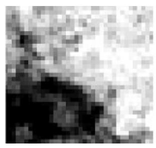
UI	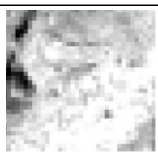	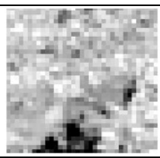	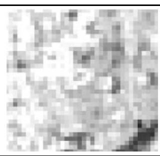	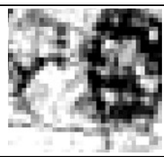	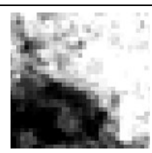
Mean LST (ºC)	36.6	34.6	35.3	32.3	33
LULC (Codes)	1.1 – (93%) 3.2 – (7%)	1.1 - (80%) 1.3 - (12%) 1.4 - (8%)	1.1 - (57%) 1.2 - (21%) 2.4 - (19%) 3.2 - (3%)	1.1 - (45%) 1.2 - (19%) 1.4 - (36%)	1.1 – (71%) 3.1 – (14%) 3.2 – (15%)
Population Density (person/ha)	360	500	480	430	580
Building Area Density	200	240	300	320	280
Mean Floor Height (m)	7	6.7	9	13.9	13.2
Green Areas Larger than 2 ha (present/absent)	absent	present	absent	present	absent

5.7. Assessment of Air Temperature and LST Values

Due to the correspondence of one or more pixels on the LST image to the locations of meteorological stations, five different-sized buffer zones of 100, 200, 300, 400, and 500 meters have been created. The cell size of the LST image is 30x30 meters. Therefore, 100-meter intervals have been determined in the buffer zone to accommodate more pixels. The correlation between the average LST values of fifteen stations belonging to five different buffer zones and air temperatures has been examined based on the 2018 values (Table 26).

Table 26. Pearson Correlation between Air Temperature and LST 2018

		LST 2018				
		Buffer_100	Buffer_200	Buffer_300	Buffer_400	Buffer_500
Air Temperature	Pearson's r	**0.645****	**0.649****	**0.642****	**0.635****	**0.667****
	p	0.005	0.004	0.005	0.005	0.003
	n	15	15	15	15	15

Pearson’s r > 0.5 (bold), (**) Correlation is significant at the 0.01 level.

As a result of the analysis, a strong positive correlation and a significant relationship have been found between the LST 2018 values and air temperature. The correlation coefficients calculated according to the buffers are as follows: Buffer_100: r=0.645, p<0.01; Buffer_200: r=0.649, p<0.01; Buffer_300: r=0.642, p<0.01; Buffer_400: r=0.635, p<0.01; Buffer_500: r=0.667, p<0.01. Accordingly, the 500-meter buffer, which has the strongest correlation with air temperature, has been selected.

To ensure consistency, the dates of Landsat satellite image usage and the dates of air temperatures are the same. The evaluated dates by year are as follows: for 1990, July 6, and August 23; for 2000, July 25, and August 10; for 2006, July 10, and August 27; for 2012, July 10, and July 26; for 2018, July 3, and August 20. Only two of the fifteen stations in the study area (İzmir Adnan Menderes Havalanı and İzmir Bölge) provide temperature data for five years. Since average air temperature and LST values will be taken for the stations by year, the values must be consistent. Therefore, the average air temperatures of two stations for specific days in 1990, 2000, 2006, 2012, and 2018 have been compared with the LST values covering the 500-meter buffer zone.

It is observed that there existed a mean difference of 5.82 ºC between LST values and temperature values obtained from meteorological stations over five years. In 2000, it is observed that the LST value and air temperature decreased compared to other years. In 2006, although the air temperature increased from the previous year, a decrease in LST value is observed. Generally, it is observed that the LST value and air temperature values linearly increased in 2012 and 2018. In addition, it is observed that in 2006, the minimum difference between air temperature and LST value was 5.05 ºC, and the maximum difference was 6.80 ºC in 2000. Generally, it can be said that there is an increasing trend in average temperature values between 1990 and 2018 (Figure 35).

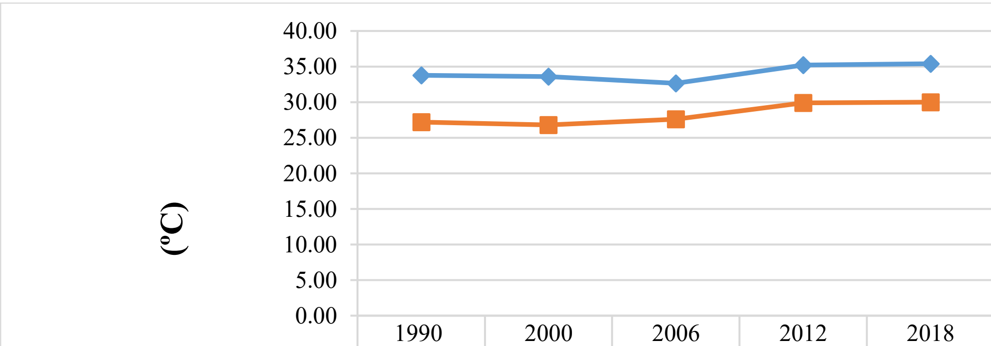

	1990	2000	2006	2012	2018
Mean of LST (ºC)	33.75	33.60	32.65	35.20	35.40
Mean Air Temperature of Meteorological Stations (ºC)	27.20	26.80	27.60	29.90	30.00

Figure 35. Temperature relationship between meteorological station and LST

When the temperature data belonging to meteorological stations (Table 14) are examined, temperature data are found only for the year 2018 for fifteen stations. Therefore, the LST values within the 500-meter buffer areas of each station were compared with the temperature values in Figure 36. Konak/Alsancak Liman Feneri station is the station with the least difference (0.1ºC) between LST and temperature values. Çiğli Havalimanı is the station with the highest difference (7.2ºC). It is generally observed that the mean difference between stations is 4.28 ºC.

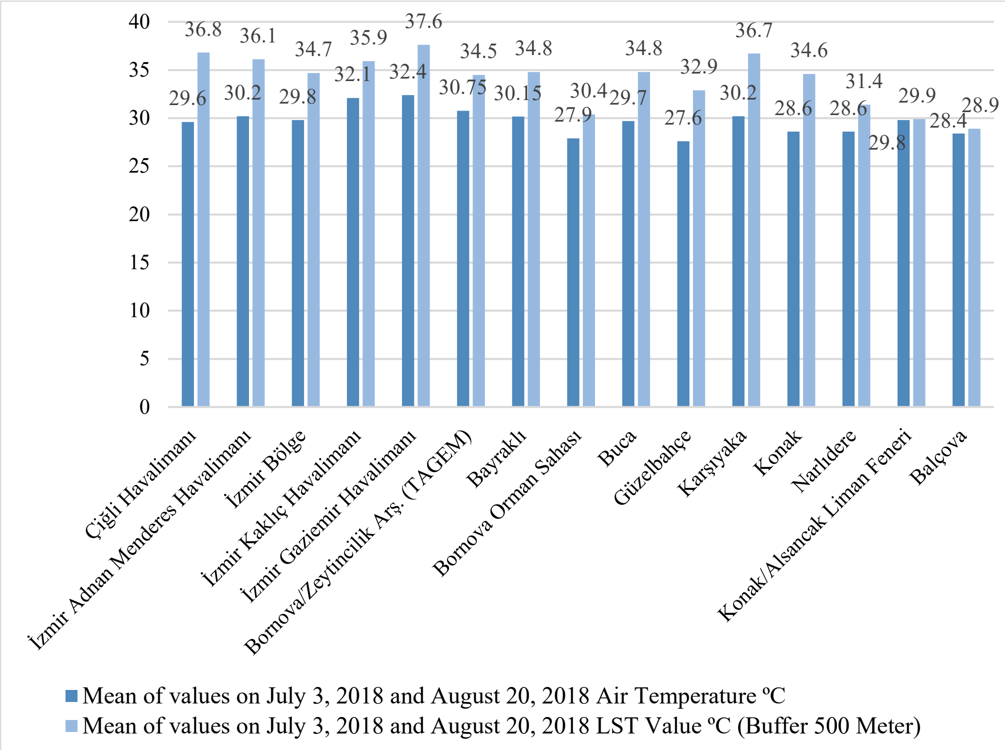

Figure 36. Comparison of mean LST and mean air temperature for 2018

CHAPTER 6

CONCLUSION

With the increasing world population, it is estimated that by 2050, 68% of the world's population will live in cities. As a result of this, many problems arise in cities, such as the reduction of vegetation, the intensification of impermeable surfaces and buildings, and significant transformations in water and energy balance, vegetation, topography, and building materials. UHI due to climate change and increasing temperatures as a result of UHI can harm human health, lead to extreme weather events, and reduce air quality by increasing energy consumption as well as greenhouse gas emissions. Therefore, monitoring urban development in the context of global climate change is of great importance.

In this study, the SUHI effect in 11 districts of the İzmir Metropolitan Area was examined in terms of spatial and temporal changes based on various urban parameters, including LST, LULC, spectral indices, and built-up indices. The time series of the study includes the years 1990, 2000, 2006, 2012, and 2018. Spatial and statistical analysis methods such as zonal statistics, correlation, and regression analysis were utilized to establish relationships between LST/SUHI and related parameters.

Within the scope of the research question of the thesis study "How Does Land Use/Land Cover Classes Affect LST Values?":

- LST values are higher in "Urban Fabric", "Industrial, Commercial, and Transport Units", "Mine, Dump, and Construction Sites", and "Heterogeneous Agricultural Areas" while lower in forest areas and green areas. This means that the presence of dense green areas in cities reduces the SUHI effect.

- LST values are higher in "Pastures", "Arable Land", "Artificial, Non-Agricultural Vegetated Areas", "Industrial, Commercial, and Transport Units", and "Urban Fabric" respectively while lower in "Marine Waters", "Coastal Wetlands", and "Forests".

- When the LULC change by the years is analyzed, "Heterogeneous Agricultural Areas and Forest" areas have been largely replaced by "Urban Fabric", and Industrial, Commercial, and Transport Units" leading to an increase in LST values, affecting the formation of SUHI.

Within the scope of the research question of the thesis study "How Are The Spectral Indices as Urban Parameters Related to LST/SUHI?":

- Correlation analysis has shown that LST is highly correlated with NDBI, UI, Albedo, and NDVI variables. There is a high correlation between LST with NDBI ($r=0.776$; $p<0.01$) (positive), UI ($r=0.749$; $p<0.01$) (positive), Albedo ($r=0.665$; $p<0.01$) (positive), and NDVI ($r=-0.664$; $p<0.01$) (negative), respectively, while there is a moderate positive correlation with NDWI ($r=0.512$; $p<0.01$).

- In the regression model, 60.4% of the variability of the dependent variable is explained by NDBI and NDVI.

- In the study, the most effective spectral index among the appropriate indicators of SUHI effects is NDBI (71.3%). In addition, NDVI (7.6%) is also an effective parameter to reduce the SUHI effect.

Within the scope of the research question of the thesis study "What Findings Emerge from Comparing LST Values with Built-up Indices as Urban Parameters?":

- To further investigate the SUHI effects in the built environment, designated built-up indices (population density, building area density, mean floor height, and surrounding green areas larger than 2 ha) were evaluated in conjunction with LST, LULC, and spectral indices.

- The most effective built-up indices on LST are green areas larger than 2 ha. The LST value is low in areas with more than 2 ha of green space. It cannot be said that other indices alone affect LST. When evaluated together with the LULC change, meaningful results emerge.

When LST values are compared with meteorological values, an average difference of 5.82ºC was observed over five years. Additionally, in the comparison made based on station data for 2018, it was observed to reach up to 7ºC. This is because LST is measured during daylight hours while air temperature is measured throughout the day.

Limitations

- Wind is an important parameter for SUHI. The lack of access to air corridor data in the study was restrictive in addressing the wind issue of the study. In further studies, a more comprehensive evaluation can be made based on wind direction and air corridor data.

- LST characterizes SUHI. Since air temperature could not be measured in this study, LST data was used. In further studies, the area can be explored with more mobile stations. Thus, a more accurate result regarding UHI will emerge than that given by SUHI.

- Due to the use of openly available sources, Sky View Factor (SVF), and Road Network Density (RND) built-up indices could not be evaluated in the study. If it is desired to make an evaluation specific to the built environment in further studies, further evaluation can be made using these indices.

Recommendations

Based on the findings obtained within the scope of the thesis study, various intervention tools that can be applied in cities to contribute to the reduction and minimization of the SUHI effect through minor improvements and structural interventions are presented for urban planning and design processes.

Recommendations obtained according to the research question "How Does Land Use/Land Cover Classes Affect LST Values?":

- Çiğli is the district with the highest LST value. Therefore, to reduce heat island formation, cool, green, and permeable coating materials should be used in areas with large impermeable surfaces (e.g. shopping mall parking lots, gardens of public buildings, and industrial areas).

- Green space is not available in sufficient quantity in the study area. Greening works should be carried out in the work area and green areas should be planned to be 10 m² per person under the Planning Principles Regulation in the Zoning Law No. 3194. New planned areas should be planned in harmony with green areas.

Recommendations obtained according to the research question "How Are The Spectral Indices as Urban Parameters Related to LST/SUHI?":

- The NDBI value, which has a significant relationship with SUHI, should be reduced in the study area. Therefore, controlling urban sprawl should be a priority.

- The number of bicycle paths needs to be increased, especially in Buca, Bornova, Çiğli, and Karabağlar districts, where LST values are high. In order to prevent floods that occur as a result of excessive rain events in İzmir, the concept of "Sponge City" should be adopted in order to collect rainwater in the area where it falls as much as possible.

Recommendations obtained according to the research question "What Findings Emerge from Comparing LST Values with Built-up Indices as Urban Parameters?":

- As a result of the study, green areas larger than 2 ha significantly reduce the LST temperature. Therefore, unnecessary large areas in the city center should be used for projects to reduce the SUHI impact. Empty areas such as the demolished prison in Buca, İzmir are suitable for such projects.

- Establish institutional structures to develop short-, medium-, and long-term spatial strategies at the national, regional, and local levels to prevent and reduce the formation of heat islands. Regularly creating district-based heat island maps and identifying areas with temperatures higher or lower than the city's average temperature.

Conducting research on the decrease in wind speed due to unconscious construction in air corridors in İzmir and investigating the regions where this effect may be effective.

Increasing studies forming the basis for climate analysis that includes the climatic conditions of İzmir and repeating them over many years to obtain more accurate results.

Prioritizing efforts to reduce LST temperature in areas with high SUHI density when planning for rapidly urbanizing areas.

Arranging the positions of trees on residential plots to reduce summer sun exposure and increase winter sun exposure.

Ensuring harmony between streams and greenery by using streams passing through the study area as blue corridors.

These practices can contribute to creating more sustainable and healthy urban environments by reducing the heat island effect. This study provides various urban parameters that can be examined in future research to understand the causes, spread, and effects of the SUHI effect more deeply, thereby guiding future urban planning and environmental policy decisions. Comparisons can be made with parameters that can provide more detailed results at the city scale, allowing for a more detailed evaluation of the effects on the SUHI effect.

REFERENCES

(1) IPCC. *Impacts, Adaptation, and Vulnerability. Working Group II Contribution to the IPCC Sixth Assessment Report of the Intergovernmental Panel on Climate Change; Pötner, H*; 2022. https://doi.org/10.1017/9781009325844.

(2) UNFPA. The State of the World Population 2007: Unleashing the Potential of Urban Growth. *Indian Pediatr.* 2007, *45* (6), 481–482.

(3) UNFPA. *World set to reach 8 billion people on 15 November 2022*. https://turkiye.unfpa.org/tr/dunya-nufus-gunu-2022-bb#:~:text=. (accessed 15.02. 2024).

(4) UN-Habitat. *Envisaging the Future of Cities*; 2022.

(5) McMichael, A. J.; Haines, A.; Slooff, R.; Kovats, S. Climate Change and Human Health: An Assessment Prepared by a Task Group on Behalf of the World Health Organization, the World Meteorological Organization and the United Nations Environment Programme. *Population and Development Review*. 1996, p 806. https://doi.org/10.2307/2137826.

(6) Ren, C.; Ng, E. Y. Y.; Katzschner, L. Urban Climatic Map Studies: A Review. *Int. J. Climatol.* 2011, *31* (15), 2213–2233. https://doi.org/10.1002/joc.2237.

(7) Allegrini, J.; Dorer, V.; Carmeliet, J. Influence of Morphologies on the Microclimate in Urban Neighbourhoods. *J. Wind Eng. Ind. Aerodyn.* 2015, *144*, 108–117. https://doi.org/10.1016/j.jweia.2015.03.024.

(8) IPCC. *Climate Change and Land: An IPCC Special Report on Climate Change, Desertification, Land Degradation, Sustainable Land Management, Food Security, and Greenhouse Gas Fluxes in Terrestrial Ecosystems*; 2019. https://doi.org/10.4337/9781784710644.

(9) Sun, Y.; Zhao, S. Spatiotemporal Dynamics of Urban Expansion in 13 Cities across the Jing-Jin-Ji Urban Agglomeration from 1978 to 2015. *Ecol. Indic.* 2018, *87* (July 2017), 302–313. https://doi.org/10.1016/j.ecolind.2017.12.038.

(10) Oleson, K. W.; Bonan, G. B.; Feddema, J.; Jackson, T. An Examination of Urban Heat Island Characteristics in a Global Climate Model. *Int. J. Climatol.* 2011, *31* (12), 1848–1865. https://doi.org/10.1002/joc.2201.

(11) Landsberg, H. E. Urban Energy Fluxes. *Urban Clim.* 1981, 53–82.

(12) Oke, T. . *Boundary Layer Climates, 2nd Edition*; 1987.

(13) Yusuf, Y. A.; Pradhan, B.; Idrees, M. O. Spatio-Temporal Assessment of Urban Heat Island Effects in Kuala Lumpur Metropolitan City Using Landsat Images. *J. Indian Soc. Remote Sens.* 2014, *42* (4), 829–837. https://doi.org/10.1007/s12524-013-0342-8.

(14) Santamouris, M.; Papanikolaou, N.; Livada, I.; Koronakis, I.; Georgakis, C.; Argiriou, A.; Assimakopoulos, D. N. On the Impact of Urban Climate on the Energy Consuption of Building. *Sol. Energy* 2001, *70* (3), 201–216. https://doi.org/10.1016/S0038-092X(00)00095-5.

(15) Stone, B.; Rodgers, M. O. Urban Form and Thermal Efficiency: How the Design of Cities Influences the Urban Heat Island Effect. *J. Am. Plan. Assoc.* 2001, *67* (2), 186–198. https://doi.org/10.1080/01944360108976228.

(16) Nakata, C. M.; de Souza, L. C. L. Verification of the Influence of Urban Geometry on the Nocturnal Heat Island Intensity. *J. Urban Environ. Eng.* 2013, *7* (2), 286–292. https://doi.org/10.4090/juee.2013.v7n2.286292.

(17) Oke, T. . The Energetic Basis of the Urban Heat Island. *Q. J. R. Meteorol. Soc.* 1982, *108* (455), 1–24. https://doi.org/10.1002/qj.49710845502.

(18) Kim, H. H. Urban Heat Island. *Int. J. Remote Sens.* 1992, *13* (12), 2319–2336. https://doi.org/10.1080/01431169208904271.

(19) Oke, T. R. Canyon Geometry and the Urban Heat Island. *J. Climatol.* 1981, *1*, 237–254.

(20) EPA. *Cooling summertime temperatures / strategies to reduce heat Islands*. Us. Environmental Protection Agency. https://www.epa.gov/sites/default/files/2014-06/documents/hiribrochure.pdf. (accessed 20.01.2024).

(21) Stone Jr, Brian Jr, Norman, J. M. Urban Heat Island Effects on Building Energy Use and Air Quality. *J. Build. Phys.* 2008, *31*, 105–313.

(22) Cheung, H. K. W.; Coles, D.; Levermore, G. J. Urban Heat Island Analysis of Greater Manchester, UK Using Sky View Factor Analysis. *Build. Serv. Eng. Res. Technol.* 2016, *37* (1), 5–17. https://doi.org/10.1177/0143624415588890.

(23) Rzepa, M. The Map of Sky View Factor in the Center of Lodz. *7th Int. Conf. Urban*

Clim. 2009, *2008* (July), 4.

(24) White, M.; Kimm, G. Measuring Sky View Factor of Urban Canyons Using Hacked {Gopro} Hemispheric Video Processing. *Living and {Learning}* 2015, No. December, 525–535.

(25) EPA. *Reducing Urban Heat Islands: Compendium of Strategies*. Us. Environmental Protection Agency. https://doi.org/10.1109/IICPE.2016.8079546.

(26) Streutker, D. R. Satellite-Measured Growth of the Urban Heat Island of Houston, Texas. *Remote Sens. Environ.* 2003, *85* (3), 282–289. https://doi.org/10.1016/S0034-4257(03)00007-5.

(27) Voogt, J. A.; Oke, T. R. Thermal Remote Sensing of Urban Climates. *Remote Sens. Environ.* 2003, *86* (3), 370–384. https://doi.org/10.1016/S0034-4257(03)00079-8.

(28) Weng, Q.; Lu, D.; Schubring, J. Estimation of Land Surface Temperature-Vegetation Abundance Relationship for Urban Heat Island Studies. *Remote Sens. Environ.* 2004, *89* (4), 467–483. https://doi.org/10.1016/j.rse.2003.11.005.

(29) Raisch, A.; Davis, C. L.; Alan, I.; Parker, K.; Warner, D. A. United States Patent (19). 1972, No. 19.

(30) Zhang, J.; Wang, Y.; Li, Y. A C++ Program for Retrieving Land Surface Temperature from the Data of Landsat TM/ETM+ Band6. *Comput. Geosci.* 2006, *32* (10), 1796–1805. https://doi.org/10.1016/j.cageo.2006.05.001.

(31) Rinner, C.; Hussain, M. Toronto's Urban Heat Island-Exploring the Relationship between Land Use and Surface Temperature. *Remote Sens.* 2011, *3* (6), 1251–1265. https://doi.org/10.3390/rs3061251.

(32) Ding, H.; Shi, W. Land-Use/Land-Cover Change and Its Influence on Surface Temperature: A Case Study in Beijing City. *Int. J. Remote Sens.* 2013, *34* (15), 5503–5517. https://doi.org/10.1080/01431161.2013.792966.

(33) Amiri, R.; Weng, Q.; Alimohammadi, A.; Alavipanah, S. K. Spatial-Temporal Dynamics of Land Surface Temperature in Relation to Fractional Vegetation Cover and Land Use/Cover in the Tabriz Urban Area, Iran. *Remote Sens. Environ.* 2009, *113* (12), 2606–2617. https://doi.org/10.1016/j.rse.2009.07.021.

(34) Wang, S.; Ma, Q.; Ding, H.; Liang, H. Detection of Urban Expansion and Land Surface Temperature Change Using Multi-Temporal Landsat Images. *Resour. Conserv. Recycl.* 2018, *128*, 526–534. https://doi.org/10.1016/j.resconrec.2016.05.011.

(35) Kadıoğlu, P. D. M. Türkiye'de İklim Değişikliği Risk Yönetimi. 2012.

(36) T.C Çevre ve Şehircilik. Uyum Stratejisi ve Eylem Planı. 2012.

(37) Akgündüz, S.; Odabaşı, E.; Kılıç, G.; Çamalan, G.; Erkan, M. A.; Soydam, M.; Güser, Y. Türkiye Meteorolojik Afetler Değerlendirmesi (2010-2021). 2021.

(38) Çevre Şehircilik Bakanlığı. *Türkiye'nin İklim Değişikliği Uyum Stratejisi ve Eylem Planı*.https://webdosya.csb.gov.tr/db/destek/editordosya/Iklim_Degisikligi_Uyum_Stratejisi_ve_Eylem_Plani.pdf. (accessed 22.01.2024).

(39) Stern, N. The Economics of Climate Change. *Top 50 Sustain. Books* 2017, 247–250. https://doi.org/10.4324/9781351279086-55.

(40) UNDRR. Human Cost of Disasters. *Hum. Cost Disasters* 2020. https://doi.org/10.18356/79b92774-en.

(41) World Meteorological Organization (WMO). *WMO Atlas of Mortality and Economic Losses from Weather, Climate and Water Extremes*; 2021.

(42) IPCC. *Climate Change 2007 The Physical Science Basis*; 2007; Vol. 59. https://doi.org/10.1256/wea.58.04.

(43) Turkish State Meteorological Service. 2022 Yılı İklim Değerlendirmesi. 2023.

(44) MedECC. Akdeniz Havzasi'nda İklim Değişikliği ve Çevresel Değişiklik. 2020.

(45) İzmir Governorship Provincial Disaster and Emergency Directorate. *İl Afet Risk Azaltma Planı*; 2021. https://izmir.afad.gov.tr/kurumlar/izmir.afad/E-KUTUPHANE/Il-Planlari/Izmir-IRAP.pdf. (accessed 18.01.2024).

(46) Oke, T. R. City Size and the Urban Heat Island. *Atmos. Environ.* 1973, *7* (8), 769–779. https://doi.org/10.1016/0004-6981(73)90140-6.

(47) Education, N. G. *All About Climate*. National Geographic Education. https://education.nationalgeographic.org/resource/all-about-climate/. (accessed 18.12.2023).

(48) WMO-World Meteorological Organization. The Global Climate in 2015 - 2019. *Cent. Res. Epidemiol. Disasters Natl. Inst. Sp. Res.* 2020, No. 1179, 32.

(49) IPCC. Climate Change 2001. Synthesis Report. IPCC Third Assessment Report

(TAR):A Contribution of Working Groups I, II, and III to the Third Assessment Report of the Integovernmental Panel on Climate Change. *IPCC* 2001, 409.

(50) Lamb, H., Horace , Gentilli, Joseph , Mason, Basil John , . . . Waggoner, P. E.; Krishnamurti, . T.N. , Wells, . Neil C. , Cenedese, . Claudia , Enfield, . David B.; , Davies, . Roger , Hayden, . Bruce P. , Smith, . Phillip J. , Arnfield, . A. John; Pielke, . Roger A. and Bluestein, . Howard B. *Climate*. Encyclopedia Britannica. https://www.britannica.com/science/climate-meteorology.

(51) Xie, Y.; Huang, T.; Li, J.; Liu, J.; Niu, J.; Mak, C. M.; Lin, Z. Evaluation of a Multi-Nodal Thermal Regulation Model for Assessment of Outdoor Thermal Comfort: Sensitivity to Wind Speed and Solar Radiation. *Build. Environ.* 2018, *132* (September 2017), 45–56. https://doi.org/10.1016/j.buildenv.2018.01.025.

(52) UNFCC (United Nations Framework Convention on Climate Change). *United Nations Framework Convention on Climate Change: Handbook*; 2006.

(53) WHO. *Climate Change and Human Health-Risks and Responses*; 2003; Vol. 64. https://doi.org/10.1360/N972018-00898.

(54) Morrison, P. The Discovery of Global Warming. *Phys. Today* 2004, *57* (6), 60–61. https://doi.org/10.1063/1.1784277.

(55) Energy, U. S. C. J. C. o. A. *Current Membership of the Joint Committee on Atomic Energy, Congress of the United States*. US Government Printing Office. https://original-ufdc.uflib.ufl.edu/AA00022673/00001. (accessed 10.01.2024).

(56) Bates, B., Kundzewicz, Z., ve Wu, S. *Climate and Water*; 2008; Vol. 1. https://doi.org/10.1029/90EO00112.

(57) Li, J.; Song, C.; Cao, L.; Zhu, F.; Meng, X.; Wu, J. Impacts of Landscape Structure on Surface Urban Heat Islands: A Case Study of Shanghai, China. *Remote Sens. Environ.* 2011, *115* (12), 3249–3263. https://doi.org/10.1016/j.rse.2011.07.008.

(58) Carmichael, G. *The Emerging Focus Of Urban Environments*. Report And Proceedings Of The WMO Ra II/Ra V Gaw Workshop On Urban Environment. https://library.wmo.int/viewer/41159/?offset=#page=16&viewer=thumb&o=bookmark&n=0&q=.

(59) Oke, T. R., Mills, G., Christen, A., & Voogt, J. A. *Urban Climates*; Cambridge University Press, 2017.

(60) Pickett, S. T. A.; Cadenasso, M. L.; Grove, J. M.; Boone, C. G.; Groffman, P. M.; Irwin, E.; Kaushal, S. S.; Marshall, V.; McGrath, B. P.; Nilon, C. H.; Pouyat, R.

V.; Szlavecz, K.; Troy, A.; Warren, P. Urban Ecological Systems: Scientific Foundations and a Decade of Progress. *J. Environ. Manage.* 2011, *92* (3), 331–362. https://doi.org/10.1016/j.jenvman.2010.08.022.

(61) Erell, E., Pearlmutter, D., & Williamson, T. Urban Microclimate, Designing the Spaces Between Buildings. *Hous. Stud.* 2012, *27* (2), 293–294. https://doi.org/10.1080/02673037.2011.615987.

(62) Marsh, M. M. *Landscape Planning: Environmental Applications*; 1991.

(63) Stewart, I. D. Why Should Urban Heat Island Researchers Study History? *Urban Clim.* 2019, *30* (April), 100484. https://doi.org/10.1016/j.uclim.2019.100484.

(64) Luke Howard. *The Climate of London in Two Volumes*. https://books.google.com.tr/books?id=7skTAAAAYAAJ&printsec=frontcover&hl=tr&source=gbs_ge_summary_r&cad=0#v=onepage&q&f=false. (accessed 05.01.2024).

(65) WHO, W. H. O. Heat-Waves: Risks and Responses. *Heal. Glob. Environ. Heal. Ser.* 2004, *No.2* (2), 124 pp. https://doi.org/10.1007/s00484-009-0283-7.

(66) Masson, V.; Lemonsu, A.; Hidalgo, J.; Voogt, J. Urban Climates and Climate Change. *Annu. Rev. Environ. Resour.* 2020, *45*, 411–444. https://doi.org/10.1146/annurev-environ-012320-083623.

(67) Roth, M. Urban Heat Islands. *Environ. Indic.* 2013, 67–75. https://doi.org/10.1007/978-94-017-9499-2_5.

(68) Oke, T. . The Need to Establish Protocols in Urban Heat Island Work. *8th Symp. Urban Environ. Phoenix, Arizona* 2009, *1215*, 11–15.

(69) Stewart, I. D. and Oke, T. R. A New Classification System for Urban Climate Sites. *Bull. Am. Meteorol. Soc.* 2009, *90*, 922–923.

(70) Oke, T. R. Street Design and Urban Canopy Layer Climate. *Energy Build.* 1988, *11* (1–3), 103–113. https://doi.org/10.1016/0378-7788(88)90026-6.

(71) Oke, T. R. Initial Guidance to Obtain Representative Meteorological Observations at Urban Sites. *World Meteorol. Organ.* 2006, No. 81, 51.

(72) Stewart, I. D.; Oke, T. R. Local Climate Zones for Urban Temperature Studies. *Bull. Am. Meteorol. Soc.* 2012, *93* (12), 1879–1900. https://doi.org/10.1175/BAMS-D-11-00019.1.

(73) The Handbook of Natural Resources. *Atmosphere and Climate*. https://ebrary.net/133432/environment/aims_scope#26. (accessed 10.01.2024).

(74) Zhou, D.; Xiao, J.; Bonafoni, S.; Berger, C.; Deilami, K.; Zhou, Y.; Frolking, S.; Yao, R.; Qiao, Z.; Sobrino, J. A. Satellite Remote Sensing of Surface Urban Heat Islands: Progress, Challenges, and Perspectives. *Remote Sens.* 2018, *11* (1), 1–36. https://doi.org/10.3390/rs11010048.

(75) Liang, Z.; Wu, S.; Wang, Y.; Wei, F.; Huang, J.; Shen, J.; Li, S. The Relationship between Urban Form and Heat Island Intensity along the Urban Development Gradients. *Sci. Total Environ.* 2020, *708*, 135011. https://doi.org/10.1016/j.scitotenv.2019.135011.

(76) Oke, T. R. *Urban heat islands*. The Handbook of Urban Ecology. https://books.google.com.tr/books?hl=tr&lr=&id=GH1dBwAAQBAJ&oi=fnd&pg=PA120&dq=Oke+T.R.+2011&ots=VAXOApc_LV&sig=QIEfdaGtHY3BWm0U7Hs7iUX72ZQ&redir_esc=y#v=onepage&q=Oke T.R. 2011&f=false. (accessed 05.01.2024).

(77) Kleerekoper, L.; Van Esch, M.; Salcedo, T. B. How to Make a City Climate-Proof, Addressing the Urban Heat Island Effect. *Resour. Conserv. Recycl.* 2012, *64*, 30–38. https://doi.org/10.1016/j.resconrec.2011.06.004.

(78) Das, S. A Review of UHI Formation over Changing Climate and Its Impacts on Urban Land Use and Environments and Adaptation Measures Sumanta. 2022.

(79) Yuan, F.; Bauer, M. E. Comparison of Impervious Surface Area and Normalized Difference Vegetation Index as Indicators of Surface Urban Heat Island Effects in Landsat Imagery. *Remote Sens. Environ.* 2007, *106* (3), 375–386. https://doi.org/10.1016/j.rse.2006.09.003.

(80) Harris, R.; Coutts, A. Airborne Thermal Remote Sensing for Analysis of the Urban Heat Island. *Vic. Cent. Clim. Chang. Adapt. Res.* 2011, 1–34.

(81) Nuruzzaman, M. Urban Heat Island: Causes, Effects and Mitigation Measures - A Review. *Int. J. Environ. Monit. Anal.* 2015, *3* (2), 67. https://doi.org/10.11648/j.ijema.20150302.15.

(82) Pandya, P. S. *Urban Heat: A rising global catastrophy for human health*. Medium. https://medium.com/@pranavspandya/urban-heat-a-rising-global-catastrophy-for-human-health-71b3888d1e97. (accessed 07.01.2024).

(83) EPA. *Heat Island Impacts*. https://www.epa.gov/heatislands/heat-island-impacts. (accessed 03.01.2024).

(84) Akbari, H., Gartland, L., & Konopacki, S. Measured Energy Savings of Light Colored Roofs: Results from Three California Demonstration Sites. *Environ. Energy Technol. Div.* 1998.

(85) Adinna, E. N.; Christian, E. I.; Okolie, A. T. Assessment of Urban Heat Island and Possible Adaptations in Enugu Urban Using Landsat-ETM. *J. Geogr. Reg. Plan.* 2009, *2* (2), 30–36.

(86) Kloss, P.; Nizam, K.; Maulud, A.; Nor, M. Reducing Urban Heat Island Effects : A Systematic Review to Achieve Energy Consumption Balance. 2010, No. January 2015.

(87) Schwarz, N.; Schlink, U.; Franck, U.; Großmann, K. Relationship of Land Surface and Air Temperatures and Its Implications for Quantifying Urban Heat Island Indicators - An Application for the City of Leipzig (Germany). *Ecol. Indic.* 2012, *18*, 693–704. https://doi.org/10.1016/j.ecolind.2012.01.001.

(88) Marshall Shepherd. *The Science Of Why Cities Are Warmer Than Rural Areas*. Forbes. https://www.forbes.com/sites/marshallshepherd/2015/09/25/the-science-of-why-cities-are-warmer-than-rural-areas/?sh=490f8edc1744. (accessed 28.12. 2023).

(89) McMillin, L. M. Estimation of Sea Surface Temperatures from Two Infrared Window Measurements with Different Absorption. *J. Geophys. Res.* 1975, *80* (36), 5113–5117. https://doi.org/10.1029/jc080i036p05113.

(90) Li, Z. L.; Tang, B. H.; Wu, H.; Ren, H.; Yan, G.; Wan, Z.; Trigo, I. F.; Sobrino, J. A. Satellite-Derived Land Surface Temperature: Current Status and Perspectives. *Remote Sens. Environ.* 2013, *131*, 14–37. https://doi.org/10.1016/j.rse.2012.12.008.

(91) Sun, Q.; Tan, J.; Xu, Y. An ERDAS Image Processing Method for Retrieving LST and Describing Urban Heat Evolution: A Case Study in the Pearl River Delta Region in South China. *Environ. Earth Sci.* 2010, *59* (5), 1047–1055. https://doi.org/10.1007/s12665-009-0096-3.

(92) Mather, P. M. Computer Processing of Remotely-Sensed Images: An Introduction. *Geocarto Int.* 1987, *2* (4), 64. https://doi.org/10.1080/10106048709354125.

(93) Camps-Valls, G.; Tuia, D.; Gómez-Chova, L.; Jiménez, S.; Malo, J. *Remote Sensing Image Processing*; 2012; Vol. 12. https://doi.org/10.2200/s00392ed1v01y201107ivm012.

(94) Tran, D. X.; Pla, F.; Latorre-Carmona, P.; Myint, S. W.; Caetano, M.; Kieu, H. V.

Characterizing the Relationship between Land Use Land Cover Change and Land Surface Temperature. *ISPRS J. Photogramm. Remote Sens.* 2017, *124*, 119–132. https://doi.org/10.1016/j.isprsjprs.2017.01.001.

(95) Stathopoulou, M.; Cartalis, C. Daytime Urban Heat Islands from Landsat ETM+ and Corine Land Cover Data: An Application to Major Cities in Greece. *Sol. Energy* 2007, *81* (3), 358–368. https://doi.org/10.1016/j.solener.2006.06.014.

(96) Jiang, J.; Tian, G. Analysis of the Impact of Land Use/Land Cover Change on Land Surface Temperature with Remote Sensing. *Procedia Environ. Sci.* 2010, *2*, 571–575. https://doi.org/10.1016/j.proenv.2010.10.062.

(97) Şekertekin, A.; Marangoz, A. M. Zonguldak Metropolitan Alanındaki Arazi Kullanımı Arazi Örtüsünün Yer Yüzey Sıcaklığına Etkisi. *Geomatik* 2019, *4* (2), 101–111. https://doi.org/10.29128/geomatik.497051.

(98) Ünal, M. Kentsel Yüzey Isı Adalarının Belirlenmesinde Yer Yüzey Sıcaklık Verilerinin Kullanımı. *Eur. J. Sci. Technol.* 2022, No. 33, 213–222. https://doi.org/10.31590/ejosat.1039572.

(99) Malik, M. S.; Shukla, J. P.; Mishra, S. Relationship of LST, NDBI and NDVI Using Landsat-8 Data in Kandaihimmat Watershed, Hoshangabad, India. *Indian J. Geo-Marine Sci.* 2019, *48* (1), 25–31.

(100) Külahlıoğlu, M., Şahingöz, M., Kurt, G., Çilek, Ö. Ü. A., & Berberoğlu, S. Geçirimsiz Yüzeyler ve Konumsal-Zamansal Dinamiklerin Kentsel Isı Adasına Etkilerinin Belirlenmesi: Adana İli Örneği. 2022, No. April.

(101) Daramola, M. T.; Eresanya, E. O.; Ishola, K. A. Assessment of the Thermal Response of Variations in Land Surface around an Urban Area. *Model. Earth Syst. Environ.* 2018, *4* (2), 535–553. https://doi.org/10.1007/s40808-018-0463-8.

(102) Macarof, P.; Bîrlica, I. C.; Stătescu, F. Investigating the Relationship between Land Surface Temperature and Urban Indices Using Landsat-8: A Case Study of Iaşi. *Lucr. Semin. Geogr. "Dimitrie Cantemir"* 2017, *45* (0), 81–88. https://doi.org/10.15551/lsgdc.v45i0.07.

(103) Türkyılmaz, M.; Özelkan, E.; Karaman, M. Termal Uydu Görüntülerinden Üretilen Yer Yüzeyi Sıcaklığı Ile Hava Sıcaklığı İlişkisinin Değerlendirilmesi. *Eur. J. Sci. Technol.* 2020, *2019* (20), 932–948. https://doi.org/10.31590/ejosat.799722.

(104) Ersoy Tonyaloğlu, E.; Menderes Üniversitesi, A.; Fakültesi, Z.; Mimarlığı Bölümü, P. Kentleşmenin Kentsel Termal Çevre Üzerindeki Etkisinin

Değerlendirilmesi, Efeler ve İncirliova (Aydın) Örneği. *Araştırma Makal. Turkish J. Landsc. Res.* 2019, *2* (1), 1–13.

(105) Halder, B.; Bandyopadhyay, J.; Banik, P. Evaluation of the Climate Change Impact on Urban Heat Island Based on Land Surface Temperature and Geospatial Indicators. *Int. J. Environ. Res.* 2021, *15* (5), 819–835. https://doi.org/10.1007/s41742-021-00356-8.

(106) Akyürek, Ö. Termal Uzaktan Algılama Görüntüleri İle Yüzey Sıcaklıklarının Belirlenmesi: Kocaeli Örneği. *Doğal Afetler ve Çevre Derg.* 2020, *6* (2), 377–390. https://doi.org/10.21324/dacd.667594.

(107) Guha, S.; Govil, H.; Gill, N.; Dey, A. Analytical Study on the Relationship between Land Surface Temperature and Land Use/Land Cover Indices. *Ann. GIS* 2020, *26* (2), 201–216. https://doi.org/10.1080/19475683.2020.1754291.

(108) Nimish, G.; Bharath, H. A.; Lalitha, A. Exploring Temperature Indices by Deriving Relationship between Land Surface Temperature and Urban Landscape. *Remote Sens. Appl. Soc. Environ.* 2020, *18* (November 2019), 100299. https://doi.org/10.1016/j.rsase.2020.100299.

(109) Kaçmaz, G.; Gürbüz, E. Arazi Örtüsü Değişiminin Arazi Yüzey Sıcaklığına Etkisinin Uzaktan Algılama ve CBS Entegrasyonu Ile Belirlenmesi: Aksaray İli Örneği (Determination of the Effect of Land Cover Change on Land Surface Temperature through Remote Sensing and GIS Integration: 2022, 38–54.

(110) Khan, M. S.; Ullah, S.; Chen, L. Comparison on Land-Use/Land-Cover Indices in Explaining Land Surface Temperature Variations in the City of Beijing, China. *Land* 2021, *10* (10). https://doi.org/10.3390/land10101018.

(111) Łęczek, A., & Łachowski, W. The Impact of the Impervious Surfaces and the Condition of Vegetation on the Land Surface Temperature in Urban Centers on the Example of Wloclawek, Poland. *oint Urban Remote Sens. Event* 2023, 1–4.

(112) Gerçek, D.; Güven, İ. T. Assessment of Mutual Variation of Near-Surface Air Temperature, Land Surface Temperature and Driving Urban Parameters at Urban Microscale. *Sustainability* 2023, *15* (22), 15710. https://doi.org/10.3390/su152215710.

(113) Andrés-Anaya, P.; Sánchez-Aparicio, M.; del Pozo, S.; Lagüela, S. Correlation of Land Surface Temperature with IR Albedo for the Analysis of Urban Heat Island †. *Eng. Proc.* 2021, *8* (1), 0–3. https://doi.org/10.3390/engproc2021008009.

(114) Bonafoni, S.; Baldinelli, G.; Rotili, A.; Verducci, P. Albedo and Surface

Temperature Relation in Urban Areas: Analysis with Different Sensors. *2017 Jt. Urban Remote Sens. Event, JURSE 2017* 2017, No. July 2016, 5–8. https://doi.org/10.1109/JURSE.2017.7924612.

(115) Favretto, A. Urban Heat Island Analysis with Remote Sensing and GIS Methods: An Application in the Trieste Area (North-East of Italy). *Boll. della Soc. Geogr. Ital.* 2018, *14* (1), 215–229. https://doi.org/10.13128/bsgi.v1i1.101.

(116) Yücer, E. Albedo, Yer Yüzey Sıcaklığı ve NDVI Arasındaki İlişkinin Landsat-7 ve Landsat-8 Uydu Verileri Kullanılarak İncelenmesi: Safranbolu Örneği. *Kahramanmaraş Sütçü İmam Üniversitesi Mühendislik Bilim. Derg.* 2023, *26* (1), 177–190.

(117) Trlica, A.; Hutyra, L. R.; Schaaf, C. L.; Erb, A.; Wang, J. A. Albedo, Land Cover, and Daytime Surface Temperature Variation Across an Urbanized Landscape. *Earth's Futur.* 2017, *5* (11), 1084–1101. https://doi.org/10.1002/2017EF000569.

(118) Odunuga, S.; Badru, G. Landcover Change, Land Surface Temperature, Surface Albedo and Topography in the Plateau Region of North-Central Nigeria. *Land* 2015, *4* (2), 300–324. https://doi.org/10.3390/land4020300.

(119) İzmir'in Rakamları. *İzmir İlçelerinin Yüzölçümü ve Cinsiyet Karşılaştırmalı Nüfus Yoğunluğu*.https://izmirinrakamlari.izmir.bel.tr/tr/2022/31/IlceYuzOlcumuCinsiyetKarsilasirmaliNufusYogunlugu. (accessed 25.10.2023).

(120) İzmir Metropolitan Municipality. *İzmir'in Coğrafyası*. https://www.izmir.bel.tr/tr/IzmirinCografyasi/220/255#:~:text= (accessed 25.10.2023).

(121) Turkish State Meteorological Service. *İllere Ait Mevsim Normalleri (1991-2020)*. https://www.mgm.gov.tr/veridegerlendirme/il-ve-ilceler-istatistik.aspx?k=undefined&m=IZMIR. (accessed 12.10.2023).

(122) TÜİK. *1990 Genel Nüfus Sayımı*. https://biruni.tuik.gov.tr/nufus90app/idari.zul. (accessed 08.09.2023).

(123) TÜİK. *2000 Genel Nüfus Sayımı*. https://biruni.tuik.gov.tr/nufusapp/idari.zul. (accessed 08.09.2023).

(124) TÜİK. *Adrese Dayalı Nüfus Kayıt Sistemi Sonuçları 2007-2022*. https://biruni.tuik.gov.tr/medas/?kn=95&locale=tr. (accessed 08.09.2023).

(125) USGS Earth Explorer. *Landsat*. https://earthexplorer.usgs.gov/. (accessed 10.02.2023).

(126) Copernicus Land Monitoring Service. *CORINE Land Cover*. https://land.copernicus.eu/en/products/corine-land-cover. (accessed 15.01.2023).

(127) Meteorology 2nd Regional Directorate. *Air Temperature Value at Meteorological Station (1990-2018)*. (accessed 30.08.2023).

(128) İzmir Metropolitan Municipality. *Buildings and Number of Floor in İzmir Central Districts*. Directorate Branch of Geographical Information Systems. (accessed 12.04.2022).

(129) İzmir'in Rakamları. *İzmir İlçelerinin Ortalama Hane Halkı Büyüklüğü*. https://izmirinrakamlari.izmir.bel.tr/tr/2022/49/HaneHalkiDurumlari. (accessed 25.10.2023).

(130) OpenStreetMap Overpass Turbo. *Urban Open-Green Areas and Forest Areas*. https://overpass-turbo.eu/. (accessed 15.01.2024).

(131) Meteorology 2nd Regional Directorate. *Meteorological Station*. https://izmir.mgm.gov.tr/istasyonlar.aspx. (accessed 30.09.2023).

(132) USGS. *What is the Landsat satellite program and why is it important?* https://www.usgs.gov/faqs/what-landsat-satellite-program-and-why-it-important. (accessed 15.09.2023).

(133) USGS. *Landsat Satellite Missions*. https://www.usgs.gov/landsat-missions/landsat-satellite-missions. (accessed 13.12.2023).

(134) USGS. *Landsat 5*. https://www.usgs.gov/landsat-missions/landsat-5. (accessed 10.02.2023).

(135) USGS. *Landsat 7*. https://www.usgs.gov/landsat-missions/landsat-7. (accessed 10.02.2023).

(136) USGS. *Landsat 8*. https://www.usgs.gov/landsat-missions/landsat-8. (accessed 10.02.2023).

(137) Republic of Turkey Ministry of Agriculture and Forestry. *Corine Nedir?* https://corine.tarimorman.gov.tr/corineportal/nedir.html. (accessed 25.03.2023).

(138) Copernicus Land Monitoring Service. *Corine Land Cover Classes*. https://insitu.copernicus.eu/Corinelandcoverclasses.eps.75dpi.png/view. (accessed 15.01.2023).

(139) USGS. *Using the USGS Landsat Level-1 Data Product*. https://www.usgs.gov/landsat-missions/using-usgs-landsat-level-1-data-product. (accessed 20.07.2023).

(140) Xu, H. Q.; Chen, B. Q. Remote Sensing of the Urban Heat Island and Its Changes in Xiamen City of SE China. *J. Environ. Sci.* 2004, *16* (2), 276–281.

(141) Sandholt, I., Rasmussen, K., & Andersen, J. A Simple Interpretation of the Surface Temperature/Vegetation Index Space for Assessment of Surface Moisture Status. *Remote Sens. Environ.* 2002, *79* (2–3), 213–224. https://doi.org/10.1007/s00209-017-2029-2.

(142) Weier, J. and Herring, D. Measuring Vegetation (NDVI & EVI). *Meas. Veg. (NDVI EVI)* 2000.

(143) Jensen, J. . Remote Sensing of the Environment: An Earth Resource Perspective. *Prentice Hall, New Jersey* 2000.

(144) Deardorff, J. W. Efficient Prediction of Ground Surface Temperature and Moisture, with Inclusion of a Layer of Vegetation. *J. Geophys. Res. Ocean.* 1978, *83* (C4), 1889–1903. https://doi.org/10.1029/jc083ic04p01889.

(145) Carlson, T. N.; Ripley, D. A. On the Relation between NDVI, Fractional Vegetation Cover, and Leaf Area Index. *Remote Sens. Environ.* 1997, *62* (3), 241–252. https://doi.org/10.1016/S0034-4257(97)00104-1.

(146) Sobrino, J. A.; Jiménez-Muñoz, J. C.; Paolini, L. Land Surface Temperature Retrieval from LANDSAT TM 5. *Remote Sens. Environ.* 2004, *90* (4), 434–440. https://doi.org/10.1016/j.rse.2004.02.003.

(147) Jiménez-Muñoz, J. C.; Sobrino, J. A.; Gillespie, A.; Sabol, D.; Gustafson, W. T. Improved Land Surface Emissivities over Agricultural Areas Using ASTER NDVI. *Remote Sens. Environ.* 2006, *103* (4), 474–487. https://doi.org/10.1016/j.rse.2006.04.012.

(148) Sobrino, J. A.; Raissouni, N. Toward Remote Sensing Methods for Land Cover Dynamic Monitoring: Application to Morocco. *Int. J. Remote Sens.* 2000, *21* (2), 353–366. https://doi.org/10.1080/014311600210876.

(149) Sobrino, J. A.; Raissouni, N.; Li, Z. L. A Comparative Study of Land Surface Emissivity Retrieval from NOAA Data. *Remote Sens. Environ.* 2001, *75* (2), 256–266. https://doi.org/10.1016/S0034-4257(00)00171-1.

(150) Zha, Y.; Gao, J.; Ni, S. Use of Normalized Difference Built-up Index in Automatically Mapping Urban Areas from TM Imagery. *Int. J. Remote Sens.* 2003,

24 (3), 583–594. https://doi.org/10.1080/01431160304987.

(151) Garg, A.; Pal, Di.; Singh, H.; Pandey, D. C. A Comparative Study of NDBI, NDISI and NDII for Extraction of Urban Impervious Surface of Dehradun [Uttarakhand, India] Using Landsat 8 Imagery. *2016 Int. Conf. Emerg. Trends Commun. Technol. ETCT 2016* 2017, No. November. https://doi.org/10.1109/ETCT.2016.7882963.

(152) Kumar Gautam, V.; Murugan, P.; Annadurai, M. A New Three Band Index for Identifying Urban Areas Using Satellite Images *Red* 2017, No. January, 978–993.

(153) Kawamura, M., Jayamanna, S., & Tsujiko, Y. *Relation between social conditions and the vegetation environment in Colombo city, using Remote Sensing data*. In International Archives of Photogrammetry and Remote Sensing. 1996. https://a-a-r-s.org/proceeding/ACRS1996/Papers/GLE96-3.htm.

(154) Gao, B.-C. NDWI A Normalized Difference Water Index for Remote Sensing of Vegetation Liquid Water From Space. *Remote Sens. Environ.* 1996, *58* (3), 359–363. https://doi.org/10.1080/00220973.1955.11010524.

(155) McFeeters, S. K. The Use of the Normalized Difference Water Index (NDWI) in the Delineation of Open Water Features. *Int. J. Remote Sens.* 1996, *17* (7), 1425–1432. https://doi.org/10.1080/01431169608948714.

(156) Xu, H. Modification of Normalised Difference Water Index (NDWI) to Enhance Open Water Features in Remotely Sensed Imagery. *Int. J. Remote Sens.* 2006, *27* (14), 3025–3033. https://doi.org/10.1080/01431160600589179.

(157) Taha, H.; Sailor, D.; Akbari, H. High-Albedo Materials for Reducing Building Cooling Energy Use, Lawrence Berkeley Laboratory, University of California. 1992.

(158) Liang, S.; Shuey, C. J.; Russ, A. L.; Fang, H.; Chen, M.; Walthall, C. L.; Daughtry, C. S. T.; Hunt, R. Narrowband to Broadband Conversions of Land Surface Albedo: II. Validation. *Remote Sens. Environ.* 2001, *84* (1), 25–41. https://doi.org/10.1016/S0034-4257(02)00068-8.

(159) Taha, H.; Akbari, H.; Rosenfeld, A.; Huang, J. Residential Cooling Loads and the Urban Heat Island-the Effects of Albedo. *Build. Environ.* 1988, *23* (4), 271–283. https://doi.org/10.1016/0360-1323(88)90033-9.

(160) ESRI. *How zonal statistics tools work*. ArcGIS. https://pro.arcgis.com/en/pro-app/latest/tool-reference/spatial-analyst/how-zonal-statistics-works.htm. (accessed 17.11.2023).

(161) Bolstad, P. *GIS Fundamentals : A First Text on Geographic Information System5 Th Edition*; 2016.

(162) Selim, B. R Programlamada İstatistiksel Veri Analizleri. 2018, 54. (accessed 12.02.2024).

(163) Brien, D. O.; Scott, P. S. *Correlation and Regression (Chapter 6)*; 2012.

(164) Statistics Knowledge Portal. *Correlation*. https://www.jmp.com/en_au/statistics-knowledge-portal/what-is-correlation.html#404f1893-ae56-43ed-b84c-f6c99f313eca.

(165) Selvanathan, M.; Jayabalan, N.; Kaur, S.; Supramaniam, M.; Hussin, N. Employee Productivity in Malaysian Private Higher. *Palarch's J. Archaraology Egypt* 2020, *17* (3), 66–79. https://doi.org/10.48080/jae.v17i3.50.

(166) Hayes, A. *Stepwise Regression: Definition, Uses, Example, and Limitations*. Investing Fundamental Analysis. https://www.investopedia.com/terms/s/stepwise-regression.asp#:~:text=. (accessed 18.02.2024).

(167) Taylor S. *Multiple Linear Regression*. CFI Education. https://corporatefinanceinstitute.com/resources/data-science/multiple-linear-regression/. (accessed 18.02.2024).

(168) Cao, X.; Onishi, A.; Chen, J.; Imura, H. Quantifying the Cool Island Intensity of Urban Parks Using ASTER and IKONOS Data. *Landsc. Urban Plan.* 2010, *96* (4), 224–231. https://doi.org/10.1016/j.landurbplan.2010.03.008.

(169) Ministry of Environment, U. and C. C. *Planlı Alanlar İmar Yönetmeliği*; 2023.

(170) Krüger, E.; Givoni, B. Outdoor Measurements and Temperature Comparisons of Seven Monitoring Stations: Preliminary Studies in Curitiba, Brazil. *Build. Environ.* 2007, *42* (4), 1685–1698. https://doi.org/10.1016/j.buildenv.2006.02.019.

(171) Yokobori, T.; Ohta, S. Effect of Land Cover on Air Temperatures Involved in the Development of an Intra-Urban Heat Island. *Clim. Res.* 2009, *39* (February), 61–73. https://doi.org/10.3354/cr00800.

(172) Yan, H.; Fan, S.; Guo, C.; Hu, J.; Dong, L. Quantifying the Impact of Land Cover Composition on Intra-Urban Air Temperature Variations at a Mid-Latitude City. *PLoS One* 2014, *9* (7). https://doi.org/10.1371/journal.pone.0102124.

(173) Johnson, S.; Ross, Z.; Kheirbek, I.; Ito, K. Characterization of Intra-Urban Spatial Variation in Observed Summer Ambient Temperature from the New York City

Community Air Survey. *Urban Clim.* 2020, *31* (December 2019), 100583. https://doi.org/10.1016/j.uclim.2020.100583.

(174) Şen, S. *Regresyon*. https://sedatsen.files.wordpress.com/2016/11/8-sunum.pdf. (accessed 07.01.2024).

(175) Nayanajith, G. Relationship of Perceived Behavioral Control and Adoption of Internet Banking in the Presence of a Moderator. 2019, *2* (January), 30–41.